Figuring Time by Space:
Representing sensory motion in cortical maps

A thesis submitted for the degree of Doctor of Philosophy

September 2011

Stuart P. Wilson

Department of Psychology

The University of Sheffield

Thesis summary

How does the brain represent sensory input? When stimuli move across sensor surfaces, such as a light source moving across the retina, sound moving between the ears, or contact moving over the skin, patterns of activation propagate across sheets of neurons that form the primary sensory cortices. Understanding how the movement of stimuli across the sensor surfaces relates to the activation of the cortical sheet is a fundamental problem in neuroscience.

The thesis presents a series of computational neuroscience studies, addressing how sensory stimuli are represented in mammalian primary sensory cortex. Each study constructed a model of how tactile stimuli, experienced by rodents via the array of facial whiskers, are encoded in the barrel cortex area of the primary somatosensory cortex. Each explains how the responses of cortical neurons to sensory stimuli can be predicted from their location in the cortical sheet. In each case, simple organising principles, based on cortical connection geometry and/or local learning rules, could account for how neuronal responses vary according to sensory stimuli.

The success of these highly simplified descriptions of cortical circuitry at explaining complex neurophysiological data suggests an important role for sensory experience and neural interconnection geometry in neural computation. The roles of both have been largely overlooked in recent large-scale efforts to model somatosensory cortical processing, which have focussed instead on cataloguing descriptions of neural tissue in increasing levels of detail. Using a top-down approach to modelling, the thesis generates specific hypotheses about the functional organisation of the sensory cortex, that can be used to guide future experimental work. The contribution of the thesis will therefore have been to lay the foundations of a theoretical framework for studying tactile stimulus processing in the somatosensory cortex, which is emerging as one of the most popular model systems in modern neuroscience.

Acknowledgements

Thank you to my supervisors. Thanks to James A. Bednar (Jim) of the University of Edinburgh for helping me to identify the problems, and for patiently, tirelessly, and selflessly guiding me towards the solutions. Thanks to Tony J. Prescott (Tony) for encouraging me to think about the bigger picture; the context, the story, and the wider implications of the work. Thanks to Ben Mitchinson (Mitch) for helping me to implement solutions, and for pushing me to be as careful and meticulous as he is. Basically, cheers Mitch for helping me zoom in, cheers Tony for helping me zoom out, and cheers Jim for helping me adjust the focus!

For helpful discussions and feedback related to published sections of the thesis, myself and my supervisors would like to acknowledge Paul Wilson (Dad), Martin Pearson, Charlie Sullivan, Jason Welsby, Tony Pipe, Tom Mrsic-Flogel, Angus Silver, Judith Law, Jan Antolik, Chris Palmer, Chris Williams, Irina Erchova, Nicolas Heess, Myles Jones, Jochen Staiger, Mathew Diamond, David Golomb, Dirk Feldmeyer, Satoshi Shimegi, Hiromichi Sato, and the various anonymous reviewers.

Thank you very much to the two examiners, Daniel Shulz (CNRS-UNIC) and Kevin Gurney (Sheffield), for taking the time to properly evaluate the thesis, and for patiently allowing me to explain myself during the viva.

Thank you also to my friends at the Active Touch laboratory at the University of Sheffield (ATL@S); Mat Evans, Robyn Grant, Alex Cope, Kendra Arkley, Charles Fox and Tom Stafford, and thank you to Ian Saunders. And to the lads; Afro, Splaig, Kimbo, Dale, Tights and Squawk.

For my loving family: For Mum, Dad, Al and Duncan, for Arthur, Boris and Dinah, and for my beautiful Rachel (Piglet!).

Contents

Chapter 1

Introduction

Chapter summary

A growing body of research in modern neuroscience has been centred on a remarkable feature of the rodent sensory cortex; the presence of a small number of large cortical columns, called 'barrels', each about half a millimetre in diameter, which after chemical staining are just about visible to the naked eye on the surface of the brain. The neurons of a particular barrel respond selectively when a particular whisker on the face is touched, and the barrels are arranged on the surface of the brain such that movement of adjacent whiskers on the animal's face primarily activates neurons of adjacent barrels. In effect, neuroscientists know exactly where to look for a response when they touch a whisker. Due to the precise topological relationship between the sensor (the facial whisker) and its primary cortical representation (the barrel), the whisker to barrel pathway is an ideal system in which to ask how sensory stimuli are represented in the brain. In addition to the mapping from the whisker to the barrel, several other parameters of whisker motion may be represented spatially across the sensory cortex. Additional parameters include the direction in which the whisker is moved, the frequency of whisker movements, and the relative timing between the movements of several whiskers. A review of the literature suggests that each parameter of sensory motion is represented in the cortex by a spatial code. Reviewed in the

context of precise definitions for sensory motion and spatial coding, the evidence gives rise to a general theory of sensory motion processing, which will be referred to as *Figuring Time by Space*. In order to formulate the theory scientifically, a program of computational modelling is proposed, centred around four key research questions. This program of research constitutes the basis of the thesis presented herein.

1.1 Sensory motion and spatial coding

What is sensory motion? Motion is the change in the position of a body in space over time. Motion is described by a velocity vector, composed of a rate of change and a direction of change, relative to an observer. In sensing, the observer is a receptor cell or surface thereof, the body is an object, and the motion velocity relative to the sensor surface is a sensory stimulus. Electrical signals in the brain are generated when waves of energy disturb receptor cells. Waves can be electromagnetic, as in vision or electrosensing, or mechanical, as in touch, audition, or biosonar in some species. Following the definitions of Cavanagh and Mather (1989), a detector for first-order motion responds to the displacement of stimulus intensity at an individual point on the sensor surface, whereas a detector for second-order motion responds to the difference in stimulus intensity between pairs of points on the sensor surface. Second order motion detection requires that signals from two detectors must be processed asymmetrically and integrated non-linearly, such that the response to stimuli moving in different directions is not equal to the mean response to either direction (Borst and Egelhaaf, 1989).

What is spatial coding? If different values for a parameter of sensory stimulus reliably evoke the greatest responses in different neurons, then that parameter is represented by a *spatial code*.

For example, if stimulation of different regions of the sensor surface evokes maximal firing rates in different neurons of a particular brain region, then the parameter, position, is represented in that region by a spatial code. For the present purposes, three types of spatial code can be defined, at increasing levels of spatial order; from the *random map*, to the *topological map*, to the *topographical map* at the highest level. Distinctions between these terms, particularly between topological and topographical maps, have been somewhat arbitrary in the literature and perhaps no universal distinction is possible (see Goodhill and Sejnowski, 1997); thus the following working definitions are offered to distinguish between orders of spatial codes in the context of the present review. First, if incremental parameter values reliably evoke the greatest responses in different neurons, and adjacent neurons respond to unrelated values, then that parameter is represented by a *random map*. A random map is a spatial code distributed amongst neurons without spatial order. Second, if incremental parameter values evoke the greatest responses in neurons that are located next to each other, then that parameter is represented by a *topological map*. A topological map is a spatial code with spatial order but without consistent orientation amongst the brains of conspecifics. Third, if increasing parameter values reliably evoke the greatest responses in neurons at increasing distances from an anatomical marker, and the relationship is conserved across the brains of conspecifics, then that parameter is represented by a *topographical map*. Thus a topographical (or topographic) map can be defined as a topological map with consistent spatial orientation.

The spatial code is to be contrasted with the temporal code, which may be defined as temporal precision in the neuronal response not simply reflecting the stimulus dynamics but relating to the stimulus properties (Dayan and Abbott, 2001). For example, in a seminal paper entitled *figuring space by time*, Ahissar and Arieli (2001) proposed that the location of a tactile stimulus may be encoded by the timing of spikes locked to whisker contact times, relative to those reporting the

phase of the whisker through the whisking cycle. Broadly speaking, spatial coding herein refers to an organisation where stimuli are discriminable by differences in the identity of responding neurons, rather than by differences in the activity of a responding neuron.

One brain area can contain numerous maps of different types, which are all coextensive with respect to the constituent neurons. To illustrate, consider the primary visual area of the rodent cortex, wherein each neuron participates in (at least) a random map for the orientation of visual edges and eye dominance, coextensive with a topographic map for the location of the stimulus in the visual field (Gias et al., 2005; Schuett et al., 2002; Ohki et al., 2005).

Self-organising processes underlie the organisation of many types of topological or topographical map, and they can originate from physical or environmental constraints on the neuronal network (Miikkulainen et al., 2005). Physical constraints may be due to genetically pre-programmed restrictions on connection lengths or speeds; for example, it has been suggested that a mapping for inter-ear stimulation time differences emerges from differences between the lengths of axons carrying signals from each ear to midbrain neurons (Jeffress, 1948). Environmental constraints are due to the nature and statistical structure of external inputs. For example, ferret auditory cortex, rewired postnatally to receive visual input, develops maps for eye preference and visual edge orientation; these maps are characteristic of those normally measured in visual cortex (Sharma et al., 2000). Hence, cortical maps for features of each sensory modality are highly plastic and are shaped by a combination of physical and environmental constraints (Feldman and Brecht, 2005).

The following sections present evidence that the sensory cortex represents sensory motion by spatial coding. Specifically, they review how the barrel cortex of tactile specialists like rats,

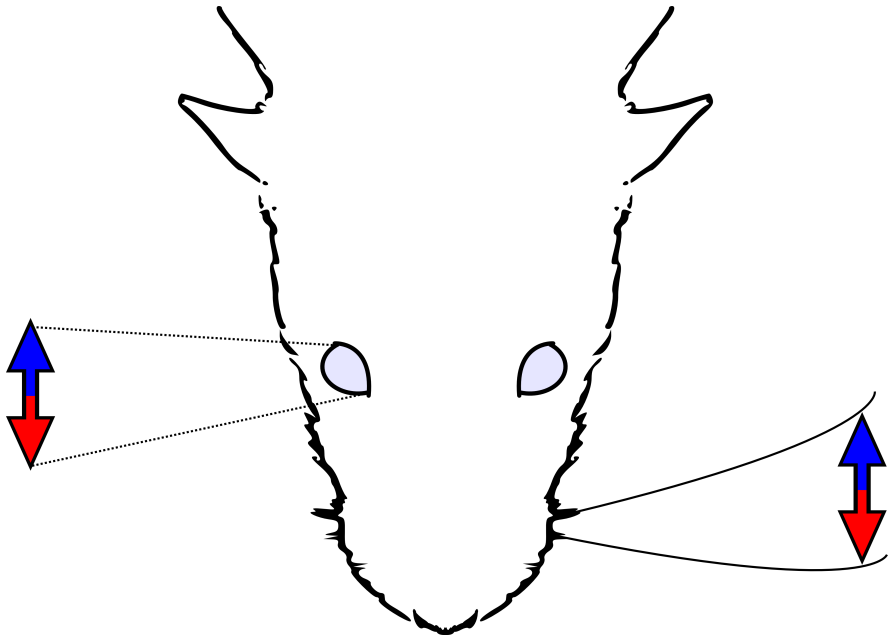

Figure 1.1. Sensory motion. Motion of an object in different directions (blue versus red) causes a response on the receptor surface via different types of wave. In vision (left), light waves travel to photoreceptors of the retina, directed by contraction of the iris relative to the lens. In the whisker system (right), mechanical waves travel to mechanoreceptors in the skin, directed by the facial vibrissae.

mice and shrews represents motion of the facial whiskers. In terms of first-order motion, maps have been measured in the barrel cortex for the identity of the stimulated whisker, for its frequency of vibration, and for its movement direction. For second-order motion, maps have been measured for the identity of maximally effective secondary whiskers, and for the velocity of stimulus movement between adjacent whiskers. As well as reviewing the evidence for these maps, the following sections serve as a focussed introduction to the anatomy and physiology of the whisker barrel system.

1.2 A spatial code for whisker identity

Tactile specialists like rats, mice, shrews and seals navigate dark environments, based on signals elicited by motion of the facial whiskers (Pisano and Storer, 1948; Hartmann, 2011; Wieskotten et al., 2011). The whiskers are arranged in an array of around 35 large whiskers on either side of the face, and many more around the lip and mouth (Welker, 1964; Brecht et al., 1997; Towal et al., 2011). Upon disturbance, the whiskers mediate a mechanical wave onto the sensor surface, which is comprised of mechanoreceptors distributed within (and, to a lesser extent, between) the corresponding hair follicles on the face (Ebara et al., 2002). It has been proposed that the physical location of the mechanoreceptor with respect to the follicle determines its response properties as either rapidly-adapting or slowly-adapting (Mitchinson et al., 2004, 2008). Similar to the way in which contracting the iris or generating a saccade regulates the flow of light onto the retina, actively controlled placement of the whiskers in space regulates the flow of the stimulus to the tactile sensor surface. (Welker, 1964; Kleinfeld et al., 2006; Mitchinson et al., 2007; Grant et al., 2009, see Figure 1.1). Whisker motion is represented in multiple, parallel,

hierarchical, sensorimotor loops, in turn via the brainstem, the thalamus, and the somatosensory and motor cortices (see Diamond et al., 2008 for an overview). See Figure 1.2 for an illustration of the pathway upon which this thesis will be focussed.

The primary somatosensory cortex contains a grid of discrete architectonic units, one unit per whisker, which after staining are visible to the naked eye (Woolsey and van der Loos, 1970; Welker and Woolsey, 1974). In layer 4, each unit is delineated in the plane tangential to the surface of the brain by a perimeter of densely-packed somata shaped like a barrel; the delineations between 'barrels' in the cortical sheet have been described mathematically as Dirichlet domains (Senft and Woolsey, 1991). Within each barrel, changes in synaptic contact density reveal regular geometric patterns, resembling, for example, a coffee bean or the Mercedes car badge (Land and Erickson, 2005; Louderback et al., 2006); these patterns are thought to emerge developmentally by self-organising processes (Ermentrout et al., 2009).

Following first-order motion at high velocity, i.e., deflection of a single whisker, neurons of a single barrel respond faster and with greater magnitude than the others. Thus the $\approx 10,000$ neurons comprising each barrel column (Beaulieu, 1993) tend to be mapped primarily to a particular whisker, called the principal whisker. The pattern of barrels in the somatosensory cortex directly corresponds to the layout of the whiskers on the face, such that adjacent whiskers are principal to adjacent barrels. This organisation is termed somatotopic, and the array of barrels is also oriented correctly (i.e., somatotopically) with respect to an overall 'ratunculus' body map in the somatosensory cortex (Woolsey and LeMessurier, 1948), which may itself arise out of self-organising processes (Farah, 1998; Stafford and Wilson, 2007). The orientation of the barrel field representation in the ratunculus is consistent amongst conspecifics (perhaps 'rodentunculus' is a sensible generalisation between rodent species), and hence the identity of

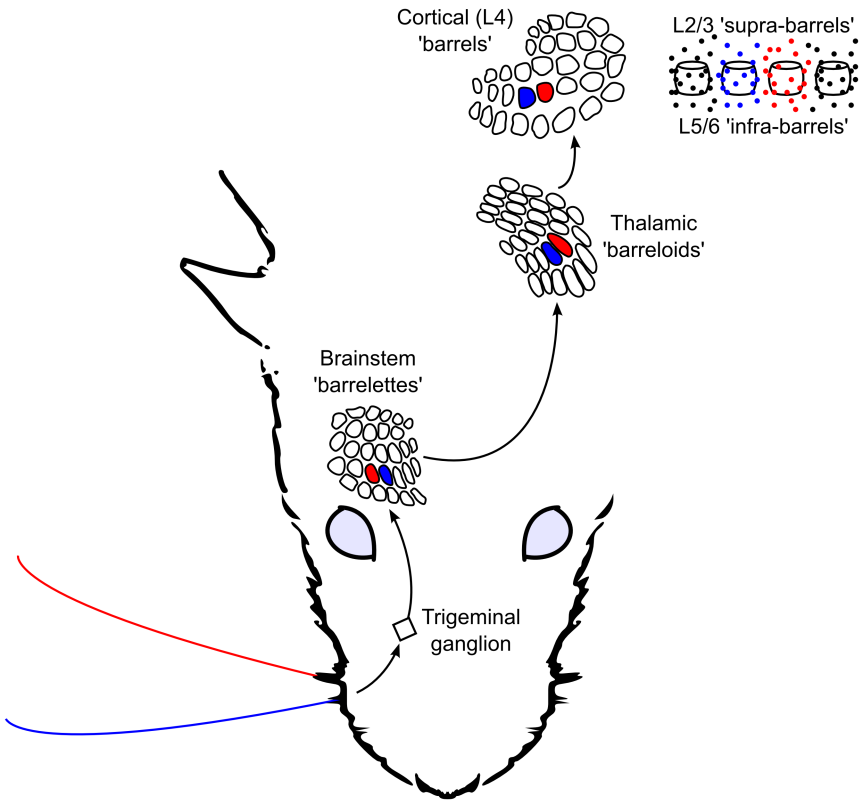

Figure 1.2. Cortico-centric view of the lemniscal processing pathway. The lemniscal pathway carries whisker signals to the cortex and beyond, via the trigeminal nucleus to ipsilateral neuronal clusters known as 'barrelettes' in the principal sensory brainstem, to contralateral 'barreloids' in the thalamic ventral posteromedial nucleus and to layer 4 cortical 'barrels'. The topographic projection of signals pertaining to two adjacent whiskers (blue and red) are traced along the neuraxis, to targets in so-called 'supra-barrel' and 'infra-barrel' regions in layer 2/3 and layer 5 barrel cortex respectively.

the deflected whisker is represented by a topographic map in the somatosensory cortex (see Figure 1.3).

The map for whisker identity amongst the barrels of granular layer 4 barrel cortex reflects a similar organisation between nuclei known as barrelettes in the brainstem (Ma and Woolsey, 1984), and as barreloids in the thalamus (van der Loos, 1976). The term supra-barrel has recently been suggested for the area of layer 2/3 supragranular barrel cortex situated directly above the barrel in layer 4 (Wilson et al., 2010), and similarly the term 'infra-barrel' will be used here to describe the region that is vertically aligned to the barrels in the infragranular layers 5 and 6. Upon whisker movement, excitation feeds forward along the neuraxis from barrelette, to barreloid, to barrel, to supra-barrel and infra-barrel, and laterally into adjacent supra- and infra-barrels (Armstrong-James et al., 1992; Lefort et al., 2009). This constitutes the lemniscal pathway; see Figure 1.2. It had been suggested that during development the organisation of topographic whisker maps unfolds in sequence along the pathway, with each whisker identity map inheriting the organisation from the antecedent layer (Killackey, 1980).

In the literature the term 'receptive field', without qualification, typically refers to the identity of whiskers whose movement can elicit significant responses in the neuron, although strictly speaking the receptive field of a neuron encompasses the full range of (multiple) whisker motion primitives (as in the original usages of Zucker and Welker, 1969; Woolsey and van der Loos, 1970). Non-principal whiskers comprising the receptive field of a neuron can increase or decrease its responses to the principal whisker, in the barreloids (Timofeeva et al., 2003; Lavallée and Deschênes, 2004; Kwegyir-Afful et al., 2005) and in the barrels (Brumberg et al., 1996; Bruno and Simons, 2002; Mirabella et al., 2001). These multi-whisker interactions are thought to subserve a kind of edge detection, and they stem from interactions between nuclei within

each level along the neuraxis (e.g., interactions between barrelettes or between barreloids; Timofeeva et al., 2004; Lavallée and Deschênes, 2004; Mirabella et al., 2001; Le Cam et al., 2011). The receptive field can be summarised by its eccentricity; a vector drawn through the whisker field, from the principal whisker to the center of mass of responses to non-principal whiskers (Andermann and Moore, 2006). The angle of eccentricity differs for different neurons within a barrel (Armstrong-James et al., 1992), such that neurons tend to prefer secondary whiskers that are represented by the nearest of the adjacent barrels (Andermann and Moore, 2006). This organisation constitutes a topographic map for the receptive field eccentricity within the barrel.

Hence a topographic map exists for first-order whisker motion (the principal whisker identity), at the resolution of the barrels (see Figure 1.4A), and for second-order whisker motion (the multi-whisker receptive field), at sub-barrel resolution.

1.3 A spatial code for whisker motion frequency?

Whiskers vary in morphology, depending on species, but in general they are curved and tapered from the base to the tip with a flat or undulating profile (Brecht et al., 1997; Chernova and Kulikov, 2011; Hanke et al., 2010; Williams and Kramer, 2010). To a first approximation the whisker behaves like a static beam with each whisker carrying a fundamental resonant frequency as well as higher-order harmonic frequencies (Birdwell et al., 2007). Thus, upon stimulation, whiskers of increasing length vibrate at decreasing frequencies (Neimark et al., 2003).

Although the whiskers have been characterised as large (the macro-vibrissae on the side of

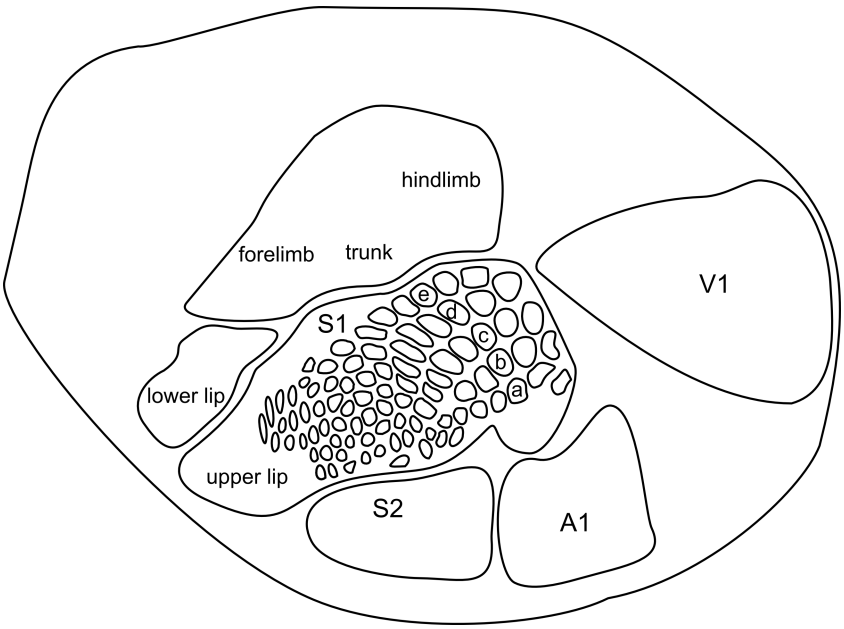

Figure 1.3. Spatial organisation of the sensory cortex. Sensory cortical areas were traced from anatomical borders, delineated by cytochrome oxidase staining in a flattened mouse cortical hemisphere. Recreated from ref. (Maier et al., 1999), their Figure 2. Rostral is to the left, caudal is to the right, medial is to the top and lateral is to the bottom. The array of cortical 'barrels' in the somatosensory cortex map in a one-to-one fashion to the array of facial whiskers. The configuration of primary visual cortex (V1) and primary auditory cortex (A1) sit in topographic register with an overall body-map organisation. Area S2 is secondary somatosensory cortex.

the face) or small (the micro-vibrissae around the mouth), in most species they are actually graded in length from small to large (Brecht et al., 1997). This grading is reflected by the band-pass tuning of barrel cortex neurons in response to controlled whisker vibration frequencies (Garabedian et al., 2003). The grading is also reflected by a topographic map for decreasing motion frequency along the barrel arcs, the major axis of the barrel array, representing whiskers of increasing length from the nose to the ear (see Figure 1.4B). Emerging from these observations, the 'cochlear hypothesis' (Andermann et al., 2004) compares the whisker array with the anatomical organisation of the cochlear in the inner ear, with its hair cells arranged by decreasing frequency preference from base to apex (Roberts et al., 1988). The cochlear hypothesis suggests a role for resonance in detecting and discriminating the spatial frequency of surface textures (Moore and Andermann, 2005). However it has been cast into doubt by evidence that barrel cortex neuronal spikes are time-locked to the 'kinetic signature' of the whisker movement (Wolfe et al., 2008), defined as the product of the frequency and the amplitude of the whisker displacement (Arabzadeh et al., 2004). The kinetic signature idea likens the whisker to a stylus on a record player, faithfully encoding the temporal pattern of small sticking and slipping events as the whisker moves over a textured surface. Accordingly, whisker resonance (and hence the resonance map) may play a more minor role in modulating near-threshold responses to whisker micromotions (Ritt et al., 2008; Andermann and Moore, 2008; Lottem and Azouz, 2009; see also Brecht, 2006; Arabzadeh et al., 2009 for a review).

1.4 A spatial code for whisker motion direction?

When the individual whisker is deflected in a particular direction at high velocity, rapidly-adapting primary afferent neurons that innervate particular structures of the whisker follicle fire strongly (Lichtenstein et al., 1990; Ebara et al., 2002; Szwed and Ahissar, 2006). Efforts to model the follicle complex have assumed that the selectivity of a primary afferent neuron for a particular deflection direction is related to the radial position of its innervation domain about the whisker base (Mitchinson et al., 2004, 2008). There is some evidence supporting the idea of a topographic mapping of deflection direction in the brainstem barrelettes, with respect to the anatomical axes of the barrelette nuclei (Furuta et al., 2006). However, stronger evidence for a topographic map for the whisker deflection direction has been measured in the thalamic barreloids (Timofeeva et al., 2003): The upward (dorsal) and forward (rostral) deflections seem to be represented by neurons located at the heads of the chilli-shaped barreloids, whereas downward (ventral) and backwards (caudal) deflections are represented by neurons located at the barreloid tails.

Evidence for a map for whisker deflection direction in the barrels has been somewhat controversial. First it was found that similar whisker deflection directions were represented by localised clusters of neurons within the barrel, but a null relationship between the directions represented in adjacent clusters was observed; i.e., a random map on the scale of the barrel (Bruno et al., 2003). Later, a positive correlation was measured between principal whisker deflection direction and the location of the neuron with respect to the barrel center (Andermann and Moore, 2006). An outwardly radiating pinwheel organisation was revealed, reminiscent of those measured in primary visual cortex, for example by Ohki et al. (2005) in cat but notably not in rodents (Ohki

et al., 2005; van Hooser et al., 2005; see also van Hooser et al., 2006). Extracellular multi-unit recordings, using tetrodes at different tangential locations through the barrel, were made whilst the principal whisker was deflected in randomly interleaved directions (Andermann and Moore, 2006). The pinwheels were topographic because movement of the whisker in the direction of an adjacent whisker on the face evoked the greatest responses in neurons located closer to the corresponding adjacent barrel (see Figure 1.4C). The strength of the correlation between neuron location and preferred direction was significantly greater in the supra-barrel compared to the barrel, suggesting that the direction map may be refined by intra-cortical circuitry.

In contrast, a subsequent two-photon calcium imaging study measured a random map in the supra-barrels (Kerr et al., 2007). However, recent additional studies have confirmed the existence of the direction map using optical imaging (Tsytsarev et al., 2010), and later using two-photon calcium imaging (Kremer et al., 2011). Results of the latter experiment went some way to resolving the previous discrepancy, revealing a non-topographic map in three-week old rats (the same age as in Kerr et al., 2007) and a topographic map in three-month old rats (the same age as in Andermann and Moore, 2006). Hence the first hypothesis that will be addressed, in chapter 2, is that, like the barrels themselves, a map for the whisker deflection direction emerges during post-natal development.

A computational model showed how correlated patterns of whisker deflection experienced during development could turn a non-topographic map for deflection direction into a topographic map in around an hour of simulated clock-time (Kremer et al., 2011; note that this model extends that presented in chapter 2; see Wilson, 2007; Wilson et al., 2010). The authors interpret this result as evidence that the map emerges during post-natal development, driven by correlations in the pattern of typical multi-whisker inputs. However, taken at face value the result

suggests that a topographic map for whisker direction could be entrained rapidly by correlated patterns of whisker deflection. Therefore the result suggests that the whisker-barrel system could be useful for exploring the process of map formation as it occurs (see Li et al., 2008 on the entraining of visual maps in ferret primary visual cortex). Suggestions for manipulating the process of self-organisation, by changing the patterns of experienced multi-whisker deflections, as well as predictions for the resulting map organisations, will be presented in chapter 2.

1.5 A spatial code for multi-whisker motion sequence?

When the rat or mouse palpates its whiskers against a surface, the whiskers make contact in sequence (Sachdev et al., 2001; Kleinfeld et al., 2006; Hartmann, 2011), and different object shapes and motion trajectories yield different patterns of whisker deflection sequence (second-order motion).

Adjacent-whisker contacts have been found to elicit supralinear responses, i.e., more than the sum of the single-whisker responses, in supra-barrel neurons located in the septal region between columns, for a range of short inter-whisker deflection intervals (Simons, 1983, 1985; Shimegi et al., 1999, 2000). It is possible that these data reflect an underlying continuum of preferences for the time interval between adjacent whisker deflections. Chapter 3 will present the hypothesis that neurons located closer to either supra-barrel center prefer increasing inter-whisker deflection intervals for stimuli beginning at the adjacent whisker. The idea is that supra-linear responses represent a topographic map for the inter-whisker motion velocity, i.e., for second-order sensory motion (see Figure 1.4D).

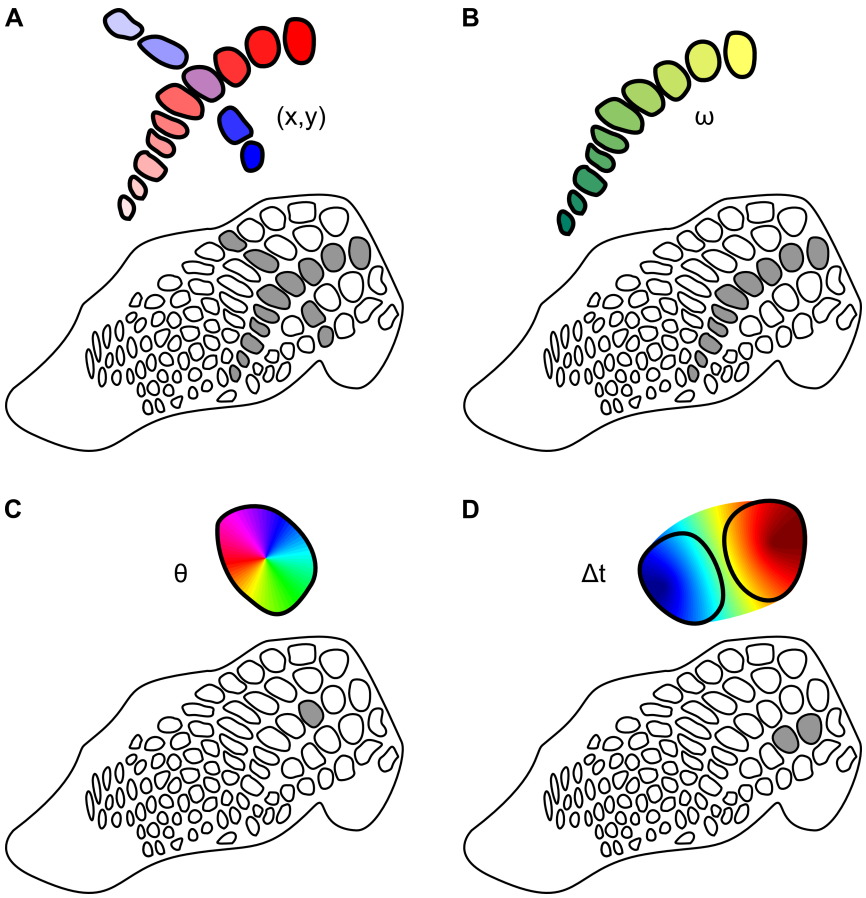

Figure 1.4. Summary of proposed spatial codes for whisker motion in the barrel cortex. **A** A map for the whisker identity across the barrels, coding for stimulus location increasing in x (stronger red along the arcs) and y (stronger blue along the rows). **B** A map for decreasing whisker resonant frequency (ω) along the arc of barrels (green to yellow for increasing x). **C** A map for the whisker receptive field eccentricity and the whisker motion direction (θ), around the radial extent of each barrel. **D** A map for inter-whisker motion sequence (Δt), extended between supra-barrels.

A recent study elegantly demonstrated that many-whisker displacement sequences are represented by a spatial code in the infra-barrels (Jacob et al., 2008). Twenty four whiskers were deflected in sequences that suggested the motion of a flat bar through the whisker field in different directions. Here a 'matrix' of individual piezoelectric stimulators aligned to each whisker (Jacob et al., 2010) allowed the individual whisker deflection directions to be independently controlled. Irrespective of the individual whisker deflection directions (first-order motion), infra-granular neurons were selective for the motion direction defined by the whisker deflection sequence (second-order motion), which is evidence for a spatial code for true second-order motion. However, the level of spatial code was not determined; random map, topological map, or topographic map? As suggested by the data of Andermann and Moore (2006) and Kremer et al. (2011), the principal whisker deflection direction is represented in a topographic pinwheel map across each barrel. However, as reported by Jacob et al. (2008), the tuning of a neuron for the principal whisker deflection direction is uncorrelated with its tuning for the motion direction implied by the multiple whisker sequence. Therefore a topographic organisation for the multiple whisker sequence direction would have to be defined with respect to axes that are distinct from the radial axes of the pinwheel maps for the principle whisker deflection direction.

1.6 Relationships between motion maps

As well as being coextensive, the organisations of maps for different stimulus features defined over the same sheet of neurons can be systematically related. The value of one stimulus parameter represented in a particular group of neurons can be predicted from the value of a second parameter represented in that group, given the map organisation for the second parameter. For

example, the iso-orientation contours of maps for visual edge orientation and the iso-direction contours of maps for visual motion direction tend to intersect at right angles across the two sheet dimensions of primate primary visual cortex; probably due to an interdependence between the two during normal visual experience (see Miikkulainen et al., 2005 and Issa et al., 2008 for an overview). So how might maps for whisker motion parameters relate?

The first-order direction map (deflection direction) seems to be correlated with the receptive field map (eccentricity), in layer 4 and 2/3 barrel cortex (Andermann and Moore, 2006). The receptive field map (eccentricity) seems to be correlated with the second-order direction map (deflection sequence), in layer 2/3 (Drew and Feldman, 2007). However, the first and second order direction maps appear not to be correlated; i.e., in layer 5 when testing using many whiskers (Jacob et al., 2008) and in layer 4 when testing using whisker pairs (Hemelt et al., 2010). A number of factors might account for this apparent discrepancy. One possibility is that stimulus motion maps in layer 2/3 and 5 might have a fundamentally different organisation. Another possibility is that colinear first-order and second-order stimulus directions used by Drew and Feldman (2007), but not by Jacob et al. (2008), might have modified the structure of the map for receptive field eccentricity. For example, Le Cam et al. (2011) recently reported that the receptive field eccentricity varies significantly depending on the first-order motion direction, in a majority of barrel cortex neurons. Hence it is a particularly interesting time to be studying map organisation, and potential correlations between maps, in the barrel cortex.

We have seen that the organisations of maps for different parameters can be systematically related within the same brain area. In addition, an elegant study revealed that maps for the same parameter in different brain areas can also influence one-another (Li and Ebner, 2007). Direct electrical stimulation of a region of the infra-barrel map for first-order motion direction

was found to modulate similar representations in the aligned thalamic barreloid. The authors stimulated infra-barrel neurons representing particular motion directions, and then measured a (recoverable) shift in the direction preference of barreloid neurons, from their original preferred direction to that preferred by the cortical neuron (Li and Ebner, 2007). The effect, and a similar effect between cortical and thalamic whisker identity maps, was measured during experiments that lasted several hours. It is not yet known whether such plasticity also occurs on shorter timescales, however it is interesting to consider whether dynamic modifications between maps within and between brain areas could subserve attention to particular stimulus feature values on behaviourally relevant timescales.

1.7 A spatial code for 'higher-order' tactile stimulus features?

If higher-order stimulus properties, such as those describing object shape, are represented by spatial coding, then they are more likely to be represented in topological rather than topographic maps; it is difficult to conceive how object representations that are invariant to spatial transformations (e.g., rotation of the object) could be maintained in a rigid topographic map that is anchored to the layout of the barrels. For example, the behavioural data of Anjum et al. (2006) show that Etruscan shrews elicit attacks when the whiskers encounter object shapes resembling the vulnerable body parts of their prey (i.e., the legs of crickets), irrespective of the direction of movement of those body parts through the whisker field. This implies that shrews maintain a Gestalt-like representation of certain tactile object shapes. Thus we might predict the presence of topological maps organised principally for higher-order relationships between object features, i.e., composed of tactile equivalents of the "Jennifer Aniston" neurons found in humans

(Quiroga et al., 2005). Unless the organisation of such an object-centered map were genetically predetermined, there should be no environmental constraints that would relate it to topographical maps for egocentric spatial relationships (e.g., for whisker identity, direction, and sequence; see Roth-Alpermann et al., 2010, for an exploration of maps in shrew cortex). The idea of maps for higher-order object representations will be explored in chapter 5.

Maps are typically measured by varying a parameter, thought by the experimenter to be of relevance to the sensory system, and then measuring the response. However it is difficult to know exactly what to look for in the barrel cortex. One approach is to control the form of the object and vary its motion. This requires formulating an hypothesis about what object forms are reliably encoded by the system; for example, that the sequence of whisker deflections pertaining to the tangential motion of a flat bar is relevant (Benison et al., 2006; Drew and Feldman, 2007; Jacob et al., 2008). However this approach becomes increasingly difficult as the represented stimuli become more abstract with respect to simple motion primitives. Another approach is to determine by experiment what type of stimulus is relevant for the animal by systematically varying tactile stimuli, and then observing a behavioural (Anjum et al., 2006) or neurophysiological response (Roth-Alpermann et al., 2010). Another method for describing spatial-temporal receptive fields for individual neurons is to consecutively track maximally effective secondary whiskers in sequence through the whisker field (Ghazanfar and Nicolelis, 1997, 1999), but this serial, single-neuron approach is difficult to apply on the scale of cortical maps.

An alternative to these methods is to avoid choosing a specific stimulus by using reverse correlation analyses. This technique involves presenting (typically low-pass filtered) white noise stimuli to the whiskers and then reconstructing the spatial and temporal profile of the maximally effective stimulus, from the maximally effective kinematics at each time-step and in each loca-

tion (each whisker). Reverse correlation analyses have been applied to the responses of primary afferent and thalamic neurons under stimulation of a single whisker (Arabzadeh et al., 2005; Petersen et al., 2008), and in the barrel cortex using multiple whiskers (Brumberg et al., 1996; Le Cam et al., 2011), and algorithms for performing efficient reverse correlation for motion stimuli are being refined for visual stimuli (Borghuis et al., 2003). However reverse correlation analyses are limited to describing only spatial-temporal receptive fields in which responses across the sensor surface combine linearly (i.e., simple-cell receptive fields; for discussion see Willmore and Smyth, 2003). Hence, whilst the approach is efficient and requires little knowledge of receptive-field structure *a priori*, it is limited when it comes to describing complex receptive-fields that may be invariant to transformations in space (e.g., a rotation of the cricket leg) or time (e.g., a slower motion of the cricket leg).

1.8 *Figuring Time by Space*

This review began with the idea that sensory motion may be represented in the sensory cortex by spatial coding. The idea is based on the fact that neurons in the barrel cortex respond to motion of the whiskers and that the spatial layout of the barrels on the surface of the brain reflects the layout of the whiskers on the face. Pursuing the idea further, the representation of additional somatosensory features, i.e., changes in whisker positions over time, could be cast as components of the more general problem of representing sensory motion by spatial coding. The idea that sensory motion is spatially encoded may therefore be conceptualised as the problem of *Figuring Time by Space*. Focussing on research conducted in the decade since Ahissar and Arieli published *Figuring space by time* (Ahissar and Arieli, 2001), the evidence was reviewed

in the context of spatial coding for first-order motion features, such as the frequency and direction of whisker movements, and second-order motion features, such as the relative timings of whisker movements.

In order to formulate the idea of *Figuring Time by Space* as a theory, it is necessary to ask of it scientific questions phrased at an appropriate level of abstraction. In reviewing the evidence it was useful to consider spatial codes of increasing spatial order in the form of random, topological, and topographic maps. In several cases the evidence suggests that maps for multiple stimulus features can lie coextensive across the same population of neurons, that the organisation of multiple maps can be correlated, and that maps can arise from developmental processes. Posed at the level of map organisation, map interaction, and map development, it is therefore appropriate to formulate theory at the level of neural systems, rather than at (or below) the level of individual neuronal and synaptic processes. As already encountered, establishing the functional organisation of cortical maps is challenging; the process often requires that a number of simplifying assumptions are made; thus maps can be difficult to interpret and the mechanisms by which they arise can be hard to evaluate. So how can these systems level problems be tackled?

Systems neuroscience has at its disposal a particularly powerful tool in the form of the computational model. Computational models are powerful theoretical formulations, because every assumption made by including or excluding part of a model constitutes an explicit hypothesis about how that part contributes to the function of the system. Modelling can complement experimental work by identifying gaps in existing knowledge, filling those gaps with explicit hypotheses, piloting experiments that may otherwise be infeasible, and establishing critical questions for future experiments. Modelling is therefore a good place to start to draw out the

plausibility of the theory that part of the function of sensory cortical processing concerns *Figuring Time by Space*.

The rodent primary somatosensory cortex has been studied in exquisite detail; a wealth of neurophysiological, neuroanatomical, neuroimaging, and behavioural data have been collected, under a variety of experimental, genetic, and pharmacological manipulations, both *in vivo* and *in vitro*. *In silico* methods have played an important role in collating a wealth of knowledge about the whisker-barrel system, and deriving from that knowledge new insights into the functional organisation of the single cortical column (notably from Kyriazi and Simons, 1993; Kyriazi et al., 1996; Pinto et al., 1996; Sarid et al., 2007; Lefort et al., 2009). However replicating this bottom up modelling approach on the scale of cortical maps is a long way off (see Markram, 2006). Meanwhile, by formulating the functional theory first and then testing it in simulation, a top down modelling approach can be equally important; research on vision in particular has a long history of complementary approaches to models at different levels of abstraction (see Table 1.1). However few, if any, top down models have been formulated in the context of the whisker barrel system. Hence the aim of this thesis will be to establish the first top down computational models of sensory processing in the whisker barrel system. These models will be used to test new ideas about barrel cortical processing, and, where possible, to derive specific, testable predictions to guide future experimental work.

Table 1.1. Results of a search on PubMed.gov (http://www.ncbi.nlm.nih.gov/pubmed) performed 12/08/2011, revealing a prevalence of computational modelling in vision compared with somatosensation.

Search term	+ 'cortex'	+ 'computational model'
'visual'	40700	355
'somatosensory'	15790	38
'barrel'	1386	14

1.9 Organisation of the thesis

Following Epstein (2008), a major motivation for modelling is to generate new theories by suggesting analogies with other known systems. Hence a major goal of the thesis is to explain somatosensory processing by analogy with that in other modalities; specifically by analogy with vision in chapter 2 and with audition in chapter 3. Another motivation is, where possible, to reveal the seemingly complex as simple (Epstein, 2008). Hence the general modelling approach will be to investigate complexity in networks interacting under simple local constraints; in particular as we explore network self-organisation in chapters 2 and 5. The approach will be one of synthesis followed by analysis (Braitenberg, 1984; Mitchinson et al., 2010); i.e., to construct the model (for example by making a physical model of the whiskers in chapter 4) and then to scientifically investigate its behaviour. Analysis at each stage will draw direct comparisons with biological data, with the caveat that a good fit alone reveals nothing about what data cannot be fit by the model, or what can be fit by alternative models (Roberts and Pashler, 2000). Hence suitable control models will be formulated where appropriate, and specific predictions for future experimental validation will be derived.

The remainder of the thesis is organised in terms of four main research questions. Together these questions constitute a theoretical framework, based on spatial coding, for understanding sensory processing in the whisker-barrel system:

Research question: ***Can a general model of cortical development explain the existence of a whisker direction map in the barrel cortex?***

In chapter 2 we will ask whether a topographic map for the individual whisker deflection direction could emerge in the barrel cortex from constraints on the patterns of tactile stim-

uli typically experienced during post-natal development. Chapter 2 is an edited version of the published article: Wilson SP, Law JS, Mitchinson B, Prescott TJ & Bednar JA (2010) Modeling the emergence of whisker direction maps in rat barrel cortex. *PLoS ONE 5: e8778* (doi: 10.1371/journal.pone.0008778).

Research question: ***Can a general model for resolving the relative timing of sensory inputs explain neuronal responses to different whisker timings in the barrel cortex?***

In chapter 3 we will ask whether a topographic map for the velocity of stimulus movements between multiple whiskers could emerge from the geometry of connections in the barrel cortex. Chapter 3 is an edited version of the published article: Wilson SP, Bednar JA, Prescott TJ & Mitchinson B (2011) Neural computation via neural geometry: A place code for inter-whisker timing in the barrel cortex? *PLoS Computational Biology* (doi: 10.1371/journal.pcbi.1002188).

Research question: ***Can spatial coding in the barrel cortex be used to reconstruct tactile stimulus features from real multi-whisker deflection patterns?***

In chapter 4 we will ask to what extent spatial coding mechanisms for first and second order motion, as identified in chapters 2 and 3, can be used to reconstruct tactile stimulus features from real (i.e., physical) multi-whisker deflection patterns.

Research question: ***How might representations of complex tactile stimulus features be organised in the barrel cortex?***

In chapter 5 we will try to predict the structure of cortical maps for complex multi-whisker stimulus parameters related to the shape, motion direction, and motion speed of tactile stimuli, asking in particular how maps for multiple tactile stimulus features may interact

across the cortical sheet.

A general discussion in chapter 6 will evaluate the general modelling approach and propose some specific experiments for the future.

Chapter 2

Modeling the emergence of whisker direction maps in rat barrel cortex

Chapter summary

Based on measuring responses to rat whiskers as they are mechanically stimulated, one recent study suggests that barrel-related areas in layer 2/3 rat primary somatosensory cortex (S1) contain a pinwheel map of whisker motion directions. Because this map is reminiscent of topographic organization for visual direction in primary visual cortex (V1) of higher mammals, we asked whether the S1 pinwheels could be explained by an input-driven developmental process as is often suggested for V1. We developed a computational model to capture how whisker stimuli are conveyed to supragranular S1, and simulate lateral cortical interactions using an established self-organizing algorithm. Inputs to the model each represent the deflection of a subset of twenty-five whiskers as they are contacted by a moving stimulus object. The subset of deflected whiskers corresponds with the shape of the stimulus, and the deflection direction corresponds with the movement direction of the stimulus. If these two features of the inputs are correlated during the training of the model, a somatotopically aligned map of direction emerges for each whisker in S1. Predictions of the model that are immediately testable, include, i) that somatotopic pinwheel maps of whisker

direction exist in adult layer 2/3 barrel cortex for every large whisker on the rat's face, even peripheral whiskers, ii) in the adult, neurons with similar directional tuning are interconnected by a network of horizontal connections, spanning distances of many whisker representations. We also propose specific experiments for testing the predictions of the model by manipulating patterns of whisker inputs experienced during early development. The results suggest that similar intracortical mechanisms guide the development of primate V1 and rat S1.

2.1 Introduction

Mammalian sensory cortex is organized firstly by modality, and secondly into topographic maps of the corresponding sensory apparatus. The prototypical example is the map of the retina in primary visual cortex (V1). Within this retinotopic map, finer scale feature maps have been found, such as for the motion direction of visual stimuli, with nearby neurons responding to similar directions (Weliky et al., 1996; Ohki et al., 2006).

Direction maps in ferret V1 emerge postnatally, and are sensitive to early visual experience (Li et al., 2006; White and Fitzpatrick, 2007), suggesting that they result from a self-organizing process driven by visual input. Map self-organization has been modeled using networks of neurons that develop receptive fields (RFs) by Hebbian learning of correlations between input and cortical activities (Swindale, 1996; Bednar and Miikkulainen, 2003; Stafford and Wilson, 2007). In such models, a balance between intracortical excitation and inhibition ensures the emergence of RFs that collectively cover the full range of motion directions; essentially, the neurons compete to respond to directions in the visual scene.

Direction maps in both real and simulated V1 are punctuated by pinwheels, where all directions are represented continuously around a central point. A similar pinwheel map has recently been measured in rat primary somatosensory cortex (S1) for the direction of deflection of the rat's whiskers (Andermann and Moore, 2006; Bruno et al., 2003). Andermann and Moore (2006) found a pinwheel map of directions spanning the domain of layer 2/3 (L2/3) neurons most responsive to one principal whisker (PW). This domain will henceforth be referred to as the supra-barrel region or just the supra-barrel, as it is located above the L4 'barrel' structure which receives thalamic input primarily from the PW. The map is somatotopically aligned to echo the overall pattern of barrels: deflection of whisker A towards whisker B evokes the strongest responses in neurons of whisker/supra-barrel A that are nearest to whisker/supra-barrel B (see Figure 2.1).

The map was measured by multi-unit tetrode recordings in approximately three-month-old rats (Andermann and Moore, 2006) but was not found in a subsequent study that used two-photon calcium imaging and rats aged approximately one month (Kerr et al., 2007). These two studies used different methods, besides the age of the animals tested and the recording techniques employed, and so the differences in their findings remain controversial (see Discussion). However, recent two-photon calcium imaging data have measured a similar map in three-month-old but not in three-week-old rats (Leger J-F., Kremer Y. & Bourdieu L., 2009, Society for Neuroscience abstract 174.13). These findings together suggest that the map for whisker deflection direction emerges during post-natal development (see Discussion). Here we explore the idea that the development of the map is driven by input from the whiskers, much as V1 feature map development is thought to be driven by input from the eyes.

Because the mapping of whisker deflection direction within the individual supra-barrel is aligned

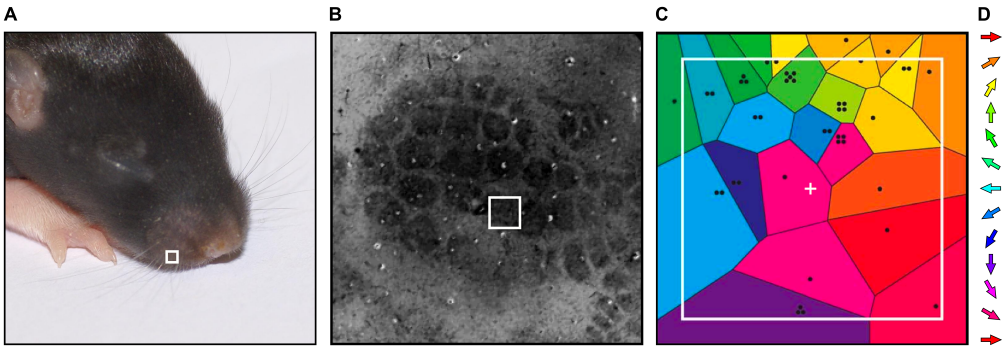

Figure 2.1. Maps in the rat whisker-barrel system. **A** The whiskers are arranged on the snout of a 10 day old rat pup in an orderly grid pattern. **B** This pattern is reproduced in barrel clusters, revealed here in a tangential section in L4 barrel cortex stained for cytochrome oxidase, such that neurons in each cluster respond preferentially to stimulation of the whisker in the corresponding position in the whiskerpad. **C** Within a supra-barrel, a pinwheel map has been measured for the direction in which the corresponding whisker is deflected (Andermann and Moore, 2006). The map is described as somatotopic because deflecting the principal whisker (PW) in the direction of an adjacent whisker on the snout selectively activates neurons in the PW's barrel that are closest to the adjacent whisker barrel. Reprinted from Andermann and Moore (2006); colors show the direction tuning of neurons in each location within a barrel, according to the color key in **D**. The black dots show positions of electrode penetrations, where multiple dots correspond to multiple-unit recordings. The white box in **A** outlines the base of the PW for the corresponding barrel outlined in **B** and whose supra-barrel is enlarged in **C**.

with the overall layout of the barrels themselves (see Figure 2.1B), we hypothesize that it is driven by tactile experiences in which the direction of the individual whisker deflection is correlated with the stimulation of adjacent whiskers. We have previously shown that when freely moving rats explore surfaces, they make contacts on a subset of whiskers (Mitchinson et al., 2007; Grant et al., 2009). Here we show in simulation that when (and only when, within the constraints of our modelling framework) the subset of deflected whiskers is consistent with the direction in which each whisker is deflected, a direction map robustly self-organizes into a somatotopic pinwheel in each supra-barrel.

2.2 Methods

2.2.1 A model of the barrel cortex

We developed a model based on LISSOM (Laterally Interconnected Synergetically Self-Organizing Map; Sirosh and Miikkulainen, 1997; Miikkulainen et al., 2005), with afferent projections that are constrained to simulate those from the layer 4 (L4) barrels to the supra-barrels in L2/3. The model was built using the Topographica simulator (Bednar et al., 2004), which is freely available at www.topographica.org.

The model comprises twenty-five whiskers arranged into a 5×5 grid, or 'whisker field' (Figure 2.2A), 25 corresponding 'barrels' in L4 S1 (Figure 2.2B), and a sheet of 105×105 L2/3 neurons (Figure 2.2C). Each barrel contains 25 directionally tuned afferent units that code for the stimulation of each whisker. Based on the afferent connections from L4, L2/3 can also

be divided into a 5×5 grid of 'supra-barrels'. There are 21×21 neurons in each supra-barrel, such that neurons located in each receive input from the L4 units coding for stimulation of the corresponding isomorphic (principal) whisker.

We first give a general overview of how the model works. An input pattern represents how the 5×5 grid of whiskers interacts with a tactile stimulus, determining whether each whisker is deflected and in what direction. This pattern is then encoded as a pattern of activation in L4. When the pattern is presented to the network, activity propagates from the L4 barrels (see Figure 2.2D) to the corresponding L2/3 supra-barrels (see Figure 2.2E), via weighted connections whose strengths are initially set to random values. L2/3 neurons then interact laterally, through recurrent connections that are net excitatory over very short distances and inhibitory over very large distances. Lateral interactions are allowed to stabilize through a number of settling steps, focusing the initial L2/3 response into discrete bubbles of activity across L2/3 (as in Figure 2.1E). Once the lateral interactions have settled, afferent and lateral weights are updated with a Hebbian learning rule, activation is reset to zero, and a new stimulus is presented to the network. The next four Methods sections describe these steps in detail.

2.2.2 Stimulating the whiskers

Each whisker w is assigned a coordinate spaced on a rectangular grid such that horizontally and vertically adjacent whiskers are 1.0 units apart, and diagonally adjacent whiskers are $\sqrt{2}$ apart. The layout of the whiskers on the grid is illustrated in Figure 2.2A. To construct each input pattern, we choose a linear boundary passing through a random point $\{x_0, y_0\} \in [-2.5, 2.5]$ and with outwardly-pointing normal in a random direction $\theta \in [0, 2\pi)$. Whiskers inside the

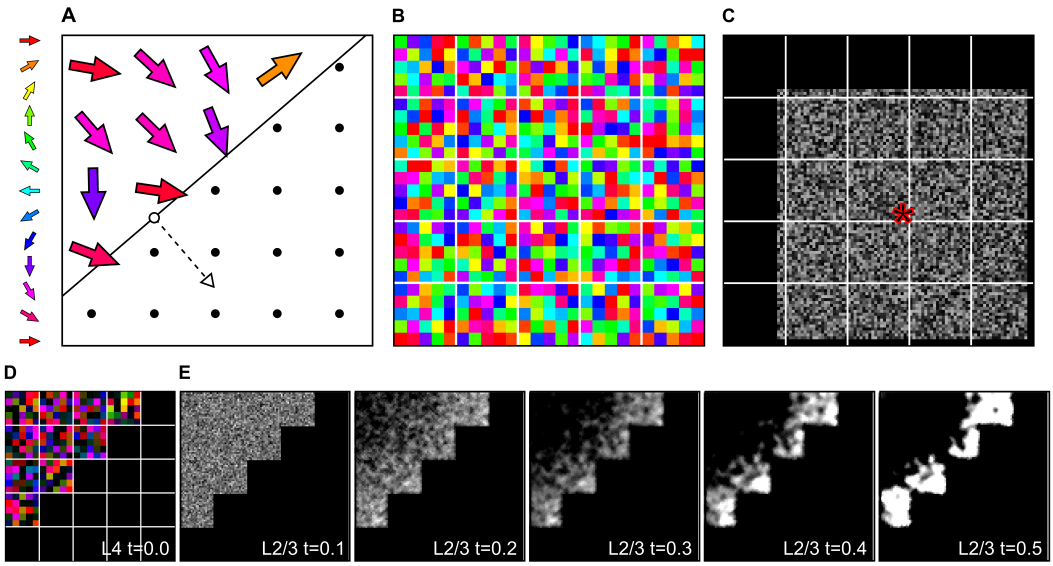

Figure 2.2. Model diagram and activity before any learning. **A** 25 whiskers are arranged in a regular grid, where some are deflected (colored arrows) and some are not (dots). Deflected whiskers are those impinged by a wide stimulus (solid line) moving in the direction of the dashed line and unfilled arrow ($\theta = 320°$). The stimulus is a half plane, which has moved almost half-way through the whisker field in this example. Deflected whiskers are those to the left of the plane. Impinged whiskers are deflected roughly in the direction of stimulus motion, but we apply normally distributed noise to each, with concentration parameter $\kappa = 3$ in the example. **B** The L4 sheet is divided into barrels (delineated by white), each containing 25 neurons with pre-assigned maximally effective directions (MEDs; pixel color) from around the circle, and located arbitrarily within the barrel. **C** L2/3 is divided into supra-barrels (21×21 neurons in each), such that each neuron receives weighted projections from all L4 neurons in the corresponding barrel. Each L2/3 neuron also receives excitatory lateral connections from itself and its 8 immediate neighbors (its lateral excitatory connection field). Each also receives inhibitory connections from all neurons that fall within a 4×4-barrel area (84×84 neurons) centered on its location; the lateral inhibitory connection field for the neuron marked * is shown. The brightness indicates connection strengths from * to each neuron before training. **D** The example input is represented in L4 by activating neurons whose MEDs are similar to the direction of deflected whiskers. **E** Initially random activity in stimulated L2/3 supra-barrels migrates to the leading edge of the stimulus as lateral interactions settle for each of steps $< t = 0.6$. All plots are normalized separately.

boundary are deflected, and those outside are not.

In line with our hypothesis that a correlation between whisker direction and the overall pattern of activated whiskers could align maps of whisker direction, we define the perfectly correlated direction for each whisker deflection to be θ. We can then control the strength of this correlation by drawing individual deflections randomly from a distribution centered on θ. We use a circular normal distribution (a Von Mises distribution; see Fisher, 1993) and vary its concentration parameter κ. This is shaped like a normal distribution for κ values between 0 and ∞, but at 0 the distribution is flat, and $\kappa = \infty$ describes a delta function. For example, when $\kappa = 0$ the whiskers would each be deflected in random directions, and when $\kappa = \infty$ they would each be deflected at θ. See Figure 2.2A for an illustration of this process.

This model is a simple abstraction of the complex (and largely unknown) pattern of whisker–stimulus interactions present during early development, focusing only on the assumption that local subsets of the whiskers are usually impinged by large stimuli moving from outside to inside the whisker field. Such stimuli might be, for example, the floor and other surfaces in the environment, a littermate's foot, tail or head, or a part of the mother's body. For clarity in the remaining sections, when we refer to a direction of motion, we mean the motion of a stimulus relative to stationary whiskers, not that of the whiskers due to locomotion or active whisking behavior. Even so, note that both types of motion would yield the same relative motion, and thus indistinguishable patterns of activation in the model.

2.2.3 Activating the barrels

Neurons located within a rat L4 barrel are tuned to the direction in which the PW is deflected (Simons, 1978; Bruno and Simons, 2002; Lee and Simons, 2004). Although neurons with similar maximally effective directions (MEDs) are clustered together, evidence for a systematic spatial arrangement of these domains in L4 is weak (Bruno et al., 2003; Andermann and Moore, 2006). L4 MEDs are consistent throughout post-natal development (Shoykhet and Simons, 2008), and neither the location nor directionality of the neuron is known to predict adjacent-whisker effects (Simons and Carvell, 1989; Khatri and Simons, 2007).

Accordingly each afferent unit in L4 represents a cluster of real neurons that have similar direction tuning. Each unit a is pre-assigned a fixed MED for deflections of the PW, chosen randomly from ($\phi_a \in [0, 2\pi)$). We use a cosine curve scaled to reflect the broad directional tuning of L4 neurons:

$$f_a = \frac{cos|\theta_w - \phi_a| + 1}{8} \tag{2.1}$$

where the firing rate f_a of each L4 unit increases when the PW is deflected in a direction more similar to its preferred direction.

2.2.4 Lateral interactions

Following deflection of a single rat whisker, excitation is relayed through corresponding groups of neurons in rat brainstem and thalamus to the isomorphic L4 barrel. Excitation then projects into the supra-barrel in L2/3, and subsequently spreads across L2/3 into adjacent domains (Armstrong-James et al., 1992). However, the overall long-distance effect of a strong whisker deflection is inhibitory, perhaps due to disynaptic inhibition. For example, Derdikman et al. (2003) measured a consistent difference-of-Gaussians profile of activity across L2/3, in which inhibitory effects range significantly further across adjacent supra-barrels than excitatory effects, for the duration of the response following PW deflection.

Studies in which adjacent whiskers are sequentially deflected also reveal strong suppression of responses to the second whisker by prior deflection of the first (Simons, 1985; Simons and Carvell, 1989; Shimegi et al., 1999; Kida et al., 2005), and the same has recently been demonstrated for stimuli that involve many whiskers (Drew and Feldman, 2007; Jacob et al., 2008). Interestingly, cross-whisker suppression is maximal at the time-scale measured as the mean interval experienced by rats trained to whisk into a stimulus (approximately $20\,\mathrm{ms}$; Sachdev et al., 2001).

With these observations in mind, we set up model L2/3 neurons to receive excitatory connections from themselves and the eight immediately adjacent neurons, so that the activity of the pre-synaptic neuron increases the response of adjacent post-synaptic neurons. Over this range and over greater lateral distances (a square area four supra-barrel widths across), neurons receive inhibitory lateral connections.

Note that these connections implement the observed net pattern of lateral interactions, and as described in the Discussion, do *not* represent any assumptions about the relative lengths of actual inhibitory and excitatory lateral connections in S1.

It is plausible that L2/3 neurons receive feed-forward input arising from multiple whiskers. However for simplicity in the model the twenty-five units of each L4 barrel all project to each of the 441 neurons in the isomorphic supra-barrel only. Hence we model the connectivity from barrel to supra-barrel as all–to–one. The excitatory and inhibitory connection fields are not restricted by the barrel borders imposed on the afferent projection from L4, but are instead centered on the location of each cortical neuron (as suggested by evidence from Bruno et al., 2009; Kerr et al., 2007; Feldmeyer et al., 2006; Helmstaedter et al., 2009; Ajima and Tanaka, 2006; see example in Figure 2.2C). Before training, the weights in the connection fields for each L2/3 neuron (afferent, excitatory and inhibitory) are uniform random values, normalized to sum to 1.0 in each connection field.

Following the reduced LISSOM model (Miikkulainen et al., 2005), the activity s_b for a L2/3 neuron at location b is the weighted sum of the activity in the corresponding barrel:

$$s_b = \sum_a \chi_a A_{ab} \tag{2.2}$$

where χ_a is the activation of afferent neuron a in the barrel projecting to cortical neuron b and A_{ab} is the corresponding afferent weight. After the initial response of a cortical neuron is calculated, activation propagates laterally across L2/3 for 9 settling steps; little change in the activation patterns is observable after 5 steps. Lateral interactions affect the activity η of a single

cortical neuron b according to:

$$\eta_b(t) = \sigma\left(s_b + \sum_c \eta_c(t-0.1)E_{cb} - \sum_c \eta_c(t-0.1)I_{cb}\right) \tag{2.3}$$

where $\eta_c(t-0.1)$ is the activity of another L2/3 neuron c during the previous settling step, E_{cb} is the excitatory lateral connection weight from that neuron to neuron b, and I_{cb} is the inhibitory connection weight. The activity is squashed through $\sigma(x)$, a piecewise-linear approximation to a sigmoidal activation function:

$$\sigma(x) = \begin{cases} 0 & x \leq l \\ (x-l)/(u-l) & l < x < u \\ 1 & x \geq u \end{cases} \tag{2.4}$$

where $l = 0.1$ is a lower-bound threshold and $u = 0.65$ is the upper bound, i.e., the saturation point of the (linearly approximated) sigmoidal region. The values for all of these parameters were determined in pilot work so that the network would group activity into bubbles on the approximate spatial scale of the supra-barrel (see example in Figure 2.2E).

2.2.5 Learning

After settling, both afferent and lateral weights are updated via a Hebbian learning rule with divisive normalization:

$$w'_{db} = \frac{w_{db} + \alpha_{bp} X_d \eta_b}{\sum_e (w_{eb} + \alpha_{bp} X_e \eta_b)} \tag{2.5}$$

where w_{db} is the current afferent or lateral connection weight from d to b, w'_{db} is the value of the weight to use in the next input presentation, X_d is the pre-synaptic activity after settling, and η_b is the activity of neuron b after settling. For unit b, $\alpha_{bp} = \frac{1}{n_p}$ is the Hebbian learning rate for connections of type p (either afferent, A, excitatory, E, or inhibitory, I), where n_p is the number of neurons in the connection field for neuron b. For example, $\alpha_{bA} = \frac{1}{25}$, as there are 25 afferent units in the afferent connection field (or barrel) connecting to each L2/3 neuron b. The afferent, excitatory, and inhibitory connections are normalized separately. We note that by using a divisive rather than subtractive normalization, weights are redistributed rather than driven to saturation after each training pattern; for a detailed discussion of this behavior see Miller and Mackay (1994). This process of input presentation, activation, settling, and learning is repeated for each of 5,000 random input patterns.

Although the initial distribution of lateral interactions in the model is uniform, the lateral weights are modifiable during self-organisation. Hence we might anticipate an anisotropic distribution of input patterns to be consolidated in a similarly anisotropic map organisation and a corresponding change in the distribution of learnt lateral connection weights. These questions

will be addressed later when we demonstrate how biased input statistics can overturn the initially unbiased cortical interactions during development in a manner consistent with data from adult barrel cortex.

2.3 Results

2.3.1 Activity bubbles migrate to the leading edge of the stimulus

When the very first stimulus is presented to the model (Figure 2.2D), activity first propagates from the barrels associated with deflected whiskers to layer 2/3, exciting each neuron in the isomorphic supra-barrels randomly (Figure 2.2E, t=0.1). L2/3 neurons then begin to interact laterally ($t > 0.1$), each becoming more active if it is similar to its immediate neighbors and dissimilar to more distant neighbors, and less active otherwise. This process continues as the network settles, and as larger groups of activity merge they migrate toward regions of least net inhibition. Hence, bubbles of activity form at the high-contrast edges of the supra-barrels that correspond to whiskers located furthest forward in the direction of the stimulus. By furthest forward we mean those inside the linear boundary that are closest to it, and hence those whiskers that would have been deflected most recently by contact with the stimulus. If the direction in which the whiskers are deflected is consistent with the orientation of the stimulus, then neurons in these regions of the supra-barrels will learn to become associated with the L4 neurons that encode the somatotopically consistent direction of whisker deflection.

As an example, a stimulus boundary moving upwards would be oriented so as to bisect the

whisker field through one of the whisker rows. It would deflect all whiskers located within and below that row in an upwards direction, and would preferentially activate L4 units representing upwards deflections. Activity in L2/3 would migrate to the top portion of the supra-barrels in the same row, and these neurons would learn stronger weighted connections to the active L4 units representing upwards deflections.

Repeated for stimuli whose leading edges bisect all points in the whisker field, at all orientations, this process will bias the network to arrange direction preferences somatotopically in each supra-barrel.

2.3.2 A somatotopic pinwheel emerges in each supra-barrel

For each value of κ = 0, 1, 2, 3, 4, 5, and ∞, 20 networks with different random initial weights were trained on different sets of 5,000 random input patterns; a total of 140 simulations were run. As a reminder, larger values of κ increase the concentration of the individual whisker deflection directions towards the movement direction of the stimulus (θ). Once the process of self-organization was complete, direction map plots were measured by deflecting each whisker through 16 directions, and then coloring each L2/3 neuron by the deflection direction that evoked the largest response. Lateral interactions and learning were turned off during this process. We note that once some learning has taken place, direction maps based on the feed-forward response are almost indistinguishable from those based on the activity after settling. We report maps based on the feed-forward response as it can be calculated more quickly for the large numbers of simulations used, and so as not to reveal an arbitrary mapping in networks that have received no previous input. An example map measured from one network trained on

$\kappa = 3$ inputs is shown in Figure 2.3A.

For the 20 networks run at each value of κ, we constructed plots of the mean preferred deflection direction at each cortical location. For $0 < \kappa < \infty$, these plots revealed a somatotopically consistent pinwheel spanning each supra-barrel; Figure 2.3B shows such a plot for the $\kappa = 3$ maps. Each is a qualitative match to that measured by Andermann and Moore (2006) in L2/3 barrel cortex. Notice that the center of the pinwheel is shifted in each supra-barrel away from the center of the cortical sheet. This reflects an implicit bias for deflections of the PW to occur more often towards the center of the whisker field, because the origin of the stimulus was confined to fall in a space not much larger than that occupied by the whiskers. Recent evidence in rat barrel cortex, based on differences in the distribution of directional preferences amongst barrels at different locations, appears to support this 'super-pinwheel' organisation predicted by the model (personal communication with Prof. Daniel Shulz, November, 2011). A super-pinwheel organisation may have important consequences for perception. By dedicating cortical territory to the representation of peripheral whisker deflections inward towards the whiskerpad centre, the super-pinwheel could increase the resolution with which inward deflection directions can be discriminated. For neurons of peripheral barrels, an enhanced resolution for these more common first-order motion directions could compensate for a reduction in the availability of second-order motion cues about the stimulus motion direction, i.e., an absence of adjacent-whisker deflections for stimuli moving inward towards peripheral whiskers.

Similar plots for the control $\kappa = 0$ reveal no global alignment (see Figure 2.6A), suggesting that a somatotopic relationship between the deflection direction and the combination of deflected whiskers is required to organize directional preferences somatotopically. Suprisingly, when the correlation is perfect ($\kappa = \infty$), map organization does not become consistent with the

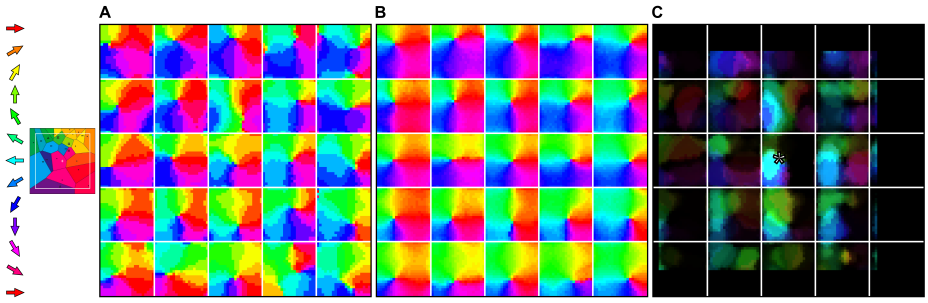

Figure 2.3. A somatotopically aligned map of whisker deflection direction emerges in each supra-barrel. **A** Example map from one network trained on 5,000 input patterns in which whisker deflection directions are each concentrated towards the orientation of the stimulus ($\kappa = 3$). Maps in each supra-barrel are a match to that measured by Andermann and Moore (2006) in which neurons on the left of each supra-barrel, for example, prefer leftward deflections of the PW. Supra-barrels are delineated by white lines. **B** Mean direction preference for neurons at each cortical location, over the 20 networks in the same data set, showing that the organization is consistent across runs. **C** Plot of the long range lateral connection strengths, from the representative example neuron at the position marked by *, to the rest of the cortical map. Pixel brightness indicates lateral weight strength, and the color indicates the preferred deflection direction of each connected neuron. This neuron becomes most strongly connected to others, some located many supra-barrels away, that are tuned to similar directions of PW deflection.

somatotopic ideal. Inspection of the individual maps suggests that $\kappa = \infty$ networks instead tend to maximize continuity of directional preferences across the entire sheet, without respecting the boundaries between supra-barrels (see below and Figure 2.6D).

2.3.3 Connections between similar directions and different whiskers

Because the Hebbian rule strengthens connections between correlated neurons, we might expect the final patterns of long-range lateral connections to reflect the fact that even distal whiskers are deflected in similar directions. Such an effect is clear in an example L2/3 map in which pixel brightness is scaled by the strength of the weights to one neuron from the rest of the sheet (Figure 2.3C). The example neuron prefers leftward ($180°$) deflections of the central whisker and becomes connected most strongly to neurons in L2/3 that also prefer leftward deflections of their PWs. Overall, we found a significant correlation between the strength of the lateral inhibitory weight between each pair of L2/3 neurons and the absolute difference between their preferred deflection directions (mean Pearson's $r = -0.531$, range -0.518 to -0.550, across 20 networks each trained on 5,000 κ = 3 inputs). Hence, the model predicts connectivity in L2/3 between patches of directionally consistent neurons with different PWs. Notice also that connection strength is greatest between neighboring neurons within the barrel, and falls off with the distance to the pre-synaptic cell (see Kerr et al., 2007).

These findings are consistent with those from experiments showing the strongest lateral interactions when whiskers are sequentially deflected in similar directions (Kida et al., 2005; Simons, 1985). Similarly, in tree shrew V1, long-ranging connections have been found to connect neurons that respond to similar orientations of visual stimulus (Bosking et al., 1997). The feature-

specific patchy connectivity that arises during map self-organisation has direct implications for perception. For example, connections linking domains of similar orientation preference in primate V1 can bind activity along the collinear edges that typically trace object contours, or separate a novel edge orientation from a background of mutually inhibiting collinear edges (depending on the sign and range of interactions) (Bednar, 2012). An analogous 'pop-out' effect between whisker deflection directions could attribute salience to the whisker field location of individual deflections reporting e.g., a crack through which to escape from a wall evoking otherwise collinear deflection directions. It is important that although we simulate the long-range interactions as inhibitory connections in the model, long range inhibition represents the net effect of responses to strong inputs that we assume drive self-organisation in real developing cortex. The patchy connections that result from self-organisation may therefore subserve more complex functionality including facilitatory effects in adult cortex when processing weaker incoming stimuli. This point we be revisited in the *Discussion*.

2.3.4 Input correlation improves pinwheel alignment but not quality

To quantify our observations, we analyzed the direction maps per supra-barrel with reference to an ideal somatotopic pinwheel template, defined for each neuron as the angle of its location from the center of each supra-barrel. More formally, each L2/3 neuron was assigned a coordinate ($x, y \in [-10, 10]$) with respect to the supra-barrel center, and its preferred deflection direction according to the template was defined using the quadrant-specific arctangent function $\mathbf{atan2}(y, x)$. The template value at the origin is undefined so the neuron at each supra-barrel center was discounted from further analyses.

An angular-angular correlation between the measured map and the template gives a score of the correspondence between the two that is rotation independent, and the absolute value of this quantity is also independent of clockwise and counter-clockwise orientation around the supra-barrel center. We can therefore define *pinwheelness* as the magnitude of the angular-angular correlation coefficient. For the 500 supra-barrel maps (20 networks times 25 supra-barrels) at each value of κ = 0, 1, 2, 3, 4, 5, and ∞, we first counted those with counter-clockwise or clockwise orientation with a correlation coefficient greater than that measured in barrel cortex ($r = 0.226$; Andermann and Moore, 2006). We classified supra-barrel maps wherein $r > 0.226$ as rotating counter-clockwise about the supra-barrel center and therefore somatotopically correct, those where $r < -0.226$ as clockwise and thus somatotopically inverted, and where $-0.226 < r < 0.226$ as non-pinwheels (see Figure 2.4A). At $\kappa = 0$, 90% of 500 supra-barrels developed pinwheels, but these were equally likely to be oriented clockwise or counter-clockwise. For $\kappa > 0$, the number of pinwheels that rotate counter-clockwise around the supra-barrel increases to a peak of 76% at $\kappa = 3$. However, when inputs had a perfect alignment between whisker deflection direction and the orientation of the edge of the stimulus ($\kappa = \infty$), the number of well-defined pinwheels dropped to just 30%.

These trends are reflected in a plot of absolute pinwheelness (Figure 2.4B), which is notable because it shows maximal pinwheelness when $\kappa = 0$. Hence, even without a consistent somatotopic relationship between the whiskers, the supra-barrels still discover the circular topology of the space of possible deflection directions, communicated by the coactivation of L4 cells with similar MEDs.

The overall trend is for pinwheelness to decrease as κ is increased. Thus an increase in somatotopic information in the inputs does not create pinwheels, but only aligns them somatotopically.

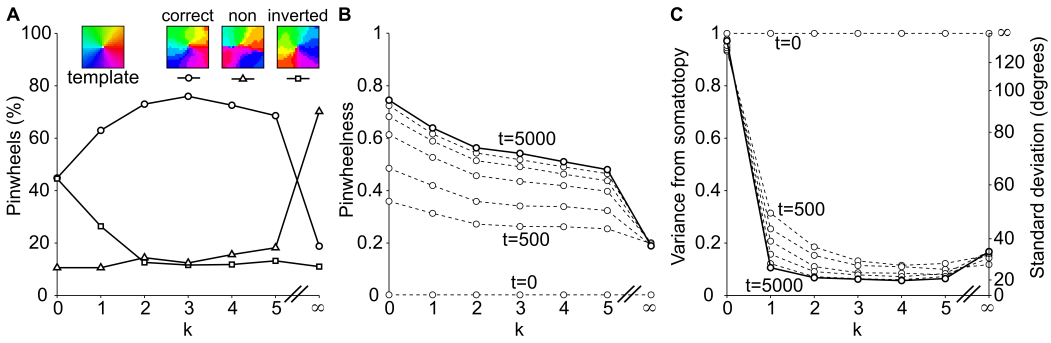

Figure 2.4. Analysis of pinwheel quality and somatotopic alignment per supra-barrel in 20 model networks. A At t = 5,000, direction maps in each supra-barrel were compared to the template pinwheel (inset) and classed as somatotopically correct pinwheels (the example map has a 'pinwheelness' score of 0.9), somatotopically inverted pinwheels (example score -0.9) or not pinwheels (score 0.2), as described in Results. When there is no correlation between the direction in which each whisker is stimulated during training ($\kappa = 0$), pinwheel maps emerge in each supra-barrel, but they are equally likely to rotate clockwise or counter-clockwise. When such a correlation is present in the inputs ($\kappa > 0$), the number of supra-barrels containing pinwheels that rotate in a somatotopically consistent way increases to a maximum of 76%. Surprisingly, perfectly correlated inputs ($\kappa = \infty$) degrade pinwheel quality. **B** This behavior is reflected in a plot of absolute 'pinwheelness' scores, in which all but the scores for $\kappa = \infty$ progress over training iterations (t=0, 500, 1,000, 2,000, 3,000, 4,000 in progressive dashed lines) toward good scores at t = 5,000 (solid line). Scores are highest for $\kappa = 0$, suggesting that networks trade a bias to maximize pinwheelness for one towards somatotopic alignment as κ is increased. **C** shows that pinwheels rotating in the correct direction become aligned to the somatotopic template, with a final circular standard deviation $< 20^\circ$ for $1 < \kappa < \infty$.

This is confirmed in a plot of the circular standard deviation between the counter-clockwise supra-barrel maps and the template (Figure 2.4C), which shows a distribution all the way around the circle for $\kappa = 0$ (std $\approx \infty^{\circ}$) which decreases to $\approx 20^{\circ}$ when whisker deflection direction and location are well correlated during training ($1 > \kappa > \infty$).

As well as associating the leading edge effect with whisker deflection directions necessary to align pinwheels somatotopically, increasing k introduces a corollary association between the afferent units of adjacent barrels that have similar directional tuning. When $k = \infty$, the activity of a given afferent unit becomes more strongly correlated with that of a neighbour-barrel unit of identical direction tuning, compared with a same-barrel unit of slightly different direction tuning. Mappings that emerge during self-organisation promote continuity in their representation of the input feature space, which in the $k = \infty$ condition is distorted by this stronger correlation between L4 barrels rather than within them. This is manifest in an example plot of $k = \infty$ map organisation, which is shown in later Figure 2.6D to accompany those produced under various other experimental distortions of the input space.

2.3.5 Biased whisker inputs create anisotropic maps.

Next we tested how a statistical bias in the distribution of θ might affect map organization (see Figure 2.5). This is important to consider because biases in the representation of certain deflection directions have been found in the barrel cortex of the adult rat (see Discussion). To this end we ran networks for 5,000 input patterns, this time drawing θ from a circular normal distribution with mean 180°. Here the concentration parameter of the distribution serves to control input pattern anisotropy, where zero anisotropy means that θ is drawn uniformly from

around the circle. In addition, we ran 20 different networks each per input anisotropy value 1, 2, 3, 4, 5 and ∞ ($\kappa = 3$). Hence, for networks in subsequent conditions, the movement of the half-plane stimulus was more likely to be around 180°.

To quantify the effects of the bias (Figure 2.5A), we summed the vectors corresponding to the preferred direction of each neuron trained under a given bias. The averaged length of this resultant vector gives a score of how concentrated the direction preferences are towards one direction, and hence provides a score of map anisotropy. A map anisotropy score of zero indicates that maps represent directions isotropically, whereas a maximum score of 1.0 indicates that the map is comprised of neurons that all prefer the same direction.

We found that as the bias for $\theta = 180^\circ$ input patterns increased, so did the proportion of neurons whose preferred direction became aligned towards 180° (mean preferred directions ranged $179^\circ - 180^\circ$ for maps trained with a bias). The trend converges to a map anisotropy score of 0.69 out of 1.0 when θ is always 180°, which is less than 1.0 owing to the broad and fixed direction tuning of the L4 input units and the $\kappa = 3$ noise applied to the individual whisker deflection directions.

For input anisotropies up to 4, the biased maps themselves still organize to represent a range of directions around 180° continuously, in a distorted pinwheel local to each supra-barrel (Figure 2.5B). Above 4, some patches opposite the biased orientation remain un-selective throughout training, because very few $\theta \approx 180^\circ$ input patterns will create a leading edge effect to drive bubbles of activity to the opposite edge of the supra-barrels (Figure 2.5C).

Thus the model predicts that strong biases in the distribution of experienced deflection directions

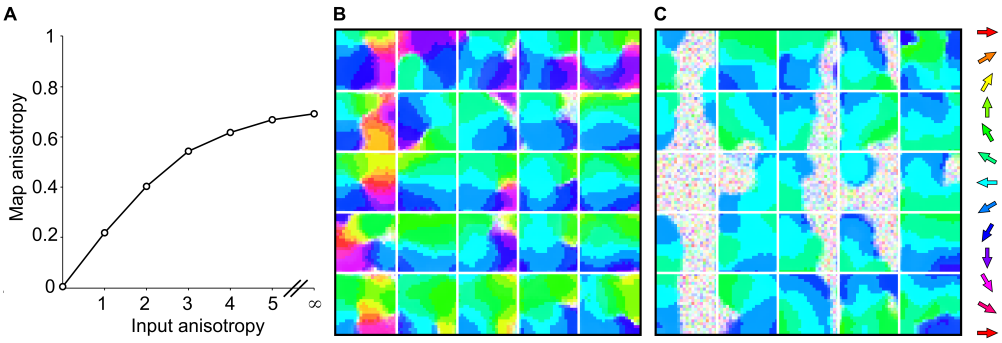

Figure 2.5. Anisotropic inputs create anisotropic maps. Values of θ were drawn from circular normal distributions with varying degrees of concentration (input anisotropy), towards a mean of $180°$. Results suggest that biased experience to a particular direction of stimulus will cause an over representation of that direction in the supra-barrels. Map anisotropy scores converge to 0.69 (out of a maximum of 1.0) when the networks are trained in a regime where half-plane stimuli always move in the same direction. **B** shows an example map from a network trained on input anisotropy 3.0, where pixel saturation indicates a lower direction selectivity for each neuron. Distorted pinwheel structures still form in many barrels, but the map is clearly dominated by neurons preferring $\approx 180°$ deflection directions. **C** shows a similar map from a network trained on input anisotropy ∞, wherein patches of non-selective neurons form on the right side of the left most supra-barrels where the leading edge of the stimulus is least likely to occur.

will be reflected in the direction maps, both as expanded regions for over represented directions, and as patches of less selective neurons in the somatotopically correct locations for under-represented directions.

2.3.6 Maps do not organize somatotopically without a correlation between whisker combination and deflection direction

We have already examined the results of the first control condition, the case where $\kappa = 0$, in which we see good pinwheel maps form in each barrel but no consistent global alignment (example in Figure 2.6A). The networks were then trained in two additional control conditions (both at $\kappa = 3$).

In the second control (Figure 2.6B), the location (but not the number) of the activated whiskers was randomly permuted for each input pattern. For example, the stimulus shown in Figure 2.2D would be reconstructed so that a random subset of ten whiskers were deflected. The activated whiskers were distributed randomly over the twenty-five possible locations on the whiskerpad and were therefore not confined to any particular region of it. Hence the global information about somatotopy was removed from each input pattern, but the level of afferent activation and the consistency between the directions in which the whiskers were deflected remained. Maps organized in this condition developed reasonably strong pinwheels, but again had no global alignment (standard deviation from the template $\approx \infty^{\circ}$). Instead, they organize more locally to be similar to primate V1 maps for orientation or direction, becoming composed of continuous regions that are punctuated by pinwheel, linear and saddle-point discontinuities (see Miikkulainen et al., 2005), largely ignoring the barrel boundaries.

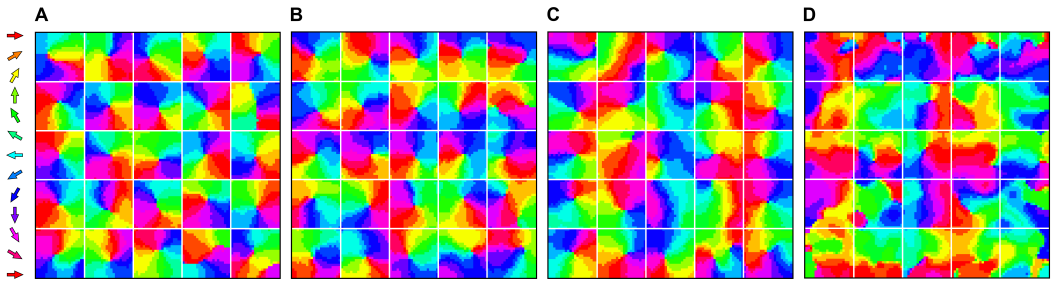

Figure 2.6. Model maps organized in control experiments and at $\kappa = \infty$. A Whisker deflection directions are independent of one another. Example direction map from a representative $\kappa = 0$ network, which develops good pinwheels in each supra-barrel but no consistent global organization. **B** Removing global correlations. Example map measured from a network trained on 5,000 inputs wherein the location of the stimulated whiskers was randomly shuffled on each iteration ($\kappa = 3$). **C** Direction map measured from one representative network trained on 5,000 inputs wherein the whiskers are deflected in the same combinations as in the normal case, but the mean direction in which they are deflected bears no relation to the stimulus direction implied by this combination ($\kappa = 3$). In both controls, maps resemble V1 orientation or direction maps rather than rodent S1 maps, because they cover all directions continuously on the local scale but have no consistent global alignment. **D** When whisker deflection directions are perfectly correlated with the whisker combination ($\kappa = \infty$), the supra-barrel borders no longer affect the input correlations, and so the map groups similar directions together rather than developing independent pinwheels.

In the third control (Figure 2.6C), the stimulus deflected whiskers in the same combinations as in the main simulation, and for each stimulus whiskers were deflected in similar directions ($\kappa = 3$). However, the mean of the distribution from which each deflection direction was drawn was random and independent of the orientation of the stimulus. Hence whisker deflection directions were again correlated with one another but unrelated to the global direction implied by the combination of activated whiskers. Again, direction maps that emerge in this control condition are more similar to primate V1 maps than rodent S1 maps because they have no overall somatotopic organization.

These results confirm that only when the overall pattern of deflected whiskers correlates with the direction in which each whisker is deflected, do somatotopic direction maps self-organize consistently within each supra-barrel.

2.3.7 Experimental manipulations

Computational models, like other theoretical formulations, should make specific predictions that can be tested through experimentation. Two such predictions, arising from the current work, are illustrated in Figure 2.7.

For the first prediction, we simulated a whisker-trimming experiment by depriving whisker input to a chessboard configuration of the barrels (Wallace and Fox, 1999; see Figure 2.7A). Although no prediction can be formulated about the organization of maps in deprived supra-barrels, somatotopically aligned maps emerge in the spared supra-barrels. Thus the model predicts that isolated whisker trimming even early in development will not have a significant

effect on the development of pinwheels in the supra-barrels for the remaining whiskers. Only when enough whiskers have been trimmed to isolate a supra-barrel from those that interact laterally with it, will somatotopic alignment be disrupted.

The second prediction is that if a central whisker is consistently deflected opposite the direction of its neighbors, the organization of direction preferences in the corresponding supra-barrel will be a pinwheel that is somatotopically inverted (see Figure 2.7B). In other words, deflections of whisker A towards whisker B will evoke the strongest responses in supra-barrel A neurons located furthest from supra-barrel B. With the advent of apparatus capable of independently stimulating up to twenty-five whiskers (Krupa et al., 2001a; Jacob et al., 2008; Drew and Feldman, 2007), the anti-correlated pinwheel experiment could now be undertaken with very precise control.

2.4 Discussion

We have demonstrated how a computational model of L2/3 barrel cortex can develop a map of whisker deflection direction that is a strong qualitative match to that measured in the rat barrel cortex by Andermann and Moore (2006). The main finding is that pinwheel maps of whisker deflection direction align somatotopically in each simulated supra-barrel. Thus the somatotopic pinwheel map should emerge across all supra-barrels provided that (i) net L2/3 interactions concentrate activity into bubbles smaller than a supra-barrel, (ii) these bubbles migrate to areas corresponding to the leading edge of a tactile stimulus, (iii) whiskers are consistently deflected away from stimuli.

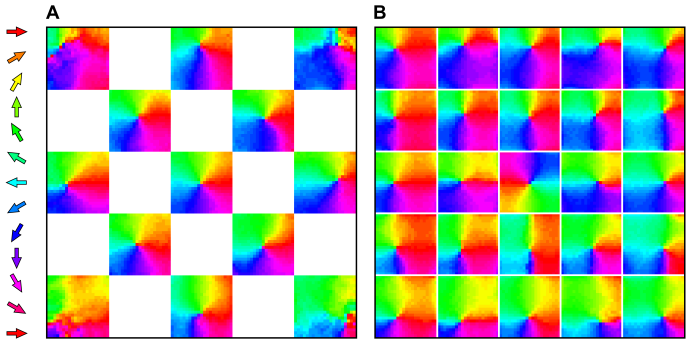

Figure 2.7. Predicting mappings for experimentally manipulated whisker inputs. A Whisker trimming experiment. Whiskers in a chessboard configuration of the model barrels were deprived of whisker input. The plot shows the mean directional preference over 20 networks. Neurons in deprived supra-barrels have no opportunity to learn connections to particular L4 neurons. However, spared supra-barrels are still able to form reasonable somatotopic pinwheel maps. Thus the model does not predict any specific reorganization of spared portions of the map for the isolated whisker trimming case. **B** Anti-correlated whisker experiment. If a central whisker is consistently deflected in the direction opposite its neighbors, neurons in the central barrel should develop RFs for deflection directions opposite those suggested by their somatotopic location, forming a somatotopically inverted pinwheel in the corresponding supra-barrel. The mean preferred direction for neurons at each location is plotted (N=20 different networks). This prediction could be tested by training rats on artificial stimuli in which the central whisker is deflected, for example, rostrally (0°) whenever the more caudal whiskers are primarily deflected, during the critical period. Although difficult to perform, this experimental paradigm would be very useful for assessing the time course of map plasticity.

The two key assumptions of the model, which need to be validated with further experimental work, are as follows. First, the model assumes that whisker contacts experienced by young rats correlate whisker combination with whisker deflection direction. Second, it assumes that the lateral extent of net excitatory interactions is less than that of net inhibitory interactions in barrel cortex, regardless of the detailed circuitry that implements these interactions. The two key predictions of the model, for normally developed barrel cortex, are as follows. First, supra-barrels for all of the large whiskers will contain a somatotopically aligned pinwheel map of PW direction, although pinwheel centers may be shifted for more peripheral whiskers. Note that only the direction map for a central supra-barrel has been established to date (Andermann and Moore, 2006, although analyses made by combining across several barrel maps have been presented; Kremer et al., 2011). Second, L2/3 neurons with similar directional tunings will be synaptically coupled, certainly with neighbors in the supra-barrel, and perhaps with those located several supra-barrels away. These predictions and the two key assumptions are testable immediately, and should not require experimental manipulation of the patterns of input to the whiskers.

In the present study, the efficacy of all whisker deflections was chosen to be equal: a whisker is either deflected or it is not. However, we could have chosen to associate different strengths to each whisker deflection, e.g. by defining a gradient of deflection strengths that decreases along the path of the stimulus. Networks trained in this way develop the same map organization as those reported (data not shown), because they essentially repeat the leading edge effect at multiple locations for each training pattern.

We chose LISSOM to model feature map development in the barrel cortex because it emphasizes lateral cortical interactions, because it produces realistic primate V1 feature maps (Mi-

ikkulainen et al., 2005), and because many comparisons have been drawn between whisker S1 and primate V1 at the level of the cortical map (Fox and Wong, 2005; Moore et al., 1999). We expect that other models (e.g. self-organizing maps or correlation-based–learning approaches) would yield similar overall map organization, if they implement similar lateral interactions. However, with the exception of the LISSOM-like model of Burger and Lang (2001), alternative models do not simulate explicit, modifiable lateral weights, and so could not reveal an emergent connectivity between directional representations that span many supra-barrels (as in Figure 2.3C).

It is important to emphasise that LISSOM does not require any assumption that long-range inhibitory interactions are implemented via long-range inhibitory connections in the cortex. The long-range inhibitory interactions measured in the barrel cortex by Derdikman et al. (2003) are presumably implemented by long-range excitation of local inhibitory neurons (Helmstaedter et al., 2009), as is thought to be the case in V1 for high contrast visual inputs (see Ren et al., 2007; Weliky et al., 1995; Martin, 2002; Somers et al., 1998; Ren et al., 2007; Silberberg and Markram, 2007, and see also Moore et al., 1999). There is now growing evidence for pervasive disynaptic inhibition in barrel cortex, at least in L4 to L2/3 circuit pathways (Swadlow, 2002; Sun et al., 2006; Higley and Contreras, 2007; Kapfer et al., 2007). Whether long-range inhibition is monosynaptic or disynaptic is not important for the modeling results, only that it be net inhibitory at long distances for strong deflections.

Given the robust emergence of pinwheel maps in the model, it is intriguing that although a recent two-photon calcium imaging study from Kerr et al. (2007) measured similar levels of directional tuning to Andermann and Moore (2006), they found no evidence for a systematic map of deflection direction in L2/3. A number of methodological differences might account

for these findings, such as anesthetics with different effects on intracortical inhibition (Kyriazi et al., 1996), or weaker stimulation velocity, as suggested by Ritt et al. (2008). The differences might be reconciled by recent two-photon calcium imaging data (Leger J-F., Kremer Y. & Bourdieu L., 2009, Society for Neuroscience abstract 174.13) which report a somatotopic pinwheel organisation in three-month old rats (the approximate age of the rats of Andermann and Moore, 2006) but no correlation between the location of the neuron and its directional tuning in three-week old rats (the data of Kerr et al., 2007 were obtained between postnatal days 25 and 35).

It also remains to be seen why an organisation for directional tuning accounts for just a portion of the variability of supragranular neuronal responses to deflection of the whiskers ($r^2 = 0.226^2 = 5\%$, Andermann and Moore, 2006). Input to the model neurons communicates only information about whisker direction, and so produces a very smooth mapping for direction in all of our simulations. However, we should assume that cortical neurons compete to represent many features of single– and multi– whisker stimuli, and so expect maps for direction to be degraded by the extent to which these additional features are described by thalamocortical input. To illustrate, consider the primary visual cortex of higher mammals, wherein each neuron participates in topographic mappings for eye preference and disparity, as well as for stimulus location, orientation, motion direction, spatial frequency, and colour. Deflection direction may not even be the best-represented feature after whisker identity, as suggested by a decrease in the information about direction carried by spikes recorded from neurons higher along the neuraxis (Bale and Petersen, 2009). The question of what additional, presumably higher-order, features are coded for by the activity of barrel cortex neurons remains an exciting and very open one.

There are numerous other phenomena in the whisker/barrel system that might yet be explained

by Hebbian learning of whisker experience. In the paralemniscal brainstem nuclei, it has been suggested that the overrepresentation of dorsal deflections (Furuta et al., 2006) may be due to the greater preponderance of dorsal deflections during rat locomotion and exploratory behavior (e.g., Grant et al., 2009) biasing cell receptive field properties via Hebbian learning. In the thalamus, competitive interactions between nuclei (Lavallée and Deschênes, 2004; Hartings et al., 2000; Brumberg et al., 1996; Brecht and Sakmann, 2002) might shape the direction map measured across the vertical extent of thalamic 'barreloids' (Temereanca and Simons, 2004; Timofeeva et al., 2003), and feedback to thalamic direction maps from those in infragranular cortical layers might also play a role (Li and Ebner, 2007). For infragranular neurons, a correlation has been reported between selectivity for motion directions administered in waves across many whiskers, and for responses to particular adjacent whiskers (Jacob et al., 2008). This data suggests the presence of a map for wave direction that is distinct from the single-whisker direction map, and might develop in a model extended to include a representation of layer 5 (see also Ghazanfar and Nicolelis, 1999; Sato et al., 2007; Drew and Feldman, 2007). Such maps could be used by the animal to discriminate stimulus features such as orientation (Polley et al., 2005).

In the adult cortex, a number of studies have reported that activity propagates preferentially along the barrel rows compared with the arcs (Petersen et al., 2003; Wirth and Lüscher, 2004; Derdikman et al., 2003), that a row bias exists also in axon distributions across layer 2/3 (Ajima and Tanaka, 2006), and that rostral and caudal deflection directions are overrepresented (Bruno et al., 2003; Andermann and Moore, 2006). These biases may reflect tendencies of adult rats to encounter objects head-on and to actively palpate the whiskers forwards and backwards, but it is difficult to determine the precise patterns of whisker deflections in live animals to use as inputs to the model. We are now beginning experiments with a mobile whiskered robot to determine what patterns of whisker deflection are common in such encounters (Fox et al., 2009), but can

predict from the results of Figure 2.5A that these would lead the model to expand representations of more common deflection directions in the map. At the time of writing we have also begun a series of experiments using robot-controlled collisions with an array of artificial whiskers to investigate the extent to which stimuli of different shapes correlate the relative position of the whisker with its deflection direction (see chapter 4 and Wilson S.P., Mitchinson B., Pearson M., Bednar J.A., Prescott T.J, 2009, Society for Neuroscience abstract 174.4).

Each of the phenomena discussed above likely involves interactions at the neural population level between multiple whisker pathways. Hence each are suitable for investigation with network models like ours, the first to explore interactions between whiskers in detail. To progress towards a complete systems-level model of multiwhisker processing, the ideas developed here can be integrated with existing models of detailed temporal processing of single-whisker events. Relevant models are available for the rat whisker (Birdwell et al., 2007), the follicle and ganglion (Mitchinson et al., 2004, 2008), the thalamus (Golomb et al., 2006) and the barrel cortex (Puccini et al., 2006; Kyriazi and Simons, 1993; Kyriazi et al., 1996; Pinto et al., 1996; Sarid et al., 2007).

Of the existing computational models, the only one to focus on S1 direction tuning is from Puccini et al. (2006). They presented whisker-direction inputs to an integrate-and-fire neuron as differences in the latency and strength of their excitatory and inhibitory components: excitation arrives faster, and both are stronger, for whisker deflections more similar to the MED (Wilent and Contreras, 2005). If this feed-forward model were to learn and evaluate inputs from adjacent-whisker cells, the relative contributions of feed-forward versus recurrent inhibition to constructing directional RFs could be detailed (see Swadlow, 2002; Swadlow and Gusev, 2002). In a network of such neurons we might hope to predict how the spatial organization of direc-

tion within a supra-barrel interacts with that for alternative features, e.g. stimulus frequency (Neimark et al., 2003).

The validity of our model could be tested using the anti-correlated whisker manipulation suggested in Figure 2.7B. If robust changes are found to the directional RFs of L2/3 neurons, without producing an anti-correlated pinwheel, then our description of either the sensory input, or of the resulting cortical interactions, is inaccurate. On the other hand, finding an anti-correlated direction map under these conditions would be very strong evidence for input-driven self-organization as a mechanism for establishing RFs in the barrel cortex. Previous studies detailing the plasticity of cortical feature maps have shown how cortical organization can be disrupted or exaggerated by altered sensory stimuli (for example see Feldman and Brecht, 2005), but if our anti-correlated pinwheel prediction is confirmed we could use it to ask, on what timescale could a very specific map organization be entrained: seconds, hours or days? Answering this question could help clarify the ongoing relationship between the sensory environment and the organization of cortical sensory areas.

Chapter 3

A place code for inter-whisker timing in the barrel cortex?

Chapter summary

The place theory proposed by Jeffress (1948) is still the dominant model of how the brain represents the movement of sensory stimuli between sensory receptors. According to the place theory, delays in signalling between neurons, dependent on the distances between them, compensate for time differences in the stimulation of sensory receptors. Hence the location of neurons, activated by the coincident arrival of multiple signals, reports the stimulus movement velocity. Despite its generality, most evidence for the place theory has been provided by studies of the auditory system of auditory specialists like the barn owl, but in the study of mammalian auditory systems the evidence is inconclusive. We ask to what extent the somatosensory systems of tactile specialists like rats and mice use distance dependent delays between neurons to compute the motion of tactile stimuli between the facial whiskers (or 'vibrissae').

We present a model in which synaptic inputs evoked by whisker deflections arrive at neurons in layer 2/3 (L2/3) somatosensory 'barrel' cortex at different times. The timing of synaptic inputs to each neuron depends on its location relative to sources of input in

layer 4 (L4) that represent stimulation of each whisker. Constrained by the geometry and timing of projections from L4 to L2/3, the model can account for a range of experimentally measured responses to two-whisker stimuli. Consistent with that data, responses of model neurons located between the barrels to paired stimulation of two whiskers are greater than the sum of the responses to either whisker input alone. The model predicts that for neurons located closer to either barrel these supralinear responses are tuned for longer inter-whisker stimulation intervals, yielding a topographic map for the inter-whisker deflection interval across the surface of L2/3. This map constitutes a neural place code for the relative timing of sensory stimuli.

3.1 Introduction

A fundamental question in computational neuroscience asks how the brain represents the relative timing of stimuli as they move between sensory receptors, e.g. as a light source moves relative to the retina, or as contact moves between touch sensors on the fingertip. For over 60 years Jeffress' place theory (Jeffress, 1948) has remained the dominant model. The idea is that coincidence detector neurons receive input from sensors after delays governed by the distance of the neuron from either sensor. The inter-sensor time difference is encoded by the location of neurons that are active because their connection delays exactly compensate the inter-sensor stimulation interval (see Figure 3.1); similar to an idea originating from vision research, each neuron essentially serves as a Reichardt motion detector (Reichardt, 1961). The place theory therefore suggests an important role for neural geometry in computing the motion of sensory stimuli.

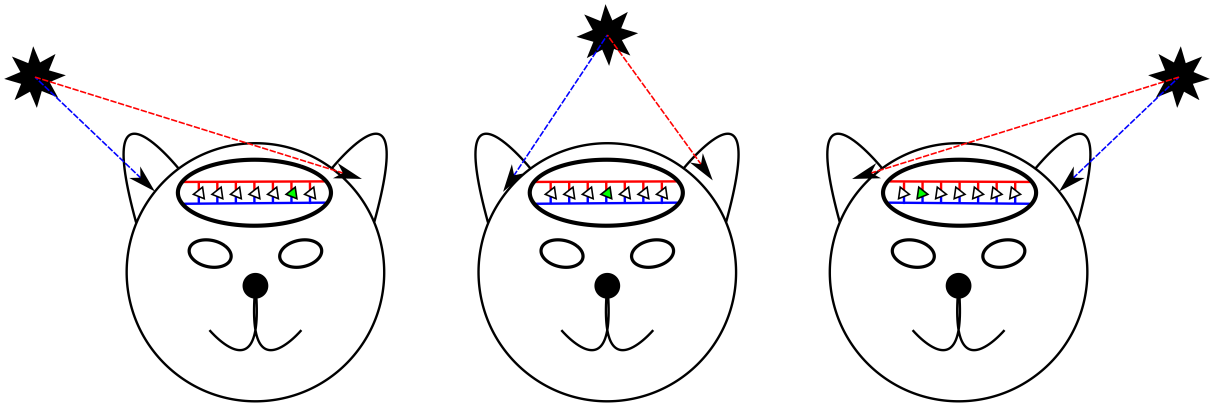

Figure 3.1. Cartoon of the Jeffress model for sound source localisation. According to the model, the distance travelled by sound waves from a source (black asterisk) to either ear (dashed lines) is compensated by internal delays that increase with the distances of neurons (white triangles) from either ear. When differences in internal signalling delays are exactly compensated by differences in inter-ear timing the incoming signals are coincident and thus sources at specific locations activate neurons at specific locations (green).

Strong support for Jeffress' place theory has been provided by a number of studies of midbrain neurons in auditory specialists like the barn owl, who locate sound sources by resolving small differences in the arrival time of sounds at either ear (see Yoris and Yin, 2006 for a review). Evidence from the mammalian auditory system is less conclusive because, for example, rabbit auditory cortex neurons are tuned to inter-ear time differences that are too long to attribute to inter-neuron distances alone (Fitzpatrick et al., 2000; see also Grothe, 2003; McAlpine and Grothe, 2003, and Seriès et al., 2002 for an alternative mechanism based on slow lateral connections). However few studies have investigated how inter-sensor time-differences might be resolved in specialist mammalian sensory systems.

Tactile specialists like rats, mice, shrews, and seals determine the form and motion of tactile stimuli using prominent arrays of whiskers (vibrissae) on the face (Welker, 1964; Mitchinson et al., 2011). For example, shrews hunting in the dark can use their whiskers to localise particular body-part shapes on fast-moving prey animals (Anjum et al., 2006). Specific to the whisker system is a precise topographic correspondence between the individual sensor and its neural representation. Deflection of adjacent whiskers A and B on the face evokes the largest amplitude and shortest latency responses in adjacent cortical columns A and B in the somatosensory (barrel) cortex. This precise mapping, as well as observations of sub-millisecond temporal precision throughout (Barth, 2003; Benison et al., 2006; Petersen et al., 2009), makes the whisker-barrel system ideal for exploring the impact of neural geometry on neural computation.

A consistent finding across studies in the rat and mouse somatosensory cortex is that responses vary with the time interval between adjacent whisker stimulation (Simons, 1983, 1985; Simons and Carvell, 1989; Ghazanfar and Nicolelis, 1999; Shimegi et al., 1999, 2000; Mirabella et al., 2001; Civillico and Contreras, 2006; Higley and Contreras, 2003, 2005; Kida et al., 2005; Drew

and Feldman, 2007). A useful metric for comparing the response to a two-whisker stimulus to the response to the individual whisker deflection is the facilitation index (Shimegi et al., 1999), defined as 'the response to paired deflection of whiskers A and B divided by the sum of the response to deflection of whisker A deflected alone and the response to whisker B deflected alone' or $\mathrm{FI} = r_{\mathrm{AB}}/(r_A{+}r_B)$. In layer 2/3 barrel cortex (L2/3) in particular, paired stimuli in which the adjacent whisker deflection precedes by 20-$50\,\mathrm{ms}$ typically evoke sublinear responses ($\mathrm{FI} < 1$). For a range of near-simultaneous deflections, a number of studies have also reported supralinear responses ($\mathrm{FI} > 1$), again particularly in L2/3 neurons (Ghazanfar and Nicolelis, 1999; Shimegi et al., 1999, 2000; Higley and Contreras, 2005; Kida et al., 2005; but see Ego-Stengel et al., 2005). Interestingly Shimegi et al. (2000) reported that septa-related neurons in L2/3, located at the midline area between two barrels, were more likely to show response facilitation for short-interval stimuli, whereas barrel-related neurons were more likely to show response suppression by prior deflection of the distal whisker at longer intervals (see Figure 3.2). Plots of the relationship between the inter-whisker-interval and the response magnitude for individual neurons showed evidence of tuning to particular short intervals. Together these results suggest that the location of the L2/3 neuron relative to the underlying barrel geometry is important in determining its response to a two-whisker stimulus.

One explanation for the different responses of barrel-related and septa-related neurons, as summarised in Table 1, is that they reflect the operation of different mechanisms for integrating adjacent-whisker signals in distinct barrel and septal circuits (see Brumberg et al., 1999; Alloway, 2008; Chakrabarti and Alloway, 2009). However an alternative hypothesis, inspired by the place theory, is that the differences reflect an underlying continuum of responses, which are determined by the location of the neuron with respect to the two cortical columns. This hypothesis would allow for, although it would not require, an essentially homogeneous population in

Table 3.1. Summary of the trends of facilitation index scores (FI), as a function of the relative stimulus timing and neuron location. t_A and d_A are the deflection time of whisker A and the distance of the neuron from the center of barrel A respectively. Thus the responses are strongly affected by the relative timing of whisker stimuli and the location of the neuron.

	$d_A < d_B$	$d_A \approx d_B$	$d_B < d_A$
$t_B < t_A$	0	0.5	1
$t_A \approx t_B$	1	> 1	1
$t_A < t_B$	1	0.5	0

L2/3.

According to this alternative hypothesis, the relationship between the inter-whisker deflection interval and the facilitation index in L2/3 neurons may be determined by differences in the arrival times of synaptic inputs that originate from either barrel. These differences may be attributed to inter-soma distance-dependent delays in the feed-forward projection from the major input in layer 4 barrel cortex (L4). This hypothesis is supported by estimates of the speed of the projection between L4 and L2/3 neuron pairs that are relatively slow, around 0.2 meters per second for excitatory and inhibitory post-synaptic neurons (Feldmeyer et al., 2002; Helmstaedter et al., 2008).

In this paper we show that simulated barrel cortex neurons that receive synaptic inputs with onset times constrained to embody this hypothesis can account for all of the trends relating to the stimulus interval in the data of Shimegi et al. (2000). We show that a natural prediction of the model is the existence of a topographic mapping of the inter-whisker deflection interval across the surface of L2/3. Specifically, supralinear population responses will peak at short non-zero intervals in neurons located closer to the barrel representing the later of the two deflected whiskers. The responses of individual L2/3 neurons satisfy the basic requirements for a motion detector, and across the population these responses encode a range of stimulus motion velocities. Results therefore suggest that two-whisker timing is represented by a place code in L2/3 barrel cortex.

More generally, the lateral displacement of active neurons due to distance-dependent delays on projections between cortical columns can be used to compute the sequence and timing of events between the sensory stimuli represented by activity in those columns. The results are

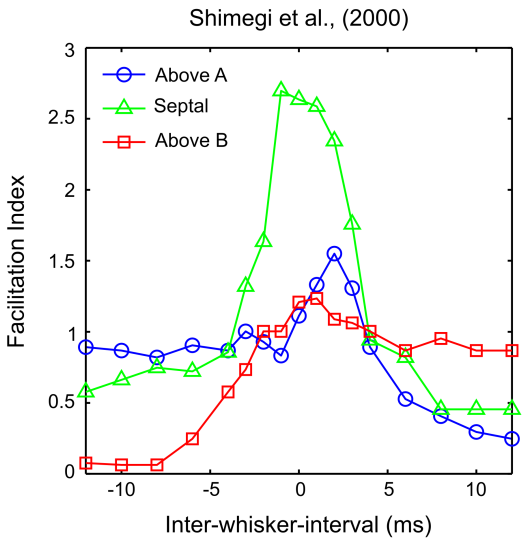

Figure 3.2. Two-whisker response interactions as reported in (Shimegi et al., 2000). L2/3 barrel cortex neurons were grouped by their position relative to the underlying barrel geometry. The spike rate over 50 stimuli at each inter-whisker deflection interval (IWI) is shown as an average for neurons located above barrel A (blue line, open circles), above barrel B (red, squares) or above the septal region between the barrel columns (green, triangles). IWI is defined as the time of the whisker A deflection relative to a whisker B deflection at time zero. When the adjacent whisker is deflected after the principal whisker, the response of neurons above the principal barrel is the linear sum of the response to either when deflected independently, as indicated by a facilitation index (FI) of 1. When the adjacent whisker is deflected prior to the principal whisker, neurons above the principal barrel are strongly suppressed, yielding a FI less than 1 and tending to zero for longer intervals. For neurons located between the barrels, longer intervals in either direction yield suppression with FI around 0.5. However in these neurons, intervals ranging $-3\,\mathrm{ms}$ to $+3\,\mathrm{ms}$ yield responses greater than the sum of the response to either whisker deflected independently and thus FI greater than 1. Notice a smaller positive FI peak in neurons above A when the whisker B deflection precedes by $2\,\mathrm{ms}$. These trends will be used to validate the model. The figure is a visualisation of the data reported in Shimegi et al. (2000), their Figure 8E, obtained from a computer-aided scan; the original error bars and statistical significance indicators are omitted, colour is added, marker styles are changed, and the axes are relabelled for clarity.

interpreted as evidence in support of the place theory as a general model of cortical processing of spatiotemporal information.

3.2 Materials and Methods

3.2.1 The distance-dependent delay hypothesis

We hypothesise that distance-dependent delays associated with inter-columar projections in sensory cortex can be used to extract the relative timing of sensory events. Specifically, delays in the projection from layer 4 (L4) to layer 2/3 (L2/3) barrel cortex might generate selectivity to the inter-whisker deflection interval for adjacent whiskers. To test the hypothesis, the latencies of synaptic inputs to a leaky integrate and fire neuron were constrained to reflect the range of geometries that characterise the L4 to L2/3 projection. To validate the model, we recreated an adjacent-whisker paired-deflection study (Shimegi et al., 2000), and compared responses of neurons in different cortical locations to stimuli in which the whiskers were deflected through a range of intervals.

The simplified model is based on three main assumptions, which are described with respect to the validation data in terms of adjacent whiskers A and B, but which in principle apply to a general model of cortical responses to arbitrarily complex multi-whisker deflection patterns.

The first assumption is that, upon whisker stimulation, inputs to L2/3 tend to originate from L4 neurons at the center of the corresponding barrel in L4. Therefore, in the model, the input layer

L4 is collapsed down to just two point sources, with activity at each source representing the deflection of the corresponding whisker A or B.

The second assumption is that the excitatory and inhibitory synaptic inputs evoked by deflection of whisker A and by deflection of whisker B arrive at a population of L2/3 neurons situated above and between corresponding barrels A and B. Therefore, in the model, each L2/3 neuron receives just four inputs, although each represents the total contribution of many similar synaptic contacts.

The third assumption is that the time taken for a L2/3 neuron to register a synaptic input is proportional to the straight-line distance between the L4 and L2/3 neuron. Therefore, in the model, we assume that the time of arrival of each synaptic input is a linear function of the distance of the L2/3 neuron from either point source in L4, and we refer to the associated constant of proportionality as the connection speed.

This simplified model of the neural geometry may deviate from the true situation. For example, if the signalling delays are due to the axonal propagation speeds, then delays could be modified by the morphology of L4 axons, which branch vertically and laterally into L2/3 (Lübke et al., 2000; Porter et al., 2001). Delays could also be modified by particular branching patterns that vary systematically with the location of the neuron in the home barrel (Petersen and Sakmann, 2000). We choose not to explicitly model the variety of axonal morphologies, firstly to keep the model formulation simple, secondly because L4 to L2/3 signalling delays are well predicted by the straight-line inter-soma distance (Feldmeyer et al., 2002; Helmstaedter et al., 2008; Armstrong-James et al., 1992), and thirdly because post-hoc simulations which considered a laterally-branching axonal morphology did not significantly alter the results. Fur-

thermore, recurrent interactions within L2/3 are not modelled explicitly, because they would occur subsequent to the initial activation of L2/3, and thus could only affect the afferent response after the critical first spike response has been determined (see *Discussion*). Similarly, modelling each L4 input source as a discrete representation of one whisker is justified because multi-whisker responses in L4 are thought to be due to latent contributions from intra-cortical mechanisms (Mirabella et al., 2001). The potential latent contributions from thalamo-cortical afferent projections will be considered in the *Discussion*. The following sections outline how each assumption is represented formally in a model that we refer to as the distance-dependent delay hypothesis. The plausibility of each assumption, the impact of each simplification, and the alternatives to each are considered in *Discussion*.

3.2.2 A simplified model of feed-forward layer 4 to layer 2/3 connectivity

The thalamocortical volley of excitation from thalamus to L4 and then up into L2/3 (Armstrong-James et al., 1992; Sato et al., 2008) is closely followed by a volley of disynaptic inhibition, mediated by a small number of interneurons in L4 (Sun et al., 2006), with a diverse range of morphologies (Porter et al., 2001). We posit that the main excitatory input to L2/3 is derived from direct synaptic connections from excitatory neurons in L4, and the main inhibitory inputs are derived indirectly from excitation of L4 inhibitory interneurons. The circuit therefore consists of three connections: an excitatory connection from L4 to L2/3, an excitatory connection onto the L4 inhibitory interneuron, and an inhibitory connection from the L4 interneuron to the L2/3 neuron.

According to the distance-dependent delay hypothesis each connection has an associated de-

lay. The onset time of the direct excitatory synaptic input at the L2/3 neuron is proportional to its distance from the barrel center. To model the indirect inhibition through an inhibitory interneuron we use a time delay proportional to the L4 to L2/3 distance plus a constant time delay accounting for the distance of the interneuron and its spike generation time.

The circuit therefore has three parameters: the speed of the excitatory pathway between L4 and the L2/3 target neuron (v_+), the speed of the inhibitory pathway between L4 and the L2/3 target neuron (v_-), and a fixed latency representing the delayed onset of the spike in the inhibitory interneuron (c) relative to the onset of excitation in L4.

For neurons in the barrel cortex, the principal whisker is typically defined as the one which, upon deflection, elicits the shortest latency and/or the largest-amplitude response. Neurons of a particular barrel column tend to share the same principal whisker, the one which on the face is isomorphic with the position of the barrel in the grid of barrels. For a given neuron all three criteria usually select the same whisker. These constraints can be built into the model if, for progressively longer inter-soma distances, whisker-evoked inhibition arrives progressively earlier than excitation. This pattern of delays requires that inhibitory connections are faster than excitatory connections, and that the onset of inhibition is delayed relative to the excitation. This is achieved in the model by setting $v_- > v_+$ and $c > 0$. An analysis of the tension created by these two factors is presented later in Figure 3.11, and the biological plausibility of these constraints will be considered in full in the *Discussion*.

3.2.3 Geometry of the L4 to L2/3 projection

In the analysis presented by Shimegi et al. (2000), against which the model will be validated, L2/3 neurons were characterised by their horizontal location with respect to two underlying barrel columns. The geometry is shown in Figure 3.3.

In the model axes x and y refer to orthogonal axes of the plane tangent to the pia matter of the brain (i.e., the plane tangential to the cortical surface; Woolsey and van der Loos, 1970); specifically x is aligned with barrels that correspond to a row of whiskers on the face, and y is orthogonal in the 'tangential plane'. The axis z is normal to the tangential plane. Axes x and z will henceforth be referred to as the horizontal and vertical axes respectively.

In the model, L2/3 neurons will be parameterised only by their horizontal location relative to the two input sources in L4. In effect, this means reducing the three spatial dimensions $\{x, y, z\}$ in which intra-cortical connections are defined to just two spatial dimensions $\{x, z\}$ by setting $y = 0$. In this way we can define the position of two sources in L4 at $\{x = \mp\alpha, z = 0\}$. Similarly we can describe L2/3 as a one-dimensional string $\{x \in \mathbb{R}, z = \beta\}$ and uniquely describe the location of individual L2/3 neurons along the string in terms of x. For example the neurons at $\{x = -\alpha, z = \beta\}$,$\{x = \alpha, z = \beta\}$, and $\{x = 0, z = \beta\}$ are L2/3 neurons located directly above barrel A, above barrel B, and above the midline respectively.

The Euclidean distance of each L2/3 neuron from the two sources can now be written in terms

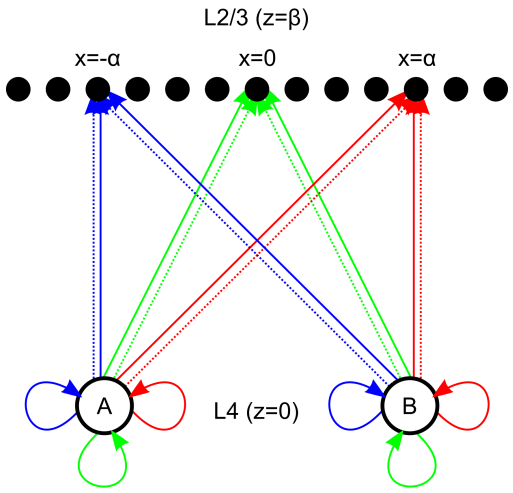

Figure 3.3. Schematic model of the L4 to L2/3 projection geometry. Input sources A and B are adjacent barrel centers in L4 that respond when corresponding whiskers A or B are deflected. Individual neurons in L2/3 (black dots) receive direct excitatory connections (solid line), or indirect inhibitory projections (dotted line) that are delayed by an additional connection (solid loop). All connections to a neuron above barrel A are shown in blue, those to the midline neuron are shown in green, and those to the neuron directly above barrel B are shown in red.

of x:

$$d_A(x) = \sqrt{[x-(-\alpha)]^2+\beta^2} \quad (3.1)$$

$$d_B(x) = \sqrt{(x-\alpha)^2+\beta^2} \quad (3.2)$$

For the analyses presented in *Results*, the input sources were located at $\{x = \mp\alpha = \mp 0.2\,\mathrm{mm}, z = 0\}$ and the two layers were separated by vertical distance $\beta = 0.4\,\mathrm{mm}$. We will henceforth refer to d_A and d_B as inter-soma distances.

Reducing the description of the neural geometry in this way makes interpretation of the behaviour of the model tractable, and it allows for a direct comparison with the available electrophysiological data. We note that using an alternative geometry has little impact on the main results, as considered in detail in *Discussion*.

3.2.4 Incorporating the distance-dependent delay hypothesis into the L4 to L2/3 projection

The L2/3 neuron receives excitatory and inhibitory synaptic inputs from each stimulated whisker. Thus, under two-whisker stimulation, the time of each input is given by:

$$t_{A+} = d_A/v_+ + \mathrm{IWI} \tag{3.3}$$

$$t_{A-} = d_A/v_- + c + \mathrm{IWI} \tag{3.4}$$

$$t_{B+} = d_B/v_+ \tag{3.5}$$

$$t_{B-} = d_B/v_- + c \tag{3.6}$$

The inter-whisker interval (IWI) is the time of deflection of whisker A, relative to whisker B, which is always deflected at time 0. Thus if $\mathrm{IWI} < 0$ whisker A was deflected before whisker B, if $\mathrm{IWI} > 0$ whisker B was deflected before whisker A, and if $\mathrm{IWI} = 0$ then the whiskers were deflected simultaneously.

The relationship between the inter-soma distance and the onset time of excitation and inhibition is illustrated in Figure 3.4A. The connection speeds were chosen to be $v_+ = 0.1\,\mathrm{m/s}$ and $v_- = 0.3\,\mathrm{m/s}$, which are in the range of estimates derived from electrophysiological data (Feldmeyer et al., 2002; Helmstaedter et al., 2008), but we note that similar analyses have estimated speeds as slow as $0.05\,\mathrm{m/s}$ (Armstrong-James et al., 1992). The constant $c = 3.7\,\mathrm{ms}$ was chosen to delay the onset of inhibition relative to excitation by $1\,\mathrm{ms}$ for the neuron located closest to either barrel center, i.e., $c = \beta/v_+ - \beta/v_- + 1\,\mathrm{ms} = 3.7\,\mathrm{ms}$.

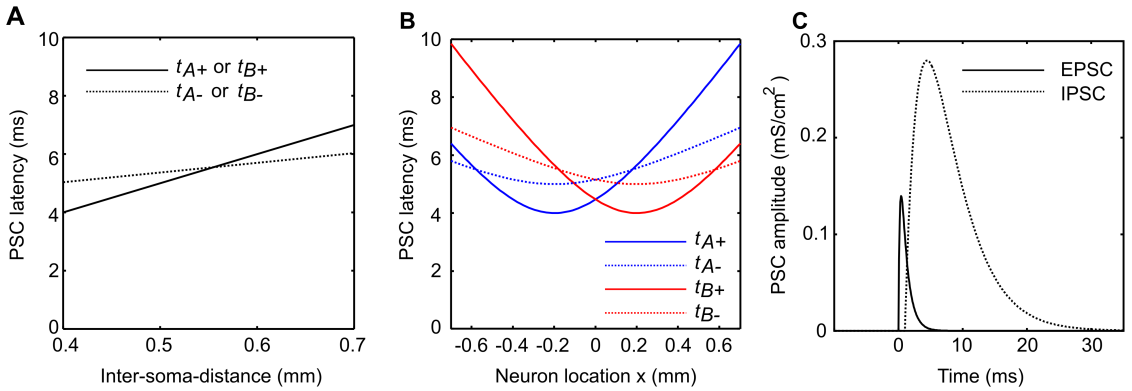

Figure 3.4. A model of distance-dependent delays in the L4 to L2/3 projection. A Distance-dependent delays in the L4 to L2/3 excitatory neuron projection. The onset of the post-synaptic conductance change (PSC) registers at the neuron after delay proportional to distance (minimum $0.4\,\mathrm{mm}$), defined by connection speed $v_+ = 0.1\,\mathrm{m/s}$ or $v_- = 0.3\,\mathrm{m/s}$ for excitatory (EPSC; solid line) and inhibitory (IPSC; dashed line) pre-synaptic neurons respectively. The inhibitory projection is in turn delayed by a constant temporal offset c. **B** Geometry of the L4 to L2/3 projection. L2/3 neurons are indexed by vertical distance $\beta = 0.4\,\mathrm{mm}$ and horizontal location x, with $x < 0$ neurons located closer to barrel center A at $\{x = -\alpha = -0.2\,\mathrm{mm}, z = 0\,\mathrm{mm}\}$, and $x > 0$ located closer to barrel B at $\{x = \alpha = 0.2\,\mathrm{mm}, z = 0\,\mathrm{mm}\}$. This geometry constrains the PSC onset latencies given by the model in **A** to be hyperbolic functions of x. Thus for simultaneous deflections of whiskers A and B the two synaptic inputs arising from deflection of whisker A (blue lines) and B (red lines) arrive in sequence depending on the location of the neuron x. The earliest input arrives at the neuron directly above the barrel center and is excitatory. **C** The timecourse of the excitatory and inhibitory PSC evoked by a whisker A stimulus is shown with relative PSC onset times for neuron $x = -\alpha$.

With the inter-soma distance constrained by the geometry of Equations 3.1 and 3.2, the input onset times, described by the linear functions in Figure 3.4A, become hyperbolic functions of the neuron location x, as shown in Figure 3.4B.

3.2.5 Leaky integrate and fire model layer 2/3 barrel cortex neuron

The model neuron is a simple integrate and fire neuron with inputs in the form of excitatory and inhibitory post-synaptic conductance changes (EPSCs and IPSCs). Parameters followed those reported by Puccini et al. (2006) as a guide for neurons in the barrel cortex.

The time course of each input P_s, following its onset at time t_{A+}, t_{A-}, t_{B+} or t_{B-}, was modelled as a normalised difference of two exponentials:

$$P_s = B(e^{-t/\tau_1} - e^{-t/\tau_2}) \tag{3.7}$$

The normalisation term $B = ((\tau_2/\tau_1)^{\tau_{\text{rise}}/\tau_1} - (\tau_2/\tau_1)^{\tau_{\text{rise}}/\tau_2})^{-1}$, where $\tau_{\text{rise}} = \tau_1\tau_2/(\tau_1 - \tau_2)$, ensures that the potential peaks at 1.

For excitatory synapses $\tau_1 = 1\,\text{ms}$ and $\tau_2 = 0.22\,\text{ms}$ simulating AMPA receptor channel opening (Sarid et al., 2007), and ensuring that excitatory inputs peak at $0.4\,\text{ms}$. For inhibitory synapses $\tau_1 = 4\,\text{ms}$ and $\tau_2 = 3\,\text{ms}$ as used by Puccini et al. (2006) to model GABA receptor channel opening, peaking later than the EPSC at $3.5\,\text{ms}$ as seen in electrophysiological data

(e.g., Wilent and Contreras, 2005). The maximum EPSC amplitude was $g_s = 0.014\,\mathrm{mS/cm^2}$ and the maximum IPSC conductance amplitude was $g_s = 0.028\,\mathrm{mS/cm^2}$ (similar to Puccini et al., 2006). The relative amplitude and time course of the excitatory and inhibitory post-synaptic currents are illustrated in Figure 3.4C.

For the L2/3 neuron we used a standard leaky integrate and fire neuron (Dayan and Abbott, 2001), again with parameters guided by those from Puccini et al. (2006):

$$\frac{dV}{dt} = \frac{1}{\tau_m}\left(E_L - V - r_m \sum_s g_s P_s (V - E_s)\right) + \eta \tag{3.8}$$

where the membrane time constant $\tau_m = 12\,\mathrm{ms}$, the resting potential $E_L = -69\,\mathrm{mV}$, the reversal potential for synapses s of type inhibitory $E_s = -85\,\mathrm{mV}$, and for excitatory synapses $E_s = 0\,\mathrm{mV}$. The leak conductance was $g_L = 0.03\,\mathrm{mS/cm^2}$ and hence the membrane resistance $r_m = \frac{1}{g_L}$. Gaussian noise η with standard deviation $0.04\,\mathrm{mV}$ was added to the membrane potential at each time step. Integration was by the forward Euler method ($dt = 0.01\,\mathrm{ms}$).

When the membrane potential reached $V_{\mathrm{threshold}} = -65\,\mathrm{mV}$ a spike was recorded, and the membrane potential was set to $V_{\mathrm{reset}} = -70\,\mathrm{mV}$.

3.3 Results

The model is validated against the data of Shimegi et al. (2000), which show a range of sublinear and supralinear facilitatory responses in neurons in different locations when paired whisker deflections occur at different inter-whisker intervals. In the following sections we show that simulated L2/3 barrel cortex neurons display the same range of interactions observed experimentally when the timing of synaptic inputs is determined by the connection geometry.

3.3.1 Responses to isolated deflections of the principal and adjacent whisker

To anticipate how a L2/3 neuron might respond to independent deflections of either whisker, we first determine when the onset times of the EPSC and IPSC evoked by deflection of that whisker will be coincident. We derive the time of coincidence by setting the onset times to be equal and rearranging:

$$t_{A+} = t_{A-} \quad \text{when} \quad x = -\alpha \pm \sqrt{[cv_-v_+/(v_- - v_+)]^2 - \beta^2} \tag{3.9}$$

$$t_{B+} = t_{B-} \quad \text{when} \quad x = \alpha \pm \sqrt{[cv_-v_+/(v_- - v_+)]^2 - \beta^2} \tag{3.10}$$

Therefore we can determine that when $t_{A+} < t_{A-}$ and hence $|x+\alpha| < \sqrt{[cv_-v_+/(v_- - v_+)]^2 - \beta^2}$ we would expect to see the largest responses to deflection of whisker A because the excitatory input precedes the inhibitory input.

To test this, neurons through the range of x locations were stimulated by applying a deflection

to either whisker A or whisker B in isolation. Analogous to the experimental procedure of Shimegi et al. (2000), each trial began $37\,\mathrm{ms}$ prior to the onset of the first whisker deflection and ended $37\,\mathrm{ms}$ after the onset of the second deflection. Spike counts were calculated over this time window for the results of all simulations, however we note that spikes were precisely timed to the whisker stimuli and so this choice of time window is not critical for the behaviour of the model (see later Figure 3.9). The spike rate is shown as an average over 50 trials in Figure 3.5A to allow direct comparison with the results of Shimegi et al. (2000), and averaged over 5000 trials for clarity in Figure 3.5B. As expected, neurons located closer to a particular barrel spike more often in response to deflection of the corresponding whisker. As the distance of the neuron from either source increases, the excitatory and inhibitory inputs evoked by the corresponding neuron register at the neuron closer together in time and thus the window of opportunity in which the EPSC can cause a spike decreases. At longer inter-soma distances, the IPSC precedes the EPSC, and effectively silences the neuron. These observations agree with the notion of the principal whisker as that represented by the barrel closest to the neuron, and which evokes the shortest latency and largest amplitude response.

Figure 3.5 shows the linear sum of the response to independent deflection of both whiskers. These values for the linear sum are later used to construct facilitation index scores from the average spike counts obtained in paired whisker-deflection trials.

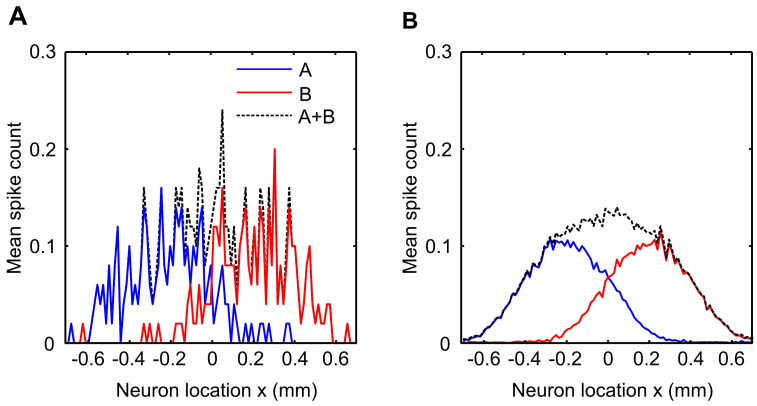

Figure 3.5. Response to independent deflection of the whiskers. Whisker A (blue line) was deflected 50 times in separate trials, and the average spike count over trials was measured in neurons at different locations in L2/3. Responses are highly variable, but are largest for neurons located directly above barrel A at $x = -\alpha = -0.2\,\mathrm{mm}$ and fall off for neurons further away from the center. Similarly responses to whisker B deflections (red line) fall off with the distance of the neuron from barrel center B at $x = \alpha = 0.2\,\mathrm{mm}$. The linear sum of the responses (dashed line) is used later to calculate the facilitation index scores. **B** Responses are shown as means over 5000 stimulus presentations for clarity.

3.3.2 The timing of synaptic inputs maps between the inter-whisker-interval and neuron location

For independent deflections of either whisker, we have seen that the spike rate is dictated by the sequence and relative timing of the synaptic inputs. Responses to paired whisker deflection stimuli are more complex because they are dictated by four PSCs rather than two and also by the IWI. However similar analysis of the relative arrival times of PSCs can be used to anticipate these responses. To this end it is useful to consider regions of the space of possible neuron location and inter-whisker deflection intervals (henceforth x–IWI space, see Figure 3.6A) that are delineated by different ordering of arrival times of the four PSCs.

These regions are delineated by loci representing coincident arrival of each possible pair amongst the four PSCs. Equations 3.9-3.10 represent two such pairs. As their solutions are not dependent on the IWI, Equations 3.9-3.10 describe four loci, which when plotted are straight lines at constant values of x that divide x–IWI space into five columns in Figure 3.6A. Solutions for the other four pairs of PSCs can be written as functions of IWI as follows:

$$t_{A+} = t_{B+} \quad \text{when} \quad \text{IWI} = (d_B - d_A)/v_+ \tag{3.11}$$

$$t_{A-} = t_{B-} \quad \text{when} \quad \text{IWI} = (d_B - d_A)/v_- \tag{3.12}$$

$$t_{A-} = t_{B+} \quad \text{when} \quad \text{IWI} = d_B/v_+ - d_A/v_- - c \tag{3.13}$$

$$t_{A+} = t_{B-} \quad \text{when} \quad \text{IWI} = d_B/v_- - d_A/v_+ + c \tag{3.14}$$

The solutions to Equations 3.11-3.14 are also plotted in Figure 3.6A, and they further divide the

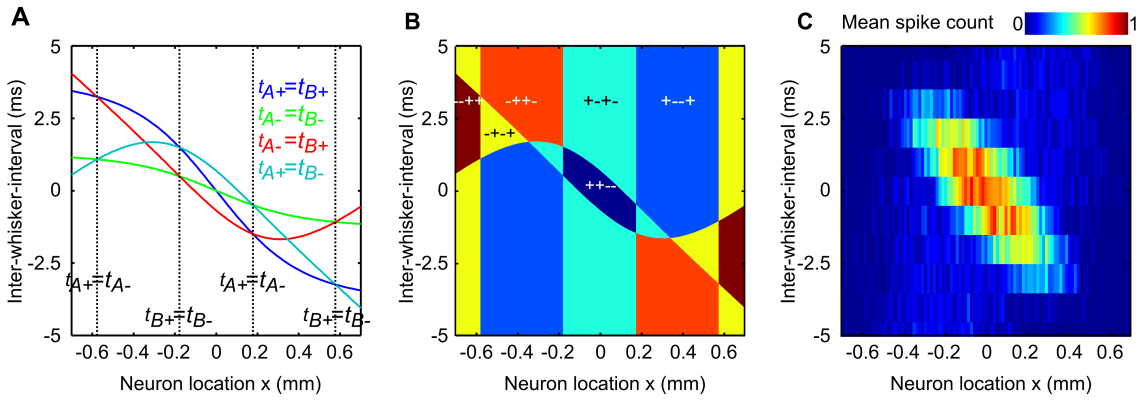

Figure 3.6. Simulated two-whisker response interactions. **A** Coincident synaptic input onsets. The model equations were rearranged to define the time at which each pair of synaptic input onsets arrives coincidently as a function of the neuron location and inter-whisker interval. **B** These solutions can be used to determine zones in which the excitatory inputs arrive in particular sequence. Neurons close to the midline register both excitatory inputs before both inhibitory inputs when the closer of the two whiskers is deflected after the more distant whisker at short intervals (dark blue zone). Under these conditions we might expect the neuron to display a large response. When these neurons are stimulated at longer intervals (cyan zone) each excitatory input immediately precedes an inhibitory input. As the excitation/inhibition pairs become separated in time the conditions are similar to the independent whisker deflections case and we might expect to observe baseline spiking. For neurons located further from the midline, when the adjacent whisker deflection precedes the principal whisker deflection by longer intervals an inhibitory input precedes both excitatory inputs, and we might expect to see a reduction in the firing rate. **C** Average spike rate measured from simulated L2/3 neurons. Neurons in different x locations were stimulated by paired-whisker deflections through a range of inter-whisker intervals. The colour of each pixel represents the average spike count averaged over 50 trials according to the colour key. The trends in the simulation data confirm the predictions formulated in reference to panel **B**. Neurons located closer to either barrel fired more often in response to a preceding adjacent whisker deflection for a range of short inter-whisker intervals, and showed the weakest responses when this interval was increased. The orientation to the patch of high activity in this space represents a topographic mapping of the two-whisker interval across L2/3.

columns into 'rows'.

For each region of the graph we can use the equations to state the sequence of inputs for each synaptic pair. This is done by setting all $=$ signs to $<$ signs in Equations 3.9-3.14. The eight inequalities that define each region of the graph can then be combined to give the order of all four synaptic PSCs, and the twenty-four possible PSC orderings take the form $t_{\mathrm{B}-} < t_{\mathrm{B}+} < t_{\mathrm{A}-} < t_{\mathrm{A}+}$, for example, in the top-left region of x–IWI space shown in Figure 3.6A.

Considering now only whether each synaptic event in the input sequence is excitatory or inhibitory, we can describe the input to the L2/3 neuron more simply. This effectively reduces the twenty-four PSC sequences to just six different orders in which excitation and inhibition can arrive at the neuron. Figure 3.6B shows how each of the six orderings delineates a zone in x–IWI space.

For a range of short interval stimuli, neurons situated near the midline receive both excitatory inputs before both inhibitory inputs. They receive inputs in the order $++--$, which can be read as 'two excitations followed by two inhibitions'. This zone is coloured dark blue in Figure 3.6B. It is in this zone that we would expect to observe the greatest spike rate because neither IPSC precedes the EPSCs. Notice that this zone is oriented diagonally in x–IWI space, and therefore neurons in different locations near the midline will prefer a range of (short) IWIs.

Similarly we can expect that the greatest suppressive interactions will be displayed in the yellow ($-+-+$), brown ($--++$), and orange zones ($-++-$), in which an IPSC event is always registered first. Of these zones the orange will be expected to yield the smallest suppression as the second IPSC is preceded by both EPSCs.

In the blue zone ($+\,-\,-+$) we might expect just one of the whisker deflections to evoke a response, as the second EPSC will be silenced by two preceding IPSCs. In the cyan zones ($+\,-\,+-$) both EPSCs are followed immediately by an IPSC. Therefore we might expect that if the two EPSC/IPSC pairs are separated sufficiently in time for the neuron to respond to them independently, i.e., if the first inhibition has little effect on the second excitation, then the response will resemble the linear sum of that evoked by either whisker deflected independently, and hence the facilitation index score here will be around one.

3.3.3 Responses to paired whisker deflections encode short inter-whisker intervals

Neurons through the range of x locations were stimulated by applying paired deflections to whisker A and whisker B in sequence. By analogy with the experimental procedure of Shimegi et al. (2000), each trial began $37\,\mathrm{ms}$ prior to the onset of the first whisker deflection and ended $37\,\mathrm{ms}$ after the onset of the second. The spike rate is shown as an average over 50 trials in Figure 3.6C.

As anticipated, the greatest activity was evoked in neurons around the midline ($x \approx 0$) when the whiskers were deflected through a range of short inter-whisker intervals ($\mathrm{IWI} \approx 0$). Within this range neurons located left of the midline and therefore closer to barrel A responded maximally to slightly positive inter-whisker intervals where whisker B was deflected before whisker A. Neurons to the right of the midline and therefore closer to barrel B responded maximally when whisker A was deflected before whisker B at short intervals.

For intervals longer than around $3\,\mathrm{ms}$ in either direction, and for neurons further from the midline than around half a millimetre, responses were much smaller. In a region of x–IWI space roughly corresponding with the light blue zone in Figure 3.6B, responses were more variable at around 0.2 spikes per stimulus.

These results from the full spiking model fit well those expected based on the relative timing of the synaptic inputs. Thus changing the relative timing of the synaptic inputs with distance-dependent delays alters the response of the neuron to paired whisker stimuli in a predictable way. A major feature predicted by the simulation data is a mapping of short interval stimuli to the location of the most active L2/3 neuron.

3.3.4 Inter-whisker interval tuning in individual L2/3 neurons

The simulation data presented thus far suggest that distance-dependent delays in the L4 to L2/3 projection can generate a spatial encoding of the relative timing of whisker inputs for short interval stimuli. But to what extent do these observations match up with experimental data? To answer this question we look first at the responses of individual model neurons to the range of different interval stimuli.

Figures 3.7A & B show the average spike rate for an individual neuron located either close to barrel B or between barrels A and B respectively. The neuron in Figure 3.7A was located approximately $0.3\,\mathrm{mm}$ to the right of the midline. Also indicated in the Figure is the linear sum of the response of this neuron to either whisker deflected in isolation. Where paired stimuli evoke responses equal to this value, a facilitation index of 1 would be measured and we would con-

clude that no facilitatory interaction had occurred. Where it is less, suppression would have been measured, and where it is greater facilitation would have been measured. The neuron in Figure 3.7A shows no facilitatory interaction when whisker B (the principal whisker) is deflected prior to the adjacent whisker A. However for slightly negative intervals strong facilitation was measured, with the average spike count exceeding the linear sum baseline three-fold or more around a peak when whisker A is deflected $2\,\mathrm{ms}$ before whisker B. When whisker A precedes by more than $4\,\mathrm{ms}$ the response is strongly suppressed and almost no spikes are evoked. The suppression recovers towards the linear sum baseline for intervals exceeding $50\,\mathrm{ms}$.

For the example midline neuron shown in Figure 3.7B facilitation appears more symmetrical around the zero inter-whisker interval. Facilitation peaks for simultaneous intervals and fluctuates around baseline for longer intervals in either direction. The peak in the average spike count is larger than that for the previous neuron, as is the linear sum response used to compute the strength of its facilitatory interaction.

Equivalent plots for individual L2/3 neurons, found in Shimegi et al. (1999, 2000); Kida et al. (2005); Drew and Feldman (2007), display similar qualitative trends to those in Figure 3.7A and Figure 3.7B, in terms of both the facilitatory interactions and of the average spike counts for independent and paired whisker stimuli.

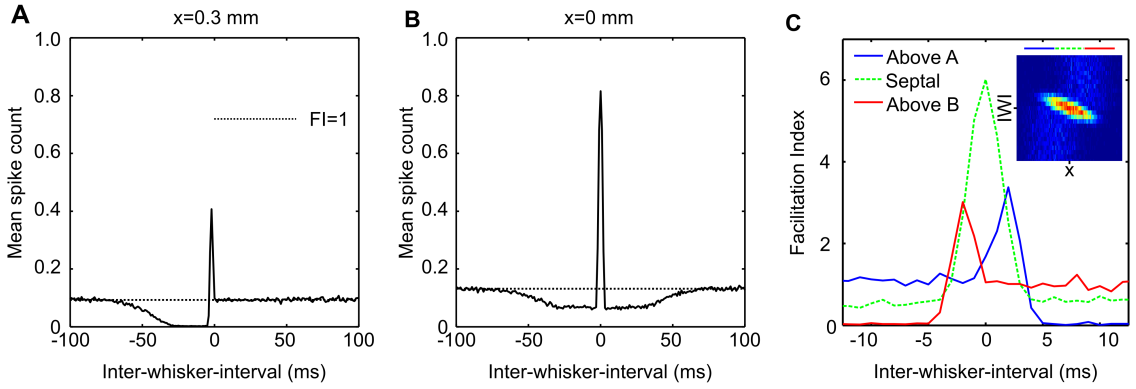

Figure 3.7. Comparing the neural and simulated data. **A** Mean spike response for the individual neuron $x = 0.3\,\mathrm{mm}$ stimulated through the range of inter-whisker intervals. Here we show the spike rate as an average over 5000 trials for clarity. The sum of the average response to either whisker deflected independently is shown by the dotted line. At positive intervals, when the principal whisker B is deflected first, responses fluctuate around baseline, whereas for longer negative IWIs the response is suppressed before recovering at intervals upwards of $50\,\mathrm{ms}$. The peak response for this neuron is at $\mathrm{IWI} = -3\,\mathrm{ms}$. **B** Equivalent data for a neuron at the midline ($x = 0\,\mathrm{mm}$). Responses to single and multi-whisker stimuli are symmetrical with respect to the inter-whisker-interval. Responses are suppressed to around 50% of the baseline firing rate for longer IWIs in either direction but are recovered for IWIs larger than $50\,\mathrm{ms}$. Peak responses are evoked by simultaneous whisker deflections. These plots are similar to those for individual L2/3 neurons reported in Shimegi et al. (1999, 2000). **C** Average response interaction for neurons located above or between the barrels. The data in Figure 3.6C are reproduced in the inset (for IWIs ranging $\pm 12\,\mathrm{ms}$) and are shown as means over neuron location in the main plot. Means were taken with respect to groups of neurons 'above A' ($-0.6\,\mathrm{mm} < x < -0.2\,\mathrm{mm}$), 'above B' ($0.2\,\mathrm{mm} < x < 0.6\,\mathrm{mm}$), and 'septal' between the two ($-0.2\,\mathrm{mm} < x < 0.2\,\mathrm{mm}$). The divisions are depicted by the position and length of the coloured bars above the inset. This plot should be compared directly with the electrophysiological data presented in Figure 3.2. Each of the major trends are reproduced by the model, including the secondary smaller peak in the above A data. In addition the model data contains a peak in the above B data, which is not clearly present in the experimental data.

3.3.5 Interval tuning over the population is a good match to the experimental data

In Figure 3.7C we group the L2/3 neurons by location as either above barrel A, above barrel B or in the septal region between the barrels. This allows for a direct comparison between the simulation data (Figure 3.7C) and the available experimental data of Shimegi et al. (2000) (compare with Figure 3.2).

The simulation data share many of the qualities of the experimental data, as summarised in Table 3.1. Septal neurons show a large facilitatory peak for near simultaneous paired whisker deflections and for longer intervals in either direction respond with an average $\mathrm{FI} \approx 0.5$, equivalent to the response to either independently deflected whisker. Neurons located above barrel B display on average a lesser facilitatory peak at $2\,\mathrm{ms}$ interval stimuli, are suppressed by prior deflection of whisker B, and display no facilitatory interactions when whisker B is deflected first (see Figure 3.2).

Geometry in the model is symmetrical about the midline and therefore the responses are symmetrical about the zero inter-whisker interval. Therefore the above barrel B population display the exact opposite interactions with respect to the interval compared with the above barrel A population. This includes a lesser peak for $-2\,\mathrm{ms}$ interval stimuli not apparent in the electrophysiological data. Notice too that the peak of the septal group in the experimental data is for a slightly negative inter-whisker interval. We will shortly demonstrate how an extension to the model, which introduces asymmetries related to the direction in which each whisker is deflected, may account for these differences. For now we note that the population response

predicted by the model affords a good match to the experimental data.

3.3.6 A place code for the inter-whisker deflection interval across the surface of L2/3

Instead of asking how L2/3 neurons in particular locations respond to different interval stimuli, we can ask how particular interval stimuli are represented across the population of L2/3. It is particularly important to consider the population response because even the most effective stimuli typically elicit less than one spike per stimulus in any particular neuron, and so individual spikes yield ambiguous information about the stimulus (Bale and Petersen, 2009).

Figure 3.8 shows the distribution of average responses across the population for a range of positive intervals. Each of the short inter-whisker deflection intervals is clearly associated with a tuning curve across the population, with a peak that shifts to the left (negative x) and scales systematically with the increase in interval. Negative intervals also evoke symmetrical results, i.e., a shift in peak responses towards neurons on the right, but we do not show them in the Figure for clarity.

Viewed in this way, it is clear that the model predicts the existence of a topographic map for the inter-whisker deflection interval across the surface of L2/3 barrel cortex. According to the model, paired whisker stimuli should elicit supralinear responses and display a systematic shift in tuning across the population for stimulus intervals ranging $-3\,\mathrm{ms}$ to $+3\,\mathrm{ms}$.

As well as the representation of the inter-whisker interval across cortical space, it is useful to

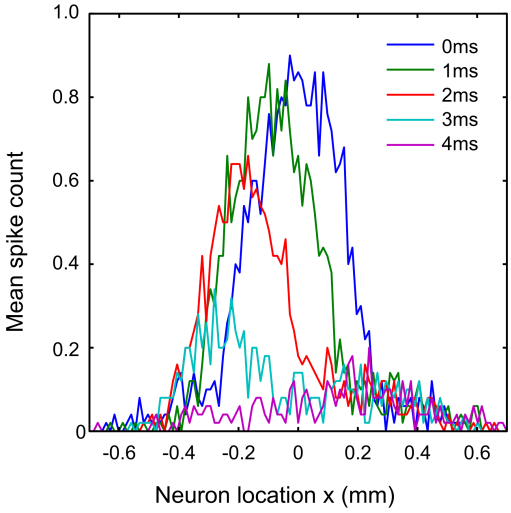

Figure 3.8. Predicted population place code for two-whisker timing. The mean spike rate plotted against neuron location reveals the population response to various inter-whisker interval stimuli. The peak response decreases and is shifted across the horizontal extent of L2/3 by stimuli varying in interval from $0\,\mathrm{ms}$ to $3\,\mathrm{ms}$ interval. Thus distance-dependent delays in the projection from L4 to L2/3 barrel cortex, coupled with the geometry of the projection, represent a mechanism by which the relative timing of two-whisker stimuli can be encoded by the population activity in L2/3 barrel cortex, for inter-whisker intervals ranging $-3\,\mathrm{ms}$ to $+3\,\mathrm{ms}$.

consider how the stimulus is represented in the timing of spikes. Inspection of maps for the spike timing revealed that in paired-whisker stimulations, spikes were precisely timed to the whisker stimuli. Moreover the largest responses reflected a combination of the delayed response to the principal whisker, as well as the superposition of excitatory influences from both whiskers (see Figure 3.9). Therefore the model predicts that the effects measured by Shimegi et al. (2000) primarily operate on the first somatosensory-evoked spikes in L2/3.

As evident in Figure 3.7A & B, the model predicts a different profile of recovery for longer inter-whisker interval stimuli beginning at the adjacent whisker. This could in principle support an inverted place code for longer inter-whisker-intervals. However, whilst the differences in response magnitude are clear in plots averaged over many trials, they are not well predicted by the location of the neuron, and the low spike rates involved (less than 0.1 spike per stimulus) render a hypothetical inverted place code for longer intervals unreliable.

3.3.7 Introducing response asymmetry via deflection direction

Barrel cortex neurons are selective for the direction in which the whiskers are deflected. The mechanism thought to underlie directional selectivity in L4 neurons is similar to that which we have outlined for two-whisker timing, but with distances measured in degrees from the preferred stimulus direction (Wilent and Contreras, 2005; Puccini et al., 2006). Several studies have suggested that direction preferences vary systematically within the barrel column, such that deflection of the principal whisker to the left or right is correlated with increased activity in neurons located to the equivalent left or right of the barrel column (Andermann and Moore, 2006; Wilson et al., 2010). Therefore we can model the effect of deflecting the whisker in either

direction by moving the L4 point source for that whisker in either direction in L4.

Accordingly, to represent a deflection of whisker A to the left (away from whisker B) we offset the point source in L4 that corresponds to whisker A by a fixed distance $r = 0.1\,\mathrm{mm}$ to obtain a new source location at $\{x = -\alpha - r, z = 0\}$. Deflecting whisker A to the right means moving the point source to $\{x = -\alpha + r, z = 0\}$ and similarly deflecting whisker B to the left or right means moving the second source to $\{x = \alpha \mp r, z = 0\}$. For two whiskers and two deflection directions, possible combinations are both deflections to the left (leftwards), both right (rightwards), A left & B right (outwards), and A right & B left (inwards). Results obtained from the model in these conditions are summarised in Figure 3.10.

For the analysis shown in Figure 3.2, Shimegi et al. (2000) deflected both whiskers to the left, and so we consider the leftwards condition first (Figure 3.10A). Conditions leftwards and rightwards produce symmetrical effects and so we only show results for the former. In the leftwards condition, the relative projections, distances, and geometry are identical to the case where the stimulus originates from the barrel centers. However, each projection is shifted to the left, and so each neuron inherits the input timing of that located $0.1\,\mathrm{mm}$ to the right. As a result the effects are still symmetrical but they are symmetrical about a new midline that is shifted to the right at $x = 0.1\,\mathrm{mm}$. When we average the data across groups defined in terms of the original midline at $x = 0$, as in Figure 3.10A, we observe systematic asymmetries in the results. The facilitatory peak in the above A group is increased, that in the septal group is shifted towards negative inter-whisker intervals, and the peak in the above B group is decreased. Thus by introducing a topology associated with the stimulus deflection direction, the model can account for each of the previously unexplained observations in the original data.

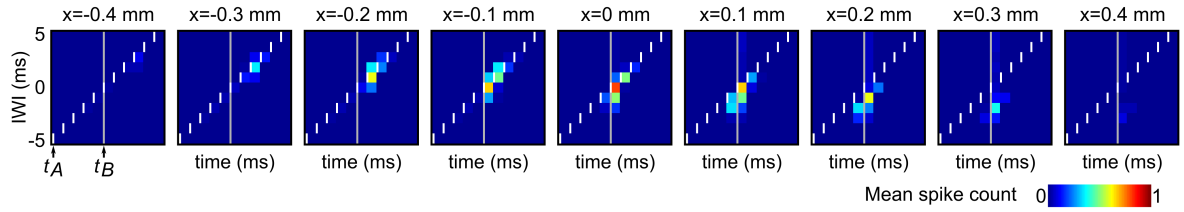

Figure 3.9. Analysis of spike timing. Spike histograms were constructed for neurons at different locations in x (shown in successive panels). In each panel, rows correspond to different inter-whisker deflection intervals (IWI), and columns show progressive simulation time. Each pixel shows the average spike count, across 5000 trials, in a $1\,\mathrm{ms}$ window. Histograms are aligned by IWI such that white ticks indicate the onset of the influence of whisker A (the first of which is labelled t_A in the first panel), and grey ticks indicate the onset of the influence of whisker B (labelled t_B). Specifically, ticks are at $t_A = \mathrm{IWI} + \beta/v_+$ and $t_B = \beta/v_+$, which is the time at which excitation from each whisker registers at the neuron closest to the corresponding input source (at $x = \pm\alpha$). In general, neurons spiked at low rates, in time with the influence of the closer whisker (diagonal versus linear trends for $x < 0$ or $x > 0$ respectively). For neurons located around the midline additional spikes occurred in time with the second whisker deflection. Interestingly, in many cases additional spikes occurred in the millisecond before the influence of the second whisker, indicating a delayed influence of the first. The maximum average spike count was 0.82 spikes per stimulus at $x = 0\,\mathrm{mm}$ and $\mathrm{IWI} = 0$, in the millisecond following the influence of whisker B.

This account is also consistent with the observations of Shimegi et al. (2000) and Kida et al. (2005) (but not Hemelt et al., 2010), that preferences for the deflection direction of the principal whisker are strongly correlated with those for the adjacent whisker deflection direction, and with the deflection direction evoking facilitatory interactions when both are deflected in that same direction at short intervals.

Predictions of the model for the two stimulus conditions not yet tested experimentally, inwards and outwards, are shown in Figure 3.10B and Figure 3.10C. Deflected towards one another (Figure 3.10B), as may occur when the whiskers encounter a concave stimulus shape, the two stimuli should be represented in the two adjacent sides of the corresponding barrels. This configuration effectively shortens all connection distances, and expands the zone in which both excitatory inputs precede both inhibitory inputs across x. Thus the facilitatory interactions are distributed more broadly across the population, and we would expect to see more similar facilitatory peaks amongst the three neuron groups. Conversely if the two whiskers are deflected away from one another (Figure 3.10C), as may occur when the whiskers encounter a convex stimulus shape or during divergent whisking movements (Sachdev et al., 2002), inputs originate from distal sides of the barrels. This configuration squeezes the zone in which we expect to see facilitatory interactions with respect to x, and concentrates them under a single peak in the septal neuron group. Demonstration of effects to the contrary could be used to falsify this aspect of the model.

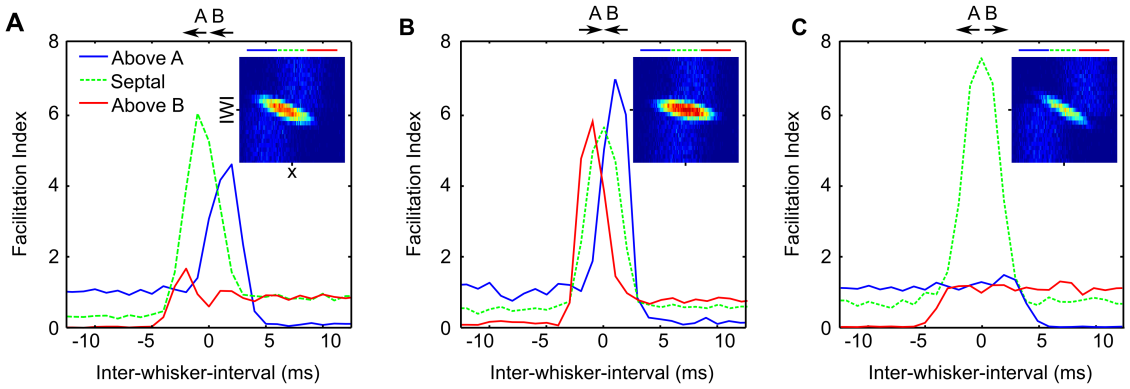

Figure 3.10. Direction-specific interactions. There is evidence that leftward or rightward deflections of the principal whisker tend to excite L4 neurons situated on the left or the right of the barrel respectively. Therefore to simulate the expected effect of deflecting the whiskers in different directions, we offset the center of activity in the model L4 by $\pm 0.1\,\mathrm{mm}$. **A** As in Shimegi et al. (2000) both whiskers were deflected to the left, as indicated by the pairs of arrows above each plot. The relationship between inter-whisker-interval and neuron location is the same but shifted for increasing intervals to neurons closer to barrel A. The resulting asymmetry is of the same form as that in Figure 3.2, increasing the secondary peak in above A neurons, decreasing that in the above B group, and shifting the septal group interval tuning negatively. **B** If the whiskers are deflected toward each other, intra-cortical distances are effectively shortened and the model predicts that facilitatory interactions will be distributed more evenly across L2/3. **C** Conversely if the whiskers are deflected away from each other, distances are increased and all facilitatory interactions are confined to the septal region. The conditions represented in panels **B** and **C** have not yet been conducted experimentally and could therefore be used to falsify the model.

3.3.8 An approximate non-linear neuron model reproduces the facilitatory interactions

The particular neuron model from which the previous results have been derived was chosen to allow comparison of the results with real biological neuron data. We have shown how the sequence of synaptic inputs due to distance-dependent delays can change the output of the neuron, but we have not yet determined the origin of the non-linear effects underlying the observed facilitatory interactions, i.e., where the facilitation index deviates from unity. To understand this better we tried to reproduce the effects using as simple a neuron model as possible.

We found that all of the trends in the full model simulations could be reproduced using a simple linear filter neuron model. The reduced model is:

$$\frac{dV}{dt} = \frac{1}{\tau_m}\left(\sum_s g_s P_s - V\right) \tag{3.15}$$

where $g_s = 1$ or $g_s = -0.5$, with output squashed using the logistic output function:

$$F(V) = \left(1 + e^{(0.2-V)/0.04}\right)^{-1} \tag{3.16}$$

The range of facilitatory interactions can be seen if we interpret either the maximum or the mean value of $F(V)$ over time as the spiking probability for each stimulus trial.

The logistic output function performs the role of the thresholding operation in the full model. Its form in the full model is affected primarily by the noise, which has a similar effect to the slope of the sigmoid (slope parameter = 0.04), and the relationship between the firing threshold and the synaptic weights and reversal potentials, which essentially sets the inflection point of the sigmoid (inflection point = 0.2).

Because both neuron models yield comparable stimulus-evoked interactions, we can be confident that the thresholding non-linearity in the full neuron model, as approximated by the sigmoidal output function in the simpler neuron model, can account for the observed non-linear effects. Comparing the two models in terms of the spike probability is valid in this instance because we observed that in the full model neurons generate less than one spike per stimulus.

3.4 Discussion

We have demonstrated how a model of the geometry of projections within the barrel cortex can generate a range of responses to paired whisker-deflection stimuli that are similar to responses measured in rat L2/3 by Shimegi et al. (2000). The main finding is that distance-dependent delays on projections from L4 to L2/3 can affect how inputs from adjacent whiskers are integrated by a non-linear neuron, in a way that is dictated by the location of the neuron relative to the underlying columnar structure. The data against which the model was validated (Shimegi et al., 2000) suggest that neurons located between the barrels combine whisker inputs supralinearly through a small range of inter-whisker deflection intervals (IWI), and when the principal whisker deflection is preceded by deflection of the adjacent whisker at longer IWIs the inputs

are combined sublinearly. In the model a discrepancy between the arrival times of excitatory and inhibitory inputs can account for each of the observed trends in the available electrophysiological data. According to our hypothesis, this discrepancy is governed by the lateral displacement between the input neurons and their targets. Therefore the discrepancy is a continuous function of the location of the neuron, and hence the range of non-linear responses is mapped continuously across the surface of L2/3. As a consequence, the model predicts that a range of short IWIs are mapped continuously across a zone of supragranular barrel cortex located between the barrel centers. This mapping constitutes a place code for the timing of the two-whisker stimulus, wherein the stimulus motion velocity (i.e., the IWI) systematically shifts the location of neurons that spike with the greatest probability.

It is useful to consider these findings in the context of the more general problem of encoding sensory stimulus motion. According to Borst and Egelhaaf (1989), the general requirements for a motion velocity detector are threefold. First, two samples or more are required to specify a motion vector, so the detector must receive two or more input signals. Second, the inputs must be asymmetrically processed, such that swapping two inputs registers a change in the output. Third, the inputs must be combined in a non-linear fashion in order that the response to stimuli in different directions is not equal to the mean response over all directions. Our results suggest that responses of individual L2/3 barrel cortex neurons satisfy each of these conditions. Inputs arising from adjacent whiskers and originating from foci in adjacent cortical columns are asymmetrically delayed in their projection to supragranular cortex. The inputs are integrated by individual L2/3 neurons by the non-linear processes involved in spike generation. Hence we propose that one function of the the L4 to L2/3 projection is to encode the stimulus motion velocity defined in terms of inter-whisker contact times.

3.4.1 Simplifications and assumptions of the model

A major simplification we made in order to construct the model was to explicitly simulate only four synaptic contacts per neuron, whereas real L2/3 neurons receive hundreds of synaptic contacts originating from L4 (Beaulieu, 1993). Where possible, the parameters of the full neuron model were derived from existing models or electrophysiological data. However to compensate for the decrease in afferent drive, the spiking threshold was lowered from a realistic $-60\,\mathrm{mV}$ to a low $-65\,\mathrm{mV}$. In the final results section we showed that the behaviour of the model is not sensitive to the form of the neuron model chosen, but that each of the trends in the electrophysiological data can be reproduced using a simple sigmoid output function neuron, as used in previous models of the barrel cortex (Kyriazi and Simons, 1993; Pinto et al., 1996).

Another simplification was to relate the delay on each projection to the straight-line distance between the input and its target. This choice was motivated by several studies reporting an approximately linear relationship between the straight-line inter-soma distance and the associated delay (Armstrong-James et al., 1992; Feldmeyer et al., 2002; Helmstaedter et al., 2008). However, the axons of L4 neurons tend to project vertically into L2/3 before turning to branch laterally (Petersen et al., 2003). Therefore it may be appropriate to consider the Manhattan distance, the vertical plus the horizontal distance, defined in the model by rewriting Equations 3.1-3.2 to be of the form $d_A(x) = |x+\alpha|+\beta$. This change has the effect of changing the hyperbolic relationship between x and the synaptic onset latency into a piecewise linear relationship. Each of the zones of synaptic input sequence is maintained in x–IWI space; hence using the Manhattan distance to compute synaptic input latencies does not change the form of the main results when they are recalculated using this alternative geometry.

The model relies implicitly on the assumption that connections between L4 and L2/3 are organised on a finer spatial scale than that defined by the column boundaries, such that the location of the L2/3 neuron determines its response properties. Evidence from several studies supports this assumption. For example calcium transients measured between pairs of neighbouring L2/3 neurons located above the barrel centers are more highly correlated than those between pairs of distant neurons located above the barrel borders (Kerr et al., 2007). These data suggest that L2/3 neurons receive input from particular regions of the L4 barrel according to their tangential location in the column (Kerr et al., 2007). More evidence for a sub-columnar spatial resolution of connections is provided by a correlation between the maximally effective direction of whisker deflection for L4 and L2/3 neuron pairs in vertically aligned sub-regions of the barrel column (Andermann and Moore, 2006). Similarly, connected thalamic and L4 neuron pairs share tuning to the whisker deflection direction (Bruno et al., 2003).

The mechanism by which the model accounts for tuning to inter-whisker interval is essentially the same as that thought to underlie tuning for the deflection direction in L4 (Swadlow, 2002; Wilent and Contreras, 2005; Puccini et al., 2006; Higley and Contreras, 2007). In both cases the relative latency of inhibition creates a short 'window of opportunity' in the post-synaptic neuron, in which excitatory input representing the preferred stimulus can evoke a response. The dependency of the preferred inter-whisker interval on the connection geometry raises the intriguing possibility that tuning for deflection direction in L4 is inherited from the geometry of the thalamo-cortical projection. A reported topographic organisation of directional preferences about the barrel center in L4 could be inherited from a map of direction preferences measured along the major anatomical axis of the thalamic input barreloid (Timofeeva et al., 2003). This idea seems plausible given that thalamocortical axon conduction times range from $0.3\,\mathrm{ms}$ to $1.3\,\mathrm{ms}$ (Simons et al., 2007), and that latencies ranging $0.5\,\mathrm{ms}$ to $1.4\,\mathrm{ms}$ can account

for responses to preferred and anti-preferred stimuli respectively (Wilent and Contreras, 2005; Puccini et al., 2006).

To account for the data of Shimegi et al. (2000), the model requires that at short inter-soma distances excitation precedes inhibition and for longer distances inhibition precedes excitation (see Figure 3.11). This we attributed to differences in axonal conduction velocity on excitatory and inhibitory projections into L2/3. The origin of the faster inhibition is unlikely to be mediated by L2/3 interneurons, because excitatory connection speeds from L4 to L2/3 interneurons are similar to those from L4 to L2/3 excitatory targets (compare Helmstaedter et al., 2008 and Feldmeyer et al., 2002 respectively). The origin is also unlikely to be thalamocortical, because L4 interneurons and L4 excitatory targets are excited after comparable latencies (Beierlein et al., 2003), although interneurons are excited via slightly thicker, shorter, and thus faster thalamocortical axons (Kimura et al., 2010). Therefore we suggest that differences in speed may be attributable to morphological differences between the axons of L4 inhibitory and L4 excitatory neurons; L4 interneurons are known to branch into L2/3 and extend well beyond the boundary of the vertically aligned barrel (Porter et al., 2001). To our knowledge, the axonal conduction velocities for this connection have not been directly measured. Therefore the critical quantitative prediction, that the L4 inhibitory axonal conduction speed must be faster than the L4 excitatory speed, can be used to validate the model in a future experiment.

Because each input source in L4 represented the deflection of one whisker, the present model assumed no contribution of sub-cortical mechanisms to the integration of multi-whisker signals. To a first approximation, the barrels in L4 can be considered as functionally separate processing units (Woolsey and van der Loos, 1970; Armstrong-James et al., 1992). Moreover, although non-linear multi-whisker responses can be evoked in L4 neurons (Simons, 1985; Simons and

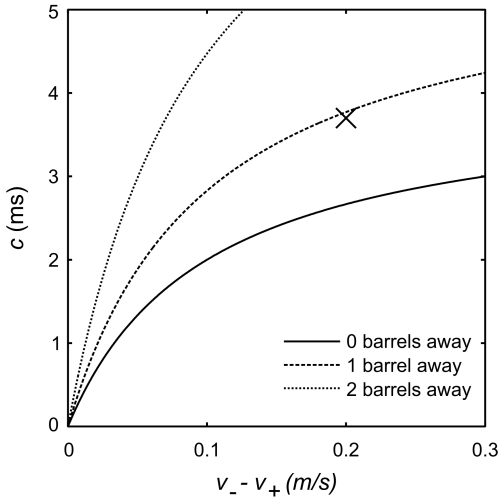

Figure 3.11. Constraints on the timing of axonal propagation. The delay on the onset of inhibition, c, required to make excitation and inhibition from the same whisker arrive coincidently, is plotted for varying inhibitory connection speeds v_- at three locations in L2/3. Solutions to the equation $c = d/v_+ - d/v_-$ are plotted for three different L4 to L2/3 inter-soma distances: First to the home barrel center $d = \beta$ (solid line), second to the adjacent barrel center $d = \sqrt{(2\alpha)^2 + \beta^2}$ (dashed line), and third to two barrel centers away $d = \sqrt{(4\alpha)^2 + \beta^2}$ (dotted line). All other parameters were fixed at the values reported in the main text ($v_+ = 0.1\,\mathrm{m/s}$, $\alpha = 0.2\,\mathrm{mm}$, and $\beta = 0.4\,\mathrm{mm}$). For choices of the parameters v_- and c that are above a line, inhibition will arrive at L2/3 neurons above the corresponding barrel center later than excitation evoked by the same whisker, and vice versa for parameters that fall below that line. The cross indicates the choice of v_- and c used for the simulations in the main text, which make excitation and inhibition coincident for neurons located approximately one barrel away from the source. Measurements of v_- and c below the solid line would falsify the model because no facilitatory zone and hence no map for the inter-whisker interval could exist in L2/3. Values much greater than the dashed line would map inter-whisker intervals between adjacent barrel centers with poor coverage.

Carvell, 1989; Brumberg et al., 1996), much of the effect may be due to intra-cortical rather than thalamocortical mechanisms (Mirabella et al., 2001), which are most pronounced in non-granular layers (Drew and Feldman, 2007; Jacob et al., 2008), and which would shape responses only after the first stimulus-evoked spikes had been determined.

However, we note that a recent study measured multi-whisker receptive fields in L4 neurons that were effectively isolated from cortico-cortical influences (Roy et al., 2011). This suggests a thalamo-cortical component of multi-whisker integration that is neglected in the present model by assuming a mono-whisker afferent projection into L4. Roy et al. (2011) found that the latency of L4 responses to non-principal whiskers increases with the distance of the non-principal whisker from the principal, which suggests that latency differences associated with the thalamo-cortical projection could play a similar role to the L4-L2/3 projection in establishing inter-whisker interval tuning in L4. The contribution of sub-cortical mechanisms to multi-whisker integration should not be overlooked; an extended version of the model will be required to explore this important issue in more detail.

By appealing to differences in axonal path lengths, the present model has not ruled out potential contributions of dendritic mechanisms to the encoding of the stimulus velocity. In contrast to the Jeffress model, the classic model of Rall (1964) shows how different synaptic input sequences can lead to different activity in the cell if synaptic potentials are evoked in particular sequences along the length of dendritic cables. As a temporal coding mechanism for velocity tuning, Rall's original passive formulation of the model requires dendrites with very large electrotonic length to support meaningful velocity discriminations. However, recent glutamate uncaging experiments activating synapses along the dendritic length have revealed a more active interaction between synapses when they are sequentially activated (Branco et al., 2010). These

experiments have to some extent confirmed Rall's central prediction for sequence coding, in L2/3 cortical neurons with dendrites of regular electrotonic lengths. Whether these results relate to velocity tuning for multi-whisker stimuli is at present unclear. The critical question is whether the relative placement of synapses along the dendritic length corresponds with the relative placement of the neuron between the barrels, i.e., does a L2/3 neuron closer to barrel A receive input from barrel A afferents at synapses located systematically closer to the soma than those from barrel B? Whilst this is certainly plausible, distance dependent axonal delays and dendritic non-linearities may both interact to enhance the representation of input velocity, and thus axonal and dendritic models may represent complementary rather than competing theories.

3.4.2 Extending the model

Tactile stimuli which include three or more whiskers cause suppressive interactions across barrel cortex which serve to enhance the representation of complex multi-whisker deflection patterns (Ghazanfar and Nicolelis, 1999; Mirabella et al., 2001; Drew and Feldman, 2007; Jacob et al., 2008). We investigated how additional whiskers are represented according to the model, by simulating the effect of a stimulus moving at various speeds through a row of whiskers which included two, three, four, or five whiskers (see Figure 3.12). When the whiskers were deflected simultaneously, the resulting activity across L2/3 was widespread and large and formed a symmetrical pattern, but when the whiskers were deflected consecutively the activity decreased across L2/3 in the direction corresponding to the stimulus motion. In agreement with previous studies the model predicts the existence of an activity gradient that is steeper for slower stimulus motions.

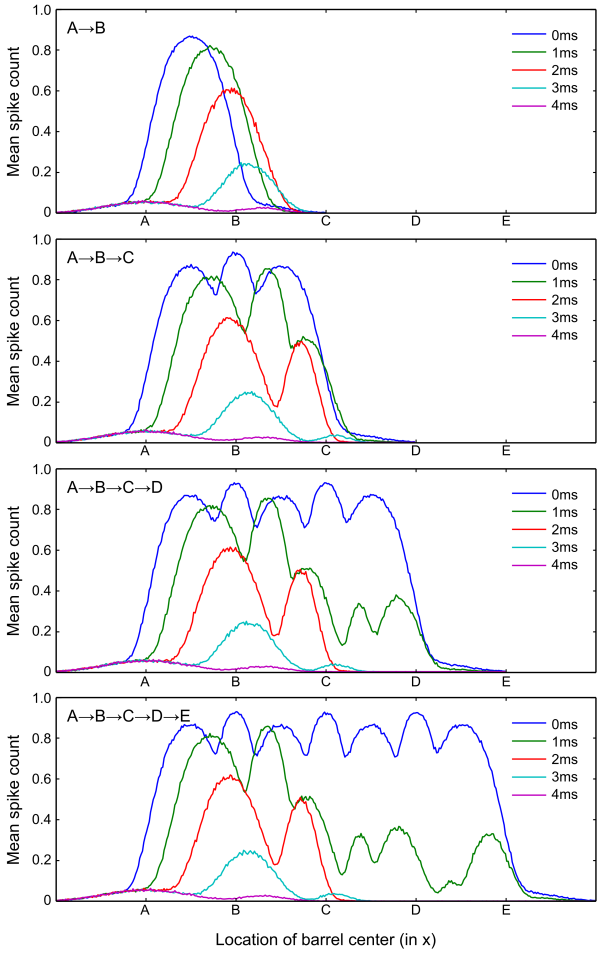

Figure 3.12. Predicted responses to additional whiskers. Responses across a large region of barrel cortex were generated by deflecting increasing numbers of whiskers. The top panel shows the mean spike count, over 5000 trials, to deflection of whisker A followed by whisker B after intervals ranging $0\,\mathrm{ms}$ to $4\,\mathrm{ms}$ (see legend). Ticks along the x–axis mark the location of the barrel centers, at 2α spacing, for columns corresponding to whiskers A to E in a row on the snout. The top panel is comparable with Figure 3.8 from the main text. Successive panels include deflections of additional whiskers, each deflected a fixed time after deflection of the adjacent whisker to the left. When three or more whiskers are deflected simultaneously ($0\,\mathrm{ms}$ interval) the response resembles the superposition of adjacent two-whisker tuning functions, punctuated by additional peaks. When stimulated consecutively, the two-whisker tuning function between each pair of columns is modulated by an overall response decrease in the direction corresponding to the stimulus movement direction. Thus, when additional whiskers are included by tactile stimuli, the model predicts an overall trend for responses to decrease in the direction of the stimulus movement.

A previous modelling study suggested that a spatial gradient in the afferent activation of L2/3 could represent the direction of stimulus motion through the whisker field, and that this representation in L2/3 would be sharpened by recurrent inhibitory interactions (Wilson et al., 2010). The present model did not consider recurrent inhibition, which is prevalent in L2/3 (Derdikman et al., 2003; Kapfer et al., 2007; Sato et al., 2008; Adesnik and Scanziani, 2010), because it considered primarily how subthreshold inputs interact to generate the earliest spikes in L2/3 (see Figure 3.9). We are currently working on a model which extends the present study and that of Wilson et al. (2010), to test the hypothesis that regions of contrast in activity due to initial feed-forward interactions are enhanced by subsequent lateral inhibition. This model will also explore how stimulus coding might be affected by distance-dependent weights on synaptic connections, as suggested by recent experiments (Derdikman et al., 2003; Adesnik and Scanziani, 2010).

3.4.3 The impact of neural geometry on neural computation

The present simulation results afford an existence proof for a more general hypothesis that the geometry of projections between neighbouring cortical columns could be useful for encoding relative inter-sensor motion speed and direction.

In its weakest form the implication of the hypothesis is that interconnection geometry and connection speeds should be considered in detailed cortical microcircuit models if they are to accurately predict the response properties of individual cortical neurons. Given the remarkable spatial relationship between the whisker and its associated barrel column, it is surprising that, with the exception of Benusková et al. (1999), Ermentrout et al. (2009) and our own previous

model (Wilson et al., 2010), connection geometry has not been an important factor in computational neuroscience models of the barrel system.

In its strongest form the implication is that the cortex could carry out specific computations by reading out the tangential position of active cortical neurons. This is essentially the same idea as the place theory proposed by Jeffress (Jeffress, 1948). The principle behind our model and the Jeffress model are essentially the same. In both, a bank of coincidence detectors receive input from spatially separated sources after delays governed by the distance from either source, and thus activity in detectors whose connection delays compensate that of the stimulus motion reports the stimulus velocity. It remains to be shown whether tactile specialists such as rats and mice can discriminate adjacent whisker contact times over the range generated in the model, although emerging techniques are allowing the link between barrel cortex activity and performance on tactile discrimination tasks to be explored in unprecedented detail (O'Connor et al., 2010).

Jeffress' place theory can be thought of as a specific case of a more powerful computational principle, recently termed 'polychronous wavefront computation' (PWC; Izhikevich and Hoppensteadt, 2009). In PWC terminology, two sources in the Jeffress model specify a one-dimensional axis through a medium (the axonal web), along which the placement of detector neurons determines their inter-stimulus interval selectivity. However, sources and detectors can be arranged in two- or higher- dimensional media, such as the barrel cortex, to perform non-trivial computations. The barrel cortex, with the precise correspondence between the grid of cortical columns and the grid of whisker sensors, is an ideal structure in which to investigate the role of neural geometry in neural computation.

The simplicity of the current model affords its explanatory power. However, a future study will be required to verify under what conditions the behaviour of the model is retained, when many hundreds of neurons and thousands of synaptic contacts are modelled explicitly. The barrel column is currently the target of a number of detailed modelling efforts (Markram, 2006; Helmstaedter et al., 2007; Sarid et al., 2007; Lefort et al., 2009). Complementing these approaches, the power of our simple geometric model to explain a series of complex observations suggests that the geometry of synaptic connections in and between barrel columns should be considered if we are to understand the function of cortical microcircuitry.

Chapter 4

Tactile discrimination using artificial whiskers and cortical maps

Chapter summary

The facial whiskers (or 'vibrissae') afford natural touch specialists, like rats and mice, with a rich representation of their immediate surroundings. A number of artificial whisker technologies are currently being developed to mimic this high-acuity sensory system. However methods for combining whisker signals have drawn little inspiration from the primary somatosensory cortex (S1), wherein multi-whisker signals seem to be integrated. Here we present the first systems-level description of the primary (lemniscal) processing pathway from the whiskers to their representation in S1. Movement signals were collected using robot-controlled collisions between physical stimuli of different shapes and an array of artificial whisker sensors. According to the model, these signals are first i) filtered for high-velocity movements in particular directions by sub-cortical neurons, then ii) mapped onto neurons at specific locations in the sensory cortex, and finally iii) integrated between whiskers, via connection delays that increase with the distances between cortical input and output neurons. After processing by the model, the whisker movements could be classified by the tactile stimulus shapes, and motion directions and speeds that caused those

movements, using a simple linear classifier. The model ascribes specific functional roles to sub-cortical and intra-cortical neural circuitry, derived at each stage from existing neurophysiological data.

4.1 Introduction

Tactile specialists like rats, mice, seals and shrews rely on facial whiskers (or 'vibrissae') to mediate information about the shape and motion of tactile stimuli to the sensory brain; Around thirty-five large whiskers on either side of the face (the macrovibrissae), and many smaller whiskers around the lip (the microvibrissae), constitute a high-acuity sensor surface (Welker, 1964; Ahl, 1986; Brecht et al., 1997; Towal et al., 2011; see Figure 4.1A). Whisker-mediated sensing is thought to be important for guiding natural exploration and navigation behaviours (Mitchinson et al., 2007; Grant et al., 2009; Dehnhardt et al., 2001; Hartmann, 2011; Mitchinson et al., 2011), as well as for hunting, foraging and fighting (Vincent, 1912; Ahl, 1986; Anjum et al., 2006); and, when performing behavioral tasks, multiple whiskers seem to be better than one (Krupa et al., 2001a; Celikel and Sakmann, 2007). In the lab, behavioural and neurophysiological data suggest that rodent whisker systems can discriminate between tactile stimulus shapes (Brecht et al., 1997; Anjum et al., 2006; Benison et al., 2006; Diamond et al., 2008); sizes, positions and orientations (Carvell and Simons, 1990, 1995; Polley et al., 2005; O'Connor et al., 2010); surface textures (Arabzadeh et al., 2005; Ritt et al., 2008); and motion velocities (Drew and Feldman, 2007; Jacob et al., 2008).

The whisker system is an important model sensory system in modern neuroscience, because in-

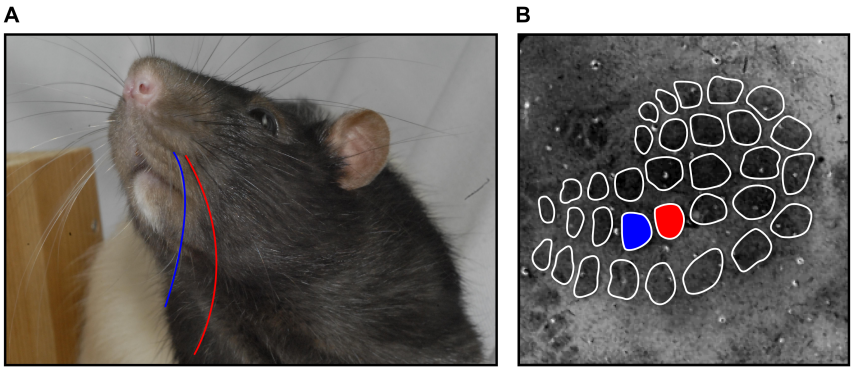

Figure 4.1. The whisker-barrel system. A The whisker system of the tactile specialist *Rattus norvegicus* (the Norwegian rat); around 35 large whiskers (the 'macrovibrissae') on either side of the face, and many more around the upper lip (the 'microvibrissae') constitute a high-acuity sensor surface. **B** A tangential section through rat barrel cortex stained for cytochrome oxidase, revealing a pattern of 'barrel' columns in layer 4; barrels are outlined in white. The layout of barrels in the cortical sheet maps precisely to the layout of whiskers on the face, such that adjacent whiskers (for example those traced in blue and red in **A**) evoke the shortest latency and greatest magnitude response in neurons of adjacent barrels (highlighted in corresponding blue and red in **B**).

put to the individual sensors (whiskers) can be precisely controlled (Krupa et al., 2001b; Jacob et al., 2010), and because the spatial layout of the sensor surface is maintained in projections through the brain to the primary sensory cortex (Woolsey and van der Loos, 1970; Welker and Woolsey, 1974). The arrangement is such that stimulation of adjacent whiskers on the face evokes maximal responses in adjacent columns of cortical neurons (Armstrong-James et al., 1992), known as 'barrels' because of their characteristic barrel-like shape. After chemical staining, the barrels are just about visible to the naked eye, on the surface of the brain, and hence the primary cortical representation of each individual sensor is easily identifiable and accessible to the experimenter (see Figure 4.1B).

Inspired by the whisker system, a number of biomimetic whisker sensor technologies have been developed in recent years (Lungarella et al., 2002; Seth et al., 2004; Russell and Wijaya, 2005; Solomon and Hartmann, 2006; Kim and Möller, 2007; Gopal and Hartmann, 2007; Pearson et al., 2007; Sullivan et al., 2011: see Solomon and Hartmann, 2008; Prescott et al., 2009 for an overview). Computational neuroscience models for processing single-whisker deflection signals have been proposed; at the level of the whiskers (Birdwell et al., 2007) and mechanoreceptors (Lottem and Azouz, 2011), at the level of the primary afferent neurons that innervate the whisker follicles (Mitchinson et al., 2004, 2008), and at the level of thalamo-cortical loops (Ahissar, 1998). However, biological mechanisms for integrating signals arising from multiple whiskers are not well understood (but see Kyriazi et al., 1996; Mitchinson et al., 2006; Gopal and Hartmann, 2007), despite a wealth of neurophysiological data describing the neural correlates of controlled multi-whisker stimulations at the level of cortical barrels (Simons, 1983, 1985; Shimegi et al., 1999, 2000; Kida et al., 2005). The aim of the present study is to collate what is known from the neurophysiology about multi-whisker integration, into the first systems-level description of the major (lemniscal) processing pathway from the whiskers

to their representation in and between the primary cortical barrels.

Two computational neuroscience models, developed recently in our lab, have suggested how whisker movement primitives are represented in the barrel cortex. These movement primitives are the direction in which a single whisker is deflected (a spatial stimulus parameter; Wilson et al., 2010, see chapter 2), and the time interval between multi-whisker deflections (a temporal stimulus parameter; Wilson et al., 2011, see chapter 3). According to these previous models, the geometry of connections between cortical columns plays a key role in determining the spatial-temporal receptive fields of neurons at different locations on a cortical sheet. The present model uses, and extends, the principles of neural interconnection geometry identified in these previous models, to represent a variety of multi-whisker movement patterns as activity patterns on a cortical sheet.

We show that the shape, direction and speed of a moving tactile stimulus can be recovered from the cortical sheet representation of multi-whisker movement patterns, collected using an array of artificial whisker sensors that were stimulated by a robot. The results therefore validate, in a real-world task, the neural model, and in particular the cortical encoding of relative whisker deflection times proposed in Wilson et al. (2011), on which the model architecture was based.

4.2 Methods and Materials

4.2.1 Overview

An array of 12 artificial whisker sensors were stimulated using tactile stimuli of different shapes, which were moved through the array by a table-top XY positioning robot. Whisker signals resulting from 2,000 collisions between the tactile stimuli and the array of whiskers were collected; 5 tactile stimulus shapes, 10 movement speeds, 8 movement directions, and 5 realisations of each stimulus combination. Signals were processed by our computational neuroscience model of the whisker-barrel processing pathway. According to this model, a population of subcortical neurons each elicit spikes when they register a high-velocity movement of the preferred whisker in a preferred direction. Subcortical spikes are relayed to a cortical sheet representing layer 4 (L4) barrel cortex, with neurons positioned on the sheet at locations that reflect the spatial pattern of whisker movements. Finally signals from multiple whiskers are integrated over time, via intra-cortical signalling delays to layer 2/3 (L2/3) barrel cortex that increase with the distance between pre-synaptic (L4) and post-synaptic (L2/3) cortical neurons.

An important aim of the study is to establish a baseline measurement of the information about the tactile stimuli that is retained by the mapping from whisker signals to the responses of model L2/3 neurons; It is important to note that the aim is not to optimise a system for the task of recognising tactile stimuli. The baseline measurement is taken to be the performance of a simple linear classifier at discriminating between tactile stimuli based on the model L2/3 population responses. Serving as a control, against which to evaluate the information retained by the mapping from the whiskers to L2/3 responses, performance of the simple linear classifier

is compared with that obtained using inputs generated via an analogous mapping based on cross-correlation from signal processing. The following sections present the details of the cortical model, with particular reference to Figure 4.2, and they present the performance measurements that were applied to the cortical and control mappings.

4.2.2 Apparatus

Twelve artificial whisker sensors were arranged in a 4 columns by 3 rows array, with the whisker shafts pointing vertically (Figure 4.3). The whiskers were stimulated using 5 differently shaped perspex edges, which served as tactile stimuli. Tactile stimuli were suspended from a platform above the whisker array so as to make contact at $2 - 3\,\mathrm{mm}$ from the whisker tips. The platform was translated by a table-top XY positioning robot (Yamaha Robotics$^{\mathrm{TM}}$, model PXYX; see Evans et al., 2010), with two motors controlling translation of the stimulus on orthogonal axes (X and Y) on the table-top. We will use a notational convention wherein real-world physical quantities, such as distances and time, are denoted by capital letters; the robot movement is repeatable to an accuracy of $\pm 0.01\,\mathrm{mm}$, so for convenience we will treat the requested robot movement as the actual robot movement, and thus also denote robot movement variables using capitals.

The $w\mathrm{th}$ whisker is identified by its table-top coordinate, by $X_w \in \{-1.5D, -0.5D, 0.5D, 1.5D\}$ and $Y_w \in \{-D, 0, D\}$, where $D = 16\,\mathrm{mm}$ is the spacing between adjacent whiskers of the same column or row, and the origin is at the center of the array. Tactile stimuli were a straight edge, and concave and convex semi-circular edges of radius $33\,\mathrm{mm}$ or $55\,\mathrm{mm}$. These shapes can be described by a single parameter R, equivalent to the semi-circle radius, which takes negative

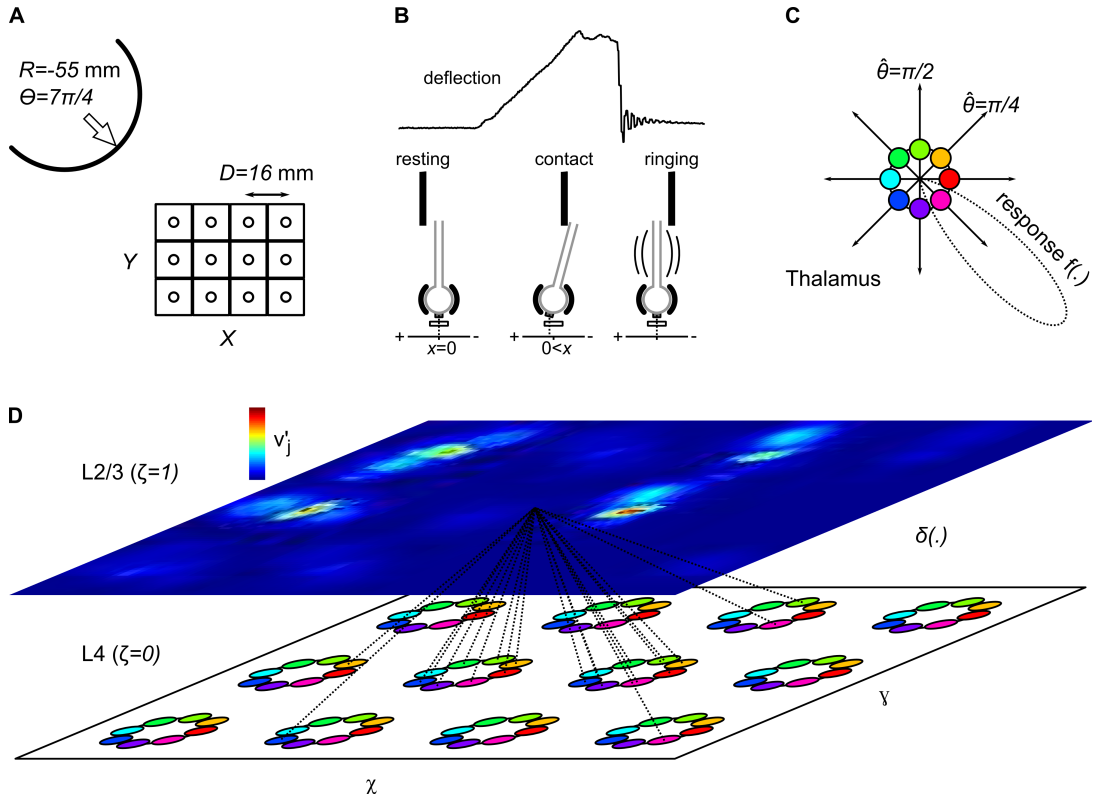

Figure 4.2. Model overview. **A** Robot-controlled stimulation of an array of artificial whisker sensors, viewed from above. The large convex stimulus edge is shown in its starting position to the northwest of an array of 4 by 3 whiskers, with the subsequent motion direction indicated by the large arrow. **B** Mechanism for measuring whisker deflections on the X–axis. When the whisker is at rest (left), a magnet at the whisker base (dark grey rectangle) is aligned to a Hall-effect sensor in the casing below (white rectangle; alignment indicated by dashed line). Upon contact with the stimulus (solid black), the whisker rotates to the right in its casing (black arcs), displacing the magnet to the left and yielding a positive voltage. Typically, at the contact offset the whisker oscillates at high frequency (ringing), as reflected in the recorded whisker deflection signal shown above ($x(t)$). **C** Encoding whisker deflections. Eight, directionally sensitive thalamic neurons (coloured circles indicate the deflection preference) respond maximally when the whisker is deflected in their preferred direction at high-velocity; $f(.)$ is largest for neurons aligned to the whisker deflection at $7\frac{\pi}{4}$ (dotted curve), and these neurons are more likely to reach the spiking threshold. **D** Architecture of the cortical model. Pre-synaptic L4 neurons inherit the stimulus selectivity of their thalamic counterparts, and are arranged in L4 so that whisker identity and deflection direction are somatotopically represented. The L4 connectivity between L4 and L2/3 is all-to-all but we show a few connections to one example L2/3 neuron, of length given by $\delta(.)$ (see Equation 4.5). A response in L2/3 to this stimulus ($S = 7\frac{S_{max}}{10}$; see Equation 4.1), consisting of individual neuron spike probabilities (v'_j; see Equation 4.8) ranging from 0 to 0.7 as shown in the colour key.

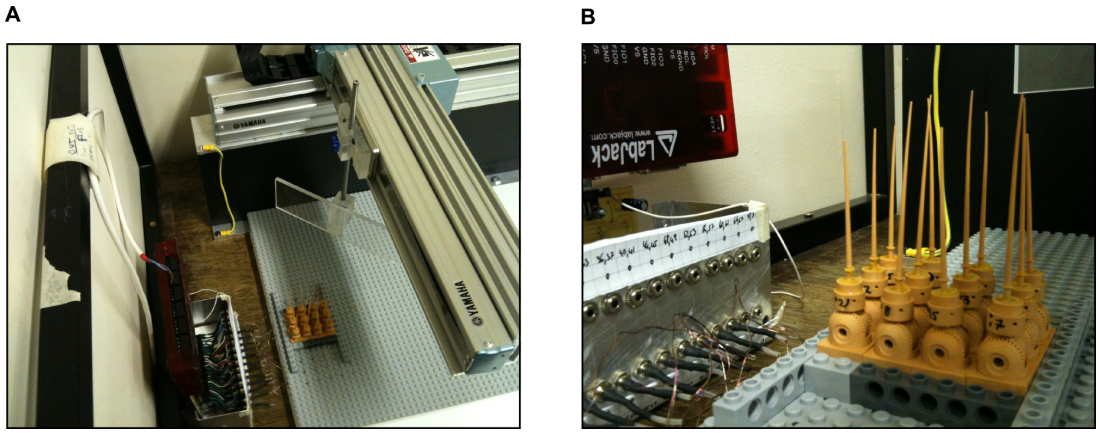

Figure 4.3. Setup and apparatus. **A** Twelve artificial whisker sensors were deflected by the movement of a straight edge tactile stimulus ($R = \infty$, shown, is a transparent rectangle) suspended by a pole from a platform attached to a table-top XY–positioning robot (X and Y axes correspond to the two arms labelled 'YAMAHA'; Yamaha$^{\mathrm{TM}}$). The stimulus was rotated on the pole so that its edge was perpendicular to the forthcoming stimulus movement ($\Theta = 5\frac{\pi}{4}$, or from-northeast-to-southwest in this example). **B** The whiskers were arranged in a 4 columns by 3 rows array; each whisker was designed to interface independently with a standard Lego$^{\mathrm{TM}}$ base. Multi-whisker deflection signals were collected via a custom-made electronic interface with a commercial LabJack$^{\mathrm{TM}}$ data acquisition card, and stored on a desktop computer.

values when the semi-circle is oriented so as to be convex relative to the whiskers, positive values when it is concave, or infinite when it is a straight edge. The five stimulus radii were thus $R \in \{-33, -55, \infty, 55, 33\}$, expressed in mm.

Before each robot movement began, the stimulus was rotated on the robot platform (by hand) so that its edge was oriented perpendicular to the forthcoming robot movement direction. Eight categories of robot movement direction were used; $\Theta \in \left\{1\frac{\pi}{4}, 2\frac{\pi}{4}, ..., 8\frac{\pi}{4}\right\}$, with angle Θ increasing anticlockwise from the positive X–axis. For example $\Theta = 7\frac{\pi}{4}$ describes a movement of the stimulus from a northwest to a southeast location, as depicted in Figure 4.3A.

The maximum movement speed allowed by each robot motor was $S_{\max} = 720\,\mathrm{mm/s}$. Ten categories of scaling on this maximum speed were used; $S \in \left\{1\frac{S_{max}}{10}, 2\frac{S_{max}}{10}, ..., 10\frac{S_{max}}{10}\right\}$. Due to intrinsic characteristics of the robot control system, the scaling was applied to the robot motors controlling translation in X and Y independently, thereby increasing the actual speed of movement $S' = S(|\cos\Theta| + |\sin\Theta|)$ by a factor of $\sqrt{2}$ for diagonal trajectories.

The geometry of whisker-stimulus interactions can be summarised by the following model, which describes the (relative) time at which the stimulus edge should make first contact with the $w\mathrm{th}$ whisker. Conceptually, we first rotate the coordinates of the whisker array to align the whiskers to the direction of stimulus movement, defining $\Theta' = -\Theta - \frac{\pi}{2}$, and obtaining $X'_w = X_w \cos\Theta' - Y_w \sin\Theta'$ and $Y'_w = X_w \sin\Theta' + Y_w \cos\Theta'$. Then, to represent the stimulus edge, we draw a semi-circle on the new Y'–axis, and divide the distance of each whisker from the semi-circle, along Y', by the robot movement speed, to obtain relative contact times:

$$T_w(R, \Theta, S) = \frac{\mathrm{sgn}(R)\sqrt{R^2 - {X'_w}^2} - Y'_w}{S'}, \tag{4.1}$$

where $\mathrm{sgn}(.)$ is the signum function.

4.2.3 Measuring whisker deflections

Each artificial whisker sensor operates like a traditional computer joystick (Figure 4.2B). When the whisker is moved from its resting axis, a magnet attached to its base is displaced relative to a Hall-effect sensor mounted in the casing below (Sullivan et al., 2011, see also Evans et al., 2010). When the whisker is moved to the right, the magnet moves to the left, and this registers as a positive voltage on a sensor aligned to the X–axis. Movement of the whisker to the left results in a negative voltage on the X–axis sensor, and equivalent whisker movements forwards or backwards result in positive or negative voltages respectively on a sensor aligned to the Y–axis. When the whisker is at rest (i.e., pointing vertically), zero voltage is registered on both axes. Voltages on each axis $V_{x,w}(t)$ and $V_{y,w}(t)$ were sampled at $2\,\mathrm{kHz}$ and relayed to a desktop computer via a custom-made multiplexing circuit, interfaced with a LabJack$^{\mathrm{TM}}$ data acquisition card (model UE9, http://labjack.com).

The voltages, $V_{x,w}(t)$ and $V_{y,w}(t)$, are approximately linearly related to the angles of deflection of the whisker, w, parallel with the X and Y axes respectively (Sullivan et al., 2011). For simplicity, we assume linearity, and define the whisker deflection signals as $x_w(t) = V_{x,w}(t)$ and $y_w(t) = V_{y,w}(t)$. The switch to lower case corresponds to the transition from physical

space to model space.

An initial validation of the dataset required a description of the variability between the sensor measurements and those that might result from a noiseless methodology and/or apparatus; the variability should indicate where systems for recognising the tactile stimulus parameters may fail. To this end, we estimated time differences between whisker deflections Δt_{ab}, for $\binom{12}{2} = 66$ pairs of whiskers labelled a and b, as the time-lag where the cross-correlation between the deflection magnitudes of whiskers a and b was maximal. We note that this analysis requires no *a priori* assumption about the deflection signals, unlike alternatives that might compare the times at which particular features in the signals occur; e.g., by comparing arbitrary threshold crossing times. Estimates were compared to those expected based on Equation 4.1, using either the standard deviation (σ) or mean deviation (μ) between Δt_{ab} and $T_a - T_b$.

4.2.4 Subcortical pre-processing of whisker movements

Neurons in the thalamic ventral posteromedial nucleus (VPM), which provide the main afferent drive to the barrel cortex, can be categorised in terms of their spatial-temporal receptive fields; they will spike maximally in response to a specific profile of movement on a particular combination of whiskers (Petersen et al., 2008). VPM neurons of one category spike selectively when a particular whisker, known as the principal whisker, is deflected at high velocity in a preferred direction (Petersen et al., 2008; Bale and Petersen, 2009). To model the differential-filtering operation performed by these neurons (Figure 4.2C), we first compute:

$$\dot{x}_w(t) = \sum_{k=1}^{10} x_w(t - k\tau) - \sum_{k=11}^{20} x_w(t - k\tau), \tag{4.2}$$

where the integration time-step was $\tau = 0.5\,\mathrm{ms}$, and the width of the filter ($10\,\mathrm{ms}$) removes the high-frequency component of the signals. A similar operation is applied to obtain $\dot{y}_w(t)$, and $\dot{x}_w(t)$ and $\dot{y}_w(t)$ are converted to polar coordinates to obtain the deflection magnitude $\dot{r}_w(t)$ and the deflection direction $\dot{\theta}_w(t)$. Next, the (binary) occurrence of spikes in 8 thalamic neurons per whisker, indexed by i, and with preferred deflection directions $\hat{\theta}_i \in \left\{1\frac{\pi}{4}, 2\frac{\pi}{4}, ..., 8\frac{\pi}{4}\right\}$, is determined by:

$$f(w, i, t) = \mathrm{H}\left(\dot{r}_w(t)\frac{e^{\alpha\cos\left(\dot{\theta}_w(t) - \hat{\theta}_i\right)}}{e^{\alpha}} - \beta\right), \tag{4.3}$$

where $\mathrm{H}(.)$ is the Heaviside step function, $\alpha = 20$ sets the directional selectivity of the thalamic neuron, and $\beta = 0.2$ sets the binary spike threshold. Finally, a record of the time since the most recent spike is maintained for each thalamic neuron at runtime. Spikes occur when the velocity of the signal, in the direction preferred by the neuron, changes from being below threshold to above threshold, i.e., at the rising edge of the signal according to:

$$t'_{w,i}(t) = \begin{cases} 0 & \text{if } f(w, i, t) - f(w, i, t - \tau) = 1 \\ t'_{w,i}(t - \tau) + \tau & \text{else} \end{cases}, \tag{4.4}$$

where $t'_{w,i}(0) = \infty$. For Equation 4.4, and hereafter, the integration time-step was $\tau = 5\,\mathrm{ms}$.

4.2.5 Mapping whisker deflections to response patterns in the barrel cortex

At the scale of cortical columns, activity in the barrel cortex reflects the spatial arrangement of stimulated whiskers of the face (Welker, 1964; Woolsey and van der Loos, 1970). At the sub-columnar scale, several studies (Andermann and Moore, 2006; Tsytsarev et al., 2010; Kremer et al., 2011), and results of a computational model developed in our lab (Wilson et al., 2010), have suggested that the representation of the whisker deflection direction varies systematically within the barrel column, such that deflection of the principal whisker toward an adjacent whisker selectively activates neurons located closer to the corresponding adjacent barrel. At the inter-columnar scale, several studies (Shimegi et al., 1999, 2000; Armstrong-James et al., 1992; Feldmeyer et al., 2002; Helmstaedter et al., 2008), and results of a computational model developed in our lab (Wilson et al., 2011), suggested that layer 2/3 (L2/3) barrel cortex neurons receive synaptic inputs after delays proportional to the straight-line distance of the cell body from regions of each barrel in layer 4 (L4) that correspond to the direction in which the principal whisker is deflected. Based on these two models, and in particular by extending the model of Wilson et al. (2011) to represent L2/3 activity patterns on a full cortical sheet, we construct here a simplified intra-cortical connection geometry to simulate the functional connectivity implied by these observations (see Figure 4.2D).

According to the model, L4 neurons directly inherit their tuning to a particular whisker stimulus from a single thalamic neuron. Therefore L4 neurons are also indexed by a preferred whisker w and a preferred deflection direction i, and L4 spike times are generated according to Equation 4.4. In the model, the only difference between the thalamic and L4 neurons is in an

ordered spatial layout of L4 neurons across a cortical sheet. L4 neurons are located in the plane $(\chi, \gamma, \zeta = 0)$, which represents the plane tangential to the surface of the brain. The axes of the cortical $\chi\gamma$–plane reflect that of the physical XY–plane, such that the center of the barrel column corresponding to the $w\text{th}$ whisker is located at coordinates $\chi_w \in \{-1.5, 0.5, 0.5, 1.5\}$ and $\gamma_w \in \{-1, 0, 1\}$. For each whisker an outwardly-radiating pinwheel arrangement of eight neurons is specified in L4, according to the preferred deflection directions of the L4 neurons, such that the L4 neuron is located at coordinates $(\chi_{w,i} = \chi_w + \rho\cos\hat{\theta}_i, \gamma_{w,i} = \gamma_w + \rho\sin\hat{\theta}_i, \zeta = 0)$, where $\rho = 0.25$ is the distance of the neuron from the corresponding barrel center.

A sheet of 120 by 90 L2/3 neurons L2/3 (indexed by j) are spaced at regular intervals on a two-dimensional grid in a plane parallel to (and directly above) L4, at $(\chi_j \in [-2, +2], \gamma_j \in [-1.5, +1.5], \zeta = 1)$. The intra-cortical geometry is expressed in Equation 4.5, which describes the straight-line distance between the pre-synaptic L4 neuron and the post-synaptic L2/3 neuron:

$$\delta(w, i, j) = \eta\sqrt{(\chi_{w,i} - \chi_j)^2 + (\gamma_{w,i} - \gamma_j)^2 + 1}. \tag{4.5}$$

The scaling factor $\eta = 0.4\,\text{mm}$ is used to simulate the dimensions of cortical tissue, based on the spacing between cortical columns in the barrel cortex. According to Equation 4.5 the model assumes strong relationships between the physical space in which the whiskers exist, whisker deflection signal space, and the physical space in which the neurons exist. Nevertheless, we use different notation (e.g., X, x, χ) for coordinates in each space to highlight that the relations between these spaces are not necessarily simple.

Parameters for the temporal processing of the signals reported in the remainder of this section were taken from our biological-scale model (Wilson et al., 2011), and then scaled by a factor of ten to reflect the larger dimensions of the artificial whisker array and an expected increase in typical inter-whisker deflection intervals, compared with biological whisker arrays. According to the model, the time at which a synaptic potential arrives at a L2/3 neuron depends on whether the potential originated from an excitatory or an inhibitory L4 neuron, and we define the time since the onset of the pre-synaptic conductance change as:

$$\lambda(w,i,j,t) = t'_{w,i}(t) - \delta(w,i,j)/s - c, \tag{4.6}$$

where $s = 10\,\mathrm{mm/s}$ is the axonal propagation speed for an excitatory connection (i.e., $100\,\mathrm{mm/s}$ in the biological scale model) and $s = 30\,\mathrm{mm/s}$ for an inhibitory connection and $c = 37\,\mathrm{ms}$ is a constant synaptic onset delay for inhibitory connections (i.e., $3.7\,\mathrm{ms}$ in the biological-scale model) and $c = 0$ for excitatory connections. The time-course of each synaptic potential is modelled as a difference of two exponentials, by:

$$p(\lambda,t) = b(e^{-\lambda/\tau_1} - e^{-\lambda/\tau_2})\mathrm{H}(\lambda), \tag{4.7}$$

where b is a normalisation term ensuring that the potential peaks at unity (see Dayan and Abbott, 2001; Puccini et al., 2006; Sarid et al., 2007; Wilson et al., 2011). For excitatory synapses $\tau_1 = 10\,\mathrm{ms}$ and $\tau_2 = 2.2\,\mathrm{ms}$ and for inhibitory synapses $\tau_1 = 40\,\mathrm{ms}$ and $\tau_2 = 30\,\mathrm{ms}$. L2/3 barrel cortex neurons are modelled as leaky integrators (Kyriazi and Simons, 1993; Wilson

et al., 2011), by:

$$v_j(t) = v_j(t-\tau) + \left(\sum_{w,i,\pm} gp(\lambda) - v_j(t-\tau) \right) \frac{\tau}{\tau_m}, \tag{4.8}$$

where $\pm$ here denotes summation over one excitatory and one inhibitory connection from each location in L4, $g = 1$ for excitatory synapses and $g = -0.5$ for inhibitory connections, and $\tau_m = 120\,\mathrm{ms}$ is the membrane potential decay constant. Hence $v_j(t)$ represents the L2/3 neuronal membrane potential after spatial integration and temporal integration of synaptic inputs (see Kyriazi and Simons, 1993). Finally, the output of each L2/3 neuron j is squashed using the logistic activation function to generate a probability of the occurrence of a spike:

$$v'_j(t) = \left(1 + e^{[0.2 - v_j(t)]/0.04}\right)^{-1}, \tag{4.9}$$

where Equation 4.9 was parameterised to simulate the non-linear responses of L2/3 barrel cortex neurons (see Wilson et al., 2011). The maximum value $v'_{j,\mathrm{trial}} = \max_t v'_j(t)$, for all t in a time window including only the whisker displacements affected by one tactile stimulus (i.e., one trial), was used as a proxy for the overall probability that neuron j would spike in response to the tactile stimulus presented in a given trial; following Wilson et al. (2011).

4.2.6 A matched control for evaluating the cortical (L2/3) mapping

To establish a baseline, against which to evaluate the cortical mapping, we defined a control mapping based on the cross-correlation function. Pairwise cross-correlations between 24 whisker displacement signals $x_w(t)$ and $y_w(t)$ were computed using each of $N_{\text{pairs}} = \binom{24}{2} = 276$ signals. The 276 cross-correlation vectors were sampled at $5\,\text{ms}$ intervals for time-lags in the range $\pm 95\,\text{ms}$. This gave reasonable coverage over the range of latencies between whisker deflections in the data, and we note that classification performance (see below) did not improve significantly for different choices of sampling frequency. The total number of features sampled in this way ($276 \times 39 = 10,764$) was comparable to the number of neurons in the cortical model (10,800 L2/3 neurons). Hence this transformation of the whisker displacement signals served as a control, matched to the output of the cortical model by dimensionality and by type; in both the control and cortical mappings, signals from multiple whiskers are offset by a series of time-lags before being integrated non-linearly to compute relative whisker deflection times.

4.2.7 Classification procedure and performance

The extent to which activity in the network encoded the parameters of the tactile stimuli was assessed by training and testing a linear classifier to recognise the stimulus parameters from the cortical responses. Multiple linear regression was used to estimate the stimulus shape (R), direction (Θ), or speed (S), using either the activity of L2/3 barrel cortex neurons ($v'_{j,\text{trial}}$) or the values of the control mapping as features.

Due to the small number of realisations of each stimulus parameter, a ‘leave one out’ design was

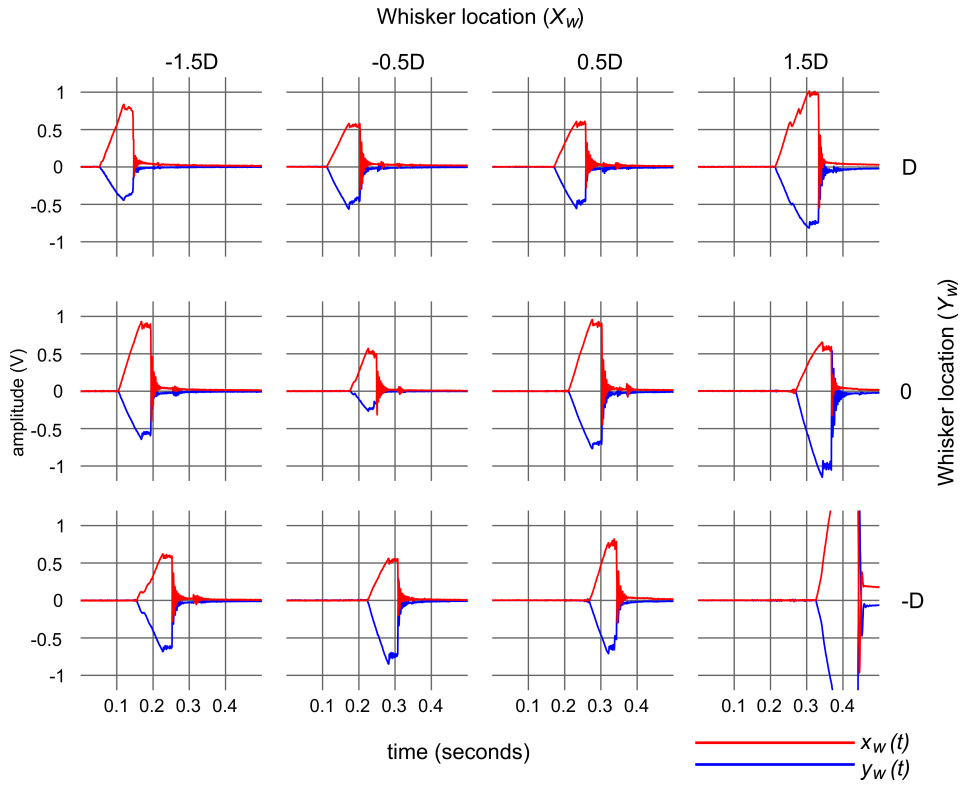

Figure 4.4. Raw artificial whisker deflection signals. Data shown are from a single collision between a straight edge tactile stimulus ($R = \infty$) and 12 artificial whiskers. The panels are arranged to reflect the spatial layout of the whiskers in their array positions. The whiskers were deflected by the sweep of an edge stimulus travelling at 0.2 meters per second in a south-easterly direction ($\Theta = 7\frac{\pi}{4}$). The whisker signals vary accordingly with positive voltages measured on the X–sensor channels (red) and negative voltages on the Y–sensor channels (blue). In particular, the onset time of the deflections progresses in time, starting at the whiskers located in the northwest and progressing through to the southeast array positions. Note the variability in response magnitude between whiskers, caused by differences in the degree of damage (during pilot work) to the rubber seal which holds the whisker shaft to its resting axis. Whilst the signals could have been renormalised post-hoc, both the cortical and control processing of these signals would be unaffected by normalisation (i.e., both operate on correlations between the signals and should not be sensitive to their absolute values); thus we present the original un-normalised amplitudes as they were processed by the model.

employed. Data from one of the five realisations in each condition (i.e., a total 400 patterns) was designated as the test set, and the remaining 1,600 patterns were the training set. This procedure was repeated using each of the 5 realisations as test data, and performance measures were averaged across realisations.

To avoid problems of multicollinearity, i.e., over-fitting due to a large ratio of features to test conditions, classification was performed using subsets of the features selected at random. Linear regression was performed on subsets consisting of progressively more features. A vector of regression weights was obtained using simple multiple linear regression. After rounding the linear regression estimates to the nearest class label, performance in classifying each stimulus parameter was measured as either the percentage of correct classifications, or by using an appropriately weighted Cohen's κ statistic (Cohen, 1968) to test the agreement between the actual and estimated classes:

$$\kappa = \frac{\sum_{ij} \mathbf{O}_{i,j}\mathbf{W}_{i,j} - \sum_{ij} \mathbf{E}_j\mathbf{W}_{i,j}}{1 - \sum_{ij} \mathbf{E}_j\mathbf{W}_{i,j}}, \tag{4.10}$$

where the square covariance matrix $\mathbf{O}_{i,j}$ is indexed by columns of actual class $i \in \{1, 2, ..., n_{\text{classes}}\}$ and rows of estimated class $j \in \{1, 2, ..., n_{\text{classes}}\}$, with entries normalised by a total 2,000 test patterns; $\mathbf{E}_j = \sum_{i=1}^{n_{\text{classes}}} \mathbf{O}_{i,j}/n_{\text{classes}}$ represents expected values. Weights, $\mathbf{W}_{i,j}$, for classification in ordinal spaces (i.e., R and S), or circular spaces (i.e., Θ), were $\mathbf{W}_{i,j} = 1-|i-j|/(n_{\text{classes}}-1)$, or $\mathbf{W}_{i,j} = |1 - 2|i - j|/n_{\text{classes}}|$, respectively. These weightings ensure higher values of κ (approaching maximum $\kappa = 1$) where misclassifications were more similar to the actual class.

4.3 Results

4.3.1 A dataset of artificial whisker deflection signals

Data were collected from an array of 12 artificial whiskers, stimulated by 5 differently shaped objects (R), moving in 8 different directions (Θ), each at 10 different speeds (S). Every collision was realised 5 times so that data from 2,000 separate multi-whisker collisions were collected in total. The raw data for each collision consisted of 24 time series ($x_w(t)$ and $y_w(t)$), which represent the amplitude of the whisker deflections from their resting positions in X and Y axes. Figure 4.4 shows an example of the raw data collected from a single collision between the whiskers and the straight edge moved at $S = 2\frac{S_{\max}}{10}$, in direction $\Theta = 7\frac{\pi}{4}$.

To explore the dataset, measured whisker deflection times were compared with those expected based on the geometry of whisker-stimulus interactions as defined by Equation 4.1 (see Figure 4.5). Values of μ were fit by a linear regression onto the inter-whisker interval. In ascending order, the slopes were 3.2% for the large convex shape, 10.7% for the straight edge, 11.2% for the large concave edge and the small concave edge, and 15.2% for the small convex edge. Similar fits for σ yielded, in ascending order, 26.1% for the straight edge, 33.5% for the large concave edge, 34.5% for the large convex edge, 55.2% for the small concave shape, and 63.2% for the small convex shape. The fits indicate first, that there was considerable noise in the relative whisker contact times (indicated by large σ), second that the robot was moving slightly faster than expected (indicated by $\mu > 0$), and third that the levels of noise were fairly similar amongst the five stimulus shapes.

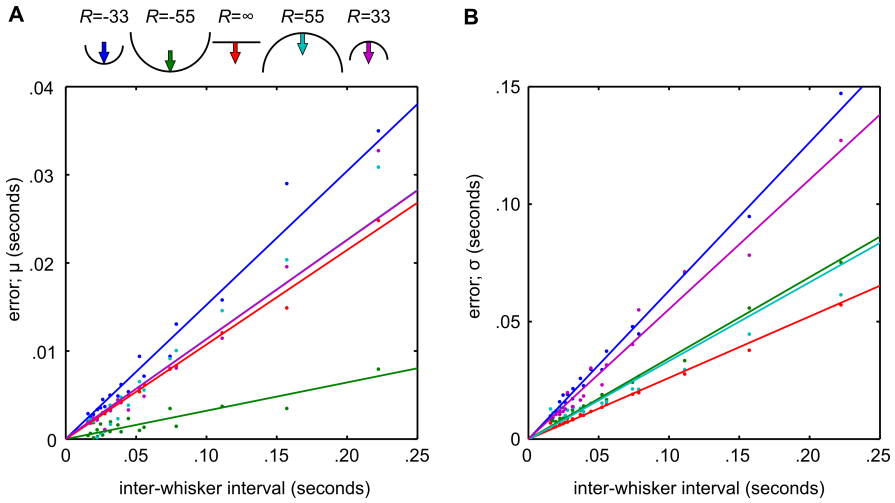

Figure 4.5. Deviation of between-whisker time differences from those predicted by the geometry. A Mean difference, μ, (expected temporal offset minus measured temporal offset) across sixty-six unique pairs from the twelve whiskers, shown as a function of the expected time taken for the robot to traverse the inter-whisker distance D. Time on both axes is measured in seconds. Each line is a linear fit to the data from twenty unique stimulus speeds collected using one of the stimulus shapes (as indicated by the shape key). For each shape the mean difference decreases as the stimulus speed increases (slower stimuli take more time), suggesting that our measurements based on the modal value of the cross-correlogram between each pair of signals underestimated the true time differences. **B** Error from the same data computed as the standard deviation of the measured time differences from those predicted from the geometric model, σ. Again, for each shape the error is greatest for the slower stimulus speeds where the expected time differences are largest. Linear regression fits to the error using both quantifications suggest that the smaller semi-circular object (dark blue and pink lines) yielded the most error. Data collecting using the small semi-circles ($R = \pm 33\,\mathrm{mm}$) are shown after discounting all measurements that included a whisker snapped during data collection.

4.3.2 Encoding whisker movement in cortical and control activity patterns

Movements of the whiskers were encoded as activity patterns, using a model of the responses of L2/3 barrel cortex neurons to paired deflections of adjacent whiskers, which vary as a function of the whisker identity, deflection direction and the interval between deflections. The model generates spatial patterns of activity across the cortical sheet, where the response of a neuron to a particular stimulus is determined by its location.

To generate activity patterns the whisker deflections were propagated through the model, and for each tactile stimulus the L2/3 response vector, $v'_{j,\mathrm{trial}}$, was computed for each of the 2,000 stimulus trials. Example response patterns are shown in Figure 4.6, which reveals that the spatial distribution of activity patterns across simulated L2/3 barrel cortex varies systematically with respect to R, Θ, and S.

The patterns consisted of small patches of activity distributed around the cortical column centers. The patches each had a characteristic ellipse-like shape (Figure 4.7), and we henceforth refer to the shape of the patches as ellipses. In the majority of cases, a central ellipse representing high activity was surrounded by two larger ellipses of less-responsive neurons. The major axes of the ellipses tended to be oriented perpendicular to a line drawn between nearby activated L4 neuron pairs, which for the bar stimulus corresponded with the direction of motion (Θ); the centers were shifted to fall between the centers of columns corresponding to consecutively stimulated whiskers (see Figure 4.7). The faster stimuli (larger S) tended to produce more ellipses and larger responses, and, for slower stimuli, more highly-active ellipses appeared between

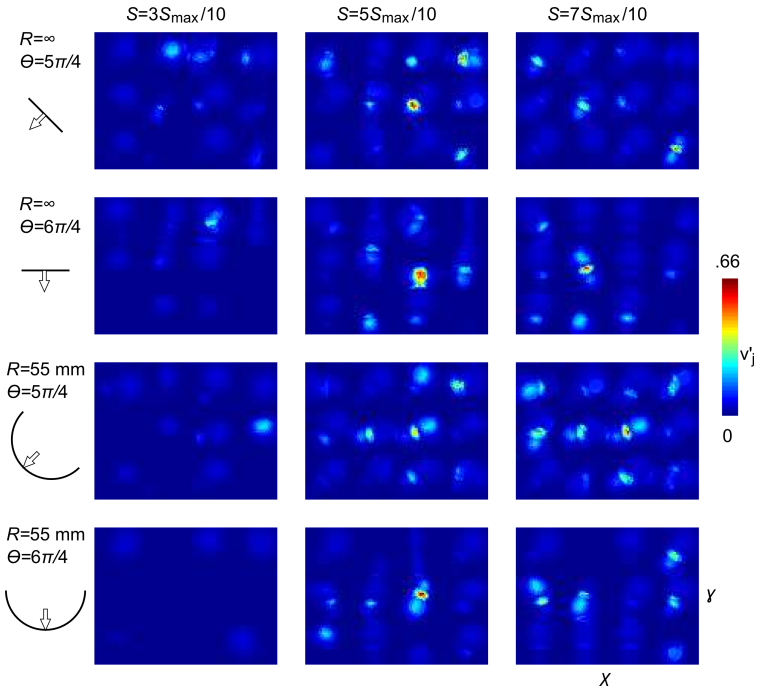

Figure 4.6. Layer 2/3 activity patterns. Each panel shows a representative activity pattern in L2/3 barrel cortex in the $\mathbf{x}, \mathbf{y}$–plane, as presented for classification (after downsampling). Patterns were obtained by propagating the 12 whisker deflections signals through the network, and storing the maximum response for each neuron over time (v'_j; one pixel corresponds to one neuron). The patterns shown were obtained by using the straight edge stimulus or the large convex stimulus moving in one of two directions (rows), at three increasing speeds (columns). See the text for a description of how cortical responses vary systematically with the associated tactile stimulus parameters.

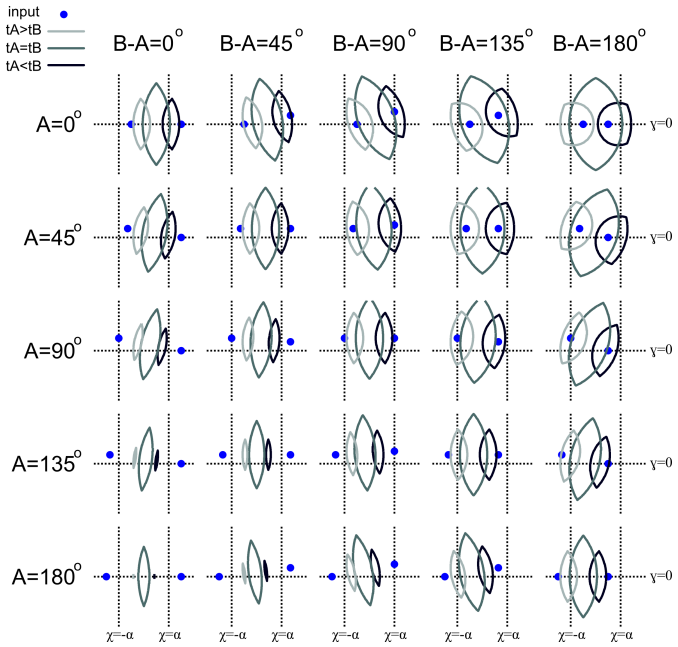

Figure 4.7. Characterising the L4 to L2/3 mapping. To investigate how the whisker deflections map to activity pattern across the L2/3 sheet, we simulated isolated deflections of two adjacent whiskers (A and B) by stimulating pairs of L4 units (blue circles) pertaining to two adjacent barrel columns. Then, across the L2/3 sheet, we traced the region in which both excitatory inputs precede both inhibitory inputs, known as the 'facilitatory zone' after Wilson et al. (2011). By varying the simulated stimulus movement direction, rightward movement in the plane perpendicular to the alignment of whiskers evoked facilitatory zones delineated by contours labelled $tA < tB$, leftward movement evoked $tA > tB$ contours, and coincident deflections evoked $tA = tB$ contours. To simulate the range of stimulus orientations we varied the angle of whisker A deflection (denoted A; varying between the rows of panels), and the difference in angle between whisker A and B deflections (denoted A-B; varying between columns). Facilitatory zones, in which we expect to see the largest L2/3 neuronal responses, had ellipse-like shapes, whose size and orientation varied systematically with the simulated stimulus movement parameters.

barrels representing whiskers displaced earlier by the stimulus. Compared with a more regular organisation generated by straight edge stimuli, curved stimuli (smaller $|R|$) yielded more irregular patterns. This is likely due to the presence of a broader range of different whisker deflection directions within a given pattern, and hence a less uniform spacing of the active input neurons in L4.

4.3.3 Recognition of tactile stimulus shape, direction and speed from cortical versus control patterns

The classification performances for stimulus shape, direction, and speed, using either the percentage correct (Figure 4.8) or the Cohen's κ (Figure 4.9) metrics are summarised in Table 4.1.

The classification of tactile stimulus shape R from control patterns was reasonable (see Figure 4.9A), but 800 features were required to obtain this performance. The maximum performance, after averaging across 10 combinations of randomly selected features at each $N_{\text{features}} \in \{10, 20, ..., 1000\}$, was $\kappa = 0.40$ for $N_{\text{features}} = 880$. In contrast, performance on the recognition of the tactile stimulus shape was improved for classification based on the cortical response patterns, reaching a maximum $\kappa = 0.47$ for $N_{\text{features}} = 570$. Control performance increased slowly as a function of increasing N_{features} to an asymptote when more than 800 features were available. In comparison, performance based on the cortical patterns increased sharply, reaching near-maximum levels for around 500 neurons, and then tailed off, presumably as a reflection of the classifier over-fitting to the training set and thus not being able to generalise to the test set.

The procedure performed less well for classification of tactile stimulus direction Θ based on

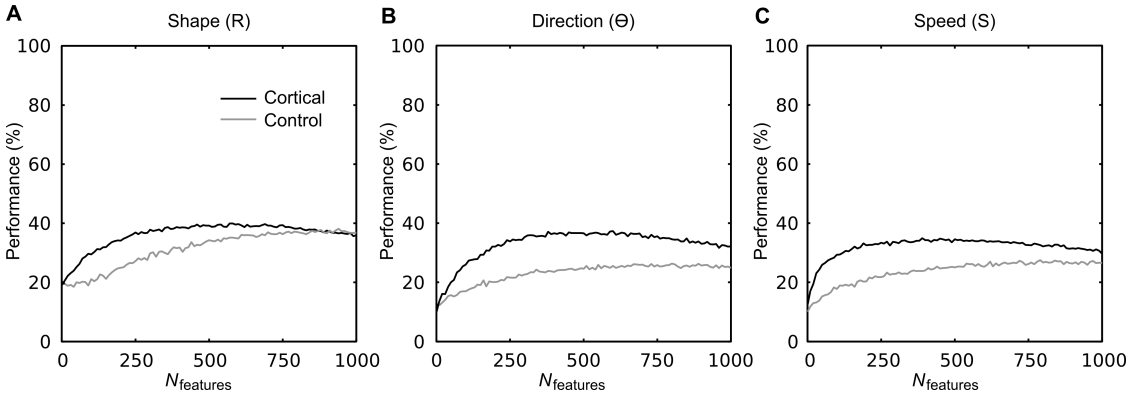

Figure 4.8. Percentage of correct classifications. A linear classifier was trained to recognise tactile stimulus shape, speed, or direction, based on either the cross-correlations between whisker displacement patterns (used as a control), or on cortical response patterns generated via the barrel cortex model. The percentage of correct classifications is plotted as a function of the number of randomly chosen features (or neurons) available to the classifier. Accuracy increased as a function of the number of available features, and it was consistently better when processing cortical versus control mappings of the whisker displacements. As the number of available features increased, performance peaked before tailing-off for cortical patterns, and increased towards asymptotes for the control patterns. Overall accuracy levels were quite low for the classification of stimulus shape **A**, direction **B** and speed **C**. The trends here were more exaggerated when using the κ measurement, which also takes into consideration the difficulty of the task and the distribution of classification errors (see Figure 4.9).

the control patterns, and performance scores were less than for the shape (see Figure 4.9B). A lower maximum at $\kappa = 0.29$ was obtained for a similar $N_{\text{features}} = 810$. However, classification performance for direction using cortical patterns reached a higher maximum using fewer features. Again, as N_{features} was increased, performance either reached an asymptote or tailed off, for the control and cortical conditions respectively.

Classification of stimulus speed, S, based on the cortical patterns, was better than for control patterns, as measured by the maximal κ. For control patterns, similar scores were reached when anything upwards of 600 features were used (see Figure 4.9C). For cortical patterns 200 or more features yielded similar levels of performance.

Similar trends, with higher classification scores obtained using cortical versus control mappings, were observed in terms of the percentage of class labels identified correctly (see Figure 4.8 and Table 4.1). Of course, these scores do not reflect the difficulty of the respective classification tasks as they do not account for the number of classes involved in each, but the fact that they display similar trends to those for κ scores adds support to conclusions based on the more informative performance measure, κ.

In summary linear classification performance based on a cortical transformation of the whisker displacement data was very much better than chance, and better than that based on a control transformation matched for type and dimensionality, at classifying previously unseen tactile stimuli.

Table 4.1. Summary of classifier performance.

Tactile stimulus	%		$\max \kappa$ at N_{features}	
	control	cortical	control	cortical
Shape	38	40	0.40@880	0.47@570
Direction	26	37	0.29@810	0.56@480
Speed	28	35	0.57@720	0.70@450

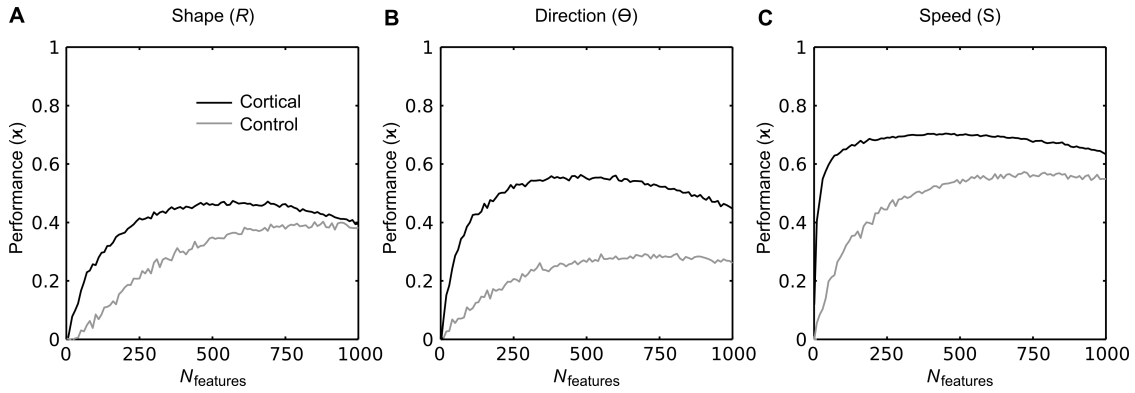

Figure 4.9. Recognising tactile stimuli. The trends in classification performance, as measured by the percentage of correct classifications, were reflected in similar trends based on the weighted Cohen's κ score, computed from the covariance matrices. Scores are the average of ten randomisations. **A** Linear classification performed remarkably well at recognising stimulus shape from the cortical data, peaking when 570 features were available at a mean performance: weighted $\kappa = 0.47$. **B** Classification of the stimulus direction, based on the cortical activation patterns, was maximal when 480 features were available: weighted $\kappa = 0.56$. **C** Classification of stimulus speed, based on the cortical responses, was maximal when 450 features were available: weighted $\kappa = 0.70$.

4.3.4 Insights from the classification errors

To understand how the cortical mapping represented the tactile stimuli, we inspected the distribution of errors in the confusion matrices for the best classifiers with respect to each stimulus parameter.

In terms of the stimulus form, as evident in Table 4.2, a curved edge was rarely mistaken for an edge of the same size curved in the opposite direction. This is interesting because, according to the geometry expressed in Equation 4.1, the distribution of Δt_{ab} amongst whisker pairs should be identical in both cases. In order for the classifier to disambiguate stimuli of opposite curvatures, the cortical mapping must have retained spatial information about the different multi-whisker deflection patterns, relating to the directions of whisker deflection and/or the identity of whiskers that were deflected earlier by the stimulus. Retention of these spatial features is to be expected, given their explicit mapping by the location of corresponding input neurons in simulated L4.

In terms of stimulus motion, the pattern of errors for the robot direction (see Table 4.3) revealed the fundamental problem of challenging a linear classifier to discover an inherently circular topology associated with Θ. This was shown by the fact that mistakes when the robot motion direction was of class 1 (arbitrarily assigned to $\Theta = 1\frac{\pi}{8}$) never mistakenly estimated the stimulus to be of class 8 ($\Theta = 8\frac{\pi}{8}$), and vice-versa, despite these classes representing adjacent parameterisations of the robot motion in circular space. Classification performance for direction could be improved significantly using a non-linear classifier; confusion matrices obtained using a parallel perceptron classifier, trained via the parallel-delta learning rule as described by Auer et al. (2008), displayed misclassification errors that wrapped around the circular space repre-

Table 4.2. Confusion matrix for the best classifier trained to recognise stimulus shape from cortical response patterns ($N_{\text{features}} = 570$). Values are the number of hits for each actual and estimated class of stimulus shape. Classes are labelled by a symbol indicating the corresponding stimulus shape, as if it were moved in the direction of the arrow. The classification performance was $\kappa = 0.44$ and 39% patterns were recognised correctly.

Estimated	Stimulus shape (R)				
$\rightarrow$	)	)	|	(	(
)	146	68	18	2	1
)	136	161	106	27	15
|	96	129	185	142	80
(	20	34	78	151	168
(	2	8	13	78	136

sented by Θ. Accordingly, performance of $\kappa > 0.8$ for $N_{\text{features}} \approx 600$ could be achieved using this non-linear classifier. We note that significant performance increases could not be obtained for shape and speed classification using the non-linear classifier, at least in our hands, and so we do not detail the procedure used for non-linear classification here. For stimulus speed, misclassification errors appeared to be more widely distributed amongst the classes as the speed increased (see Table 4.4), which is probably a reflection of the linear relationship between the stimulus speed and the variability amongst Δt_{ab}, as revealed in Figure 4.5.

4.4 Discussion

We mapped a variety of tactile stimuli to neuronal activity at discrete locations on a two-dimensional cortical sheet. The mapping was by non-linear temporal integration of signals communicating high-velocity multi-whisker directional-deflection times. These whisker deflection signals were offset in time by a geometry of cortical projections reflecting the physical space in which the whiskers moved. The tactile stimulus parameters were recovered by linear regression on the activity patterns, and the classification performance showed that the mapping of whisker displacements to cortical activity, by the geometry of cortical connections, retains essential information about the stimulus shape, direction and speed.

Table 4.3. Confusion matrix for the best classifier trained to recognise stimulus direction Θ from cortical response patterns $N_{\text{features}} = 480$. The classification performance was $\kappa = 0.54$ and 36% patterns were recognised correctly.

Estimated	Stimulus direction (Θ)							
$\frac{\pi}{8}\times$	1	2	3	4	5	6	7	8
1	120	62	20	2	1	1	0	0
2	57	81	45	5	4	0	0	0
3	50	81	74	35	37	7	0	3
4	19	18	76	103	58	27	10	5
5	4	6	28	80	78	61	41	15
6	0	2	6	17	47	101	65	59
7	0	0	0	6	21	41	69	74
8	0	0	1	2	4	12	65	94

4.4.1 Technical considerations

Using our apparatus the stimulus speed and direction were co-dependent. Thus the motion speed parameter, S, did not uniformly sample the underlying speed (S'), and the linear regression estimated the speed applied to each of the two robot motors from signals collected under the joint influence of both S and θ. That the regression faired as well as it did in this non-linear space was encouraging, and we anticipate improved performances using continuous parameterisations of speed in future studies.

Whilst efforts were made to record data for each stimulus in random order, in practise this was not entirely feasible. The first compromise meant collecting all data with a given stimulus shape at once, with speed and direction randomised. Because the concave and convex edges of a given stimulus radius were part of the same physical apparatus, the second compromise meant that data for oppositely curved edges were collected consecutively. After manual repositioning of the stimulus orientation for the forthcoming trial, data using the convex edge were always collected before those using the concave edge. A potential confound related to this procedure was that the whisker resting axes could have been systematically displaced before collection of all concave data. This would have introduced systematic measurement errors for the concave versus the convex stimuli, that could in principle have made them more easily separable for the classifier. Although we cannot rule out such an effect, there was no evidence for it in our estimations of the error for each shape, as presented in Figure 4.5. For both measures of error (μ and σ), errors associated with both small stimuli were greater than those for both large stimuli. Moreover the straight edge, which could have suffered from no such confound, generated levels of error in the estimation of Δt_{ab} that were comparable to those for each of the curved stimuli. Therefore we feel confident that potential confounds related to the order in which the data

Table 4.4. Confusion matrix for the best classifier trained to recognise stimulus speed class from cortical response patterns $N_{\text{features}} = 450$. The classification performance was $\kappa = 0.70$ and 35% patterns were recognised correctly.

Estiamted	Stimulus speed (S)									
$\frac{S_{\max}}{10} \times$	1	2	3	4	5	6	7	8	9	10
1	96	34	4	0	0	0	0	0	0	0
2	84	113	54	9	1	1	0	0	0	0
3	17	41	82	48	15	1	0	0	0	0
4	1	12	41	69	40	13	5	1	0	1
5	2	0	16	41	71	36	15	9	2	1
6	0	0	2	23	47	63	41	15	13	14
7	0	0	1	9	18	55	52	50	42	19
8	0	0	0	1	6	16	50	53	57	44
9	0	0	0	0	1	11	26	49	38	60
10	0	0	0	0	1	4	11	23	48	61

were collected were minimal, at least to within the accuracy of our model of whisker stimulus interactions (Equation 4.1).

Unlike naturalistic whisker experiences, the center of the stimuli always traversed the center of the whisker array, the orientation of the stimulus was always orthogonal to the direction of motion, all trajectories followed a straight line, and all movement was confined to the XY–plane. These constraints made a large range of different multi-whisker displacements reducible to just three dimensions (R, Θ, S). Relaxation of each constraint would require the introduction of at least one additional stimulus parameter. The space of stimulus parameters to explore increases further when parameters of the configuration of the whisker array are included; for example including static parameters like the spread of the whisker resting axes from vertical, and dynamic parameters like the frequency of whisking movements. Nature has selected a variety of configurations (Brecht et al., 1997); compare the bilaterally symmetric grid-like morphology of the rat whisker array (Towal et al., 2011) with the radially symmetric cone-like morphology of the Etruscan shrew array (Anjum et al., 2006). Perhaps particular morphologies are suited to the processing of particular stimulus parameters? There is scope to test such an hypothesis in the future, using our reconfigurable array of posable artificial whiskers, to compare how the range of array morphologies that occur naturally amongst tactile specialists changes the nature of multi-whisker deflection patterns.

4.4.2 Practical considerations

The raw whisker deflection signals were filtered to pick out the high-velocity components associated with whisker-stimulus contacts, with reference to the data of Petersen et al. (2008)

showing that a class of thalamic neurons are sensitive to the deflection velocity. However, these data revealed different classes of thalamic neuron, sensitive to either the absolute deflection magnitude, or to higher-order derivatives of the whisker deflection, i.e., filters for the whisker-position or whisker acceleration respectively. Filtering for the whisker-velocity picked out the whisker deflection offset events, i.e., the time at which the whisker was released after being in contact with the stimulus. Indeed it is plausible that deflection offsets accounted for more of the signal reaching the cortex than did deflection onsets. This may account for the tendency towards positive errors in the measurement μ (Figure 4.5A), wherein filtered deflections were compared with those expected from a geometry formulated to predict deflection onsets (Equation 4.1).

Data from high-speed video analyses of rat whisking behaviour suggest that when rats investigate objects they actively control whisker movements to make a 'light touch'; minimising the whisker impingement whilst maximising the number of whisker-stimulus contacts (Mitchinson et al., 2007; Grant et al., 2009). Such a strategy would minimise the velocity associated with deflection offsets, and thus neuronal responses to deflection offset would be less pronounced than those generated under our procedure using passive (stationary) whiskers (Evans et al., 2010).

Further studies will be required to investigate the contributions of alternative thalamic circuitry and whisking control strategies to the nature of signals received by cortex.

4.4.3 Potential alternative models

The mapping from the whiskers to the cortex, as represented by Equation 4.5, represents a highly simplified model of real cortical connection geometry. In the model all L2/3 neurons re-

ceive input from all L4 neurons, and they do so with equal strength. This is unlike real cortical circuitry, where for example sub-threshold activity in L2/3, as a consequence of direct stimulation in L4, decreases with the distance between the pre-synaptic and post-synaptic neuron (Adesnik and Scanziani, 2010; see also Petersen et al., 2003; Derdikman et al., 2003). Although its behaviour would be more difficult to interpret, a more accurate model would decrease the connection probability and the synaptic weight by some function (such as a Gaussian function) of the inter-soma distance.

The model also does not account for how plasticity shapes cortical circuits; for example our previous computational modelling study predicted that lateral interactions will be strongest between cortical loci that represent similar directions of deflection applied to nearby whiskers (Wilson et al., 2010). A more accurate model in this respect might introduce recurrent connections, with a profile of weights that sharpen synaptic inputs to amplify contrasts between adjacent whisker deflection directions.

Cortical activity generated in the model could be used to identify higher-order features of the tactile stimuli based on the multi-whisker deflection patterns, by forming representations that were invariant to the position of the stimulus in the whisker array at any given time. It may be worth considering whether the cortical mapping can maintain information about the absolute position of the stimulus. We observed that due to the somatotopy-preserving mapping, regions of the cortical sheet became active in a sequence closely related to that in which the individual whiskers were deflected, and hence the absolute position of the stimulus was retained in the gross dynamics of the network. However, we did not investigate the dynamics of the network in detail in the present study, nor did we try and constrain them to match the data of a particular experiment.

As an alternative model, differences in dynamics may identify separate cortical circuits for the processing of stimulus form and motion in real cortical networks. For example, recent imaging of network dynamics in cat primary visual cortex revealed traveling waves of activity with respect to the Cartesian axes of the retinotopic map, but standing waves of activity with respect to the circular axis of the coextensive map for visual edge orientation preferences (Benucci et al., 2007). Similar mechanisms could operate in somatosensory cortex, if domains of directional selectivity in the barrels can be thought of as the tactile equivalent of orientation tuning domains in primary visual cortex, and if somatotopic and retinotopic maps can likewise be substituted. This idea is supported by the measurement of similar lateral propagation speeds for activity in cat visual and mouse barrel cortices; compare $280\,\mathrm{mm/s}$ (Benucci et al., 2007) and $250\,\mathrm{mm/s}$ (Adesnik and Scanziani, 2010) respectively (for rat, see also Petersen et al., 2003 and Derdikman et al., 2003).

A recent study found that the receptive fields of neurons throughout the barrel column, i.e, the identity and number of whiskers that could elicit significant responses, shifted depending on the direction in which the whiskers were deflected (Le Cam et al., 2011). Differences in receptive field were related to differences in response latencies, which were predicted first by the whisker identity (principal or adjacent whisker) and second by the deflection direction (caudal or rostral). It would be interesting to see whether these differences in response profile can be predicted by the precise location of the neuron. It should be possible to draw out specific predictions from our cortical sheet model, about the timing of responses that arise when distance dependent input delays into L2/3 are constrained by superimposing directional pinwheels onto the somatotopic whisker map in L4.

Whilst the present study cannot rule out alternative models, which might have the unique ge-

ometry of interactions within the barrel cortex utilised differently, the results demonstrate the sufficiency of the geometric mapping, which was derived from neurophysiological observation, for representing tactile stimulus form and motion.

Chapter 5

Orthogonal coding of tactile stimulus features in a model of barrel cortex development

Chapter summary

The responses of mammalian primary visual cortex neurons to different features of visual input are organised systematically across the cortical sheet. Since being discovered by Hubel and Wiesel in the 1960s, maps for visual edge orientation, spatial frequency, and eye preferences have been described in exquisite detail: Visual feature maps are topological, preserving adjacency in each feature space; they are coextensive, meaning that they can be measured within a single population of neurons; and they interact predictably, with a tendency for the contours of different maps to intersect with each other orthogonally. However, much less is known about the types of feature map that may be present in non-visual cortical areas, and how coextensive non-visual feature maps may interact. Using a self-organising model of visual cortex map development, we set out to predict the potential organisation of maps in the somatosensory 'barrel' cortex, which in rats, mice and shrews, is driven by tactile stimulation of the facial whiskers.

Inputs to the model were patterns of activity in simulated layer 2/3 barrel cortex, which correspond to the different shapes, directions, and speeds of a tactile stimulus moved through an array of artificial whisker sensors. As the network self-organised, responses became organised into maps, wherein contours for shape, direction, and speed preferences intersect orthogonally. The orthogonal coding for these three tactile feature spaces was reflected by a transition from initial single-whisker neuronal receptive fields to multi-whisker receptive fields. The maps that emerged, and the connectivity patterns behind them, serve as predictions about the organisation of responses in layer 5 barrel cortex that could help guide future experiments.

5.1 Introduction

The primary visual cortex (V1) of many species is organised by maps of neuronal preferences for a variety of different visual features. For example, responses to different orientations of edges in the visual scene define a functional organisation of V1 in cat and monkey, as a locally smooth orientation map, wherein incremental changes in orientation evoke selective responses in neurons at incremental horizontal locations (Hubel and Wiesel, 1959, 1965, 1974; Ohki et al., 2006). V1 visual feature maps are shaped by the nature of sensory inputs experienced during post-natal development, and changes in map organisation correspond with changes in the extent to which those features can be perceived. For example, in kittens that have only experienced scenes composed of vertical lines, V1 neuronal receptive-fields and inter-connectivity patterns, are vertically biased (Blakemore and Cooper, 1970; Blakemore et al., 1978; Tieman and Hirsch, 1982); consequently, vertical-reared animals respond less reliably to lines of other orientation to which they are later exposed (Blasdel et al., 1977).

Maps for visual stimulus features other than orientation, for example for the location of an image (retinotopy), the eye to which it is presented (ocular dominance), and the spacing between visual edges (spatial frequency), also vary smoothly across cat and monkey V1. Thus multiple feature maps lie coextensive across the cortical sheet. These feature maps interact in such a way that promotes coverage (all features represented equally) and continuity (map smoothness; Hübener et al., 1997; Yu et al., 2005; Farley et al., 2007; see Basole et al., 2006 and Issa et al., 2008 for an overview), and that minimises connection lengths (Swindale et al., 2000; Yu et al., 2005). As a consequence, the contours of maps for different stimulus features intersect at right angles, and thus the interactions between maps in V1 describe an orthogonal encoding of multiple visual feature spaces (Issa et al., 2008).

Continuity, coverage, and orthogonal coding are all predicted by dimension-reduction models, which explain map self-organisation as a consequence of sensory experiences. Conceptually, in these models the high-dimensional space of stimulus features is folded onto the two dimensions of the cortical sheet (von der Malsburg, 1973; Kohonen, 1982; Burger and Lang, 2001; Sirosh and Miikkulainen, 1997; see Swindale, 1996 and Miikkulainen et al., 2005 for an overview). This account of map development has been used to explain numerous observations about the organisation of maps in V1. However, dimension-reduction models represent a general theory of cortical map development, and as such they should also make predictions about map development in non-visual domains. Therefore in this study, we use a general-purpose self-organising map model to ask how the representation of non-visual feature spaces may be represented in other cortical areas. Specifically, we asked how the representation of whisker movements pertaining to different features of tactile stimuli might be organised in the barrel cortex area of the primary somatosensory cortex (S1), in tactile-specialist species such as rats, mice, and shrews.

Previous models of S1 map self-organisation, including those developed in our lab, have been successful in reproducing maps for individual tactile stimulus features; explaining, for example, the origin of discontinuities in the primate 'homunculus' body-map (Stafford and Wilson, 2007), the emergence of receptive-fields for textures experienced via the finger-tip (Park et al., 2009), and maps for the direction in which the rats facial whiskers are deflected (Wilson, 2007; Wilson et al., 2011; Kremer et al., 2011). Here we use a similar approach to model map development in the rat barrel cortex, to explore for the first time, the emergence of, and interactions between, coextensive maps for multiple tactile stimulus features.

Experimentally, responses of barrel cortex neurons have been shown to correlate with various features of multi-whisker stimulation, such as the shape of a stimulus edge, i.e., a straight versus curved edge (Benison et al., 2006); the direction of stimulus motion, as implied by the whisker deflection direction (Bruno et al., 2003; Andermann and Moore, 2006) and the deflection sequence (Ghazanfar and Nicolelis, 1999; Polley et al., 2005; Drew and Feldman, 2007; Jacob et al., 2008); and the speed of stimulus motion, as represented by the inter-whisker deflection interval (Shimegi et al., 1999, 2000). The aim of the present study is to explore the interactions between maps for these three tactile stimulus features (shape, direction, and speed) in the barrel cortex, and therefore to suggest how the preference of a given neuron for one feature can predict its preference for another.

5.2 Methods and Materials

5.2.1 Overview

Layer 5 (L5) can be thought of as the major output layer of the barrel cortex, innervating large regions of layer 2/3 (L2/3) (Wright and Fox, 2010; Oberlaender et al., 2011), and projecting to numerous extra-barrel targets. Targets include the primary motor cortex and secondary somatosensory cortex (Welker et al., 1988; Hoffer et al., 2005; Fox, 2008), the thalamus (Veinante et al., 2000; Li and Ebner, 2007), the cerebellum (Mercier et al., 1990), the pons, and the superior colliculus (Hoffer et al., 2005). In general, L5 neurons have the longest stimulus-response latencies (Armstrong-James et al., 1992; Lefort et al., 2009; Adesnik and Scanziani, 2010), as well as the largest (Ito, 1992; Manns et al., 2004) and most spatial-temporally complicated receptive fields (Ghazanfar and Nicolelis, 1999; Jacob et al., 2008) compared with layers 4 and 2/3. L5 can be characterised by two layers a and b: L5a neurons are smaller, sparser, and tend to project axons reciprocally back to their afferents in L2/3 (Schubert et al., 2006). L5b consists of two functionally distinct pyramidal cell types (known as regular spiking and intrinsically bursting), based on differences in their spiking characteristics, receptive-field sizes, and modes of plasticity (Schubert et al., 2001; Jacob et al., 2012; see Ahissar and Staiger, 2010 for an overview). Whilst acknowledging a number of important distinctions within L5, for the purposes of the modelling presented here we will consider L5 to be an essentially homogenous population and henceforth refer to a single L5.

To explore how multi-whisker stimulation patterns might be represented in L5 barrel cortex, we model it as a sheet of recurrently interconnected self-organising neurons (as in Wilson et al.,

2010), and present to it many examples of multi-whisker stimulation. Activity in simulated L5 is driven by robot-controlled stimulation of 12 artificial whisker sensors, as encoded in patterns of activity on a sheet of layer 2/3 (L2/3) neurons (Wilson et al., 2011), and it is shaped by weighted lateral connections between L5 neurons. In response to each tactile stimulus, cooperative interactions within L5, mediated by short-range recurrent excitatory connections, and competitive interactions via long-range recurrent inhibitory connections, are consolidated by Hebbian learning. The process is repeated in response to many multi-whisker stimulation patterns, simulating early post-natal whisker experiences, during which L5 connections self-organise to represent whisker movements correlated by the nature of the tactile stimuli.

The following sections briefly describe, i) the procedure for collecting whisker deflection data (for details see chapter 4), ii) the representation of whisker deflections as patterns of activity in a sheet of L2/3 neurons (for details see Wilson et al., 2011 and chapter 4), and iii) the process of map self-organisation in simulated L5 barrel cortex (for details see Wilson et al., 2010). Figure 5.1 provides an overview of the network architecture. Measures of the organisation of L5 stimulus feature maps, and of the structure of neuronal receptive fields underlying those maps are also detailed, along with a model for simulating whisker deflections.

5.2.2 Generating whisker deflections and barrel cortex input patterns

A dataset of multi-whisker deflection patterns was generated using robot-controlled collisions between a variety of tactile stimuli and a regular 3 by 4 array of artificial whisker sensors (as described in chapter 4). Tactile stimuli were five semi-circular edges, each parameterised by a radius R. On each trial, one tactile stimulus shape (R), suspended from a table-top XY-

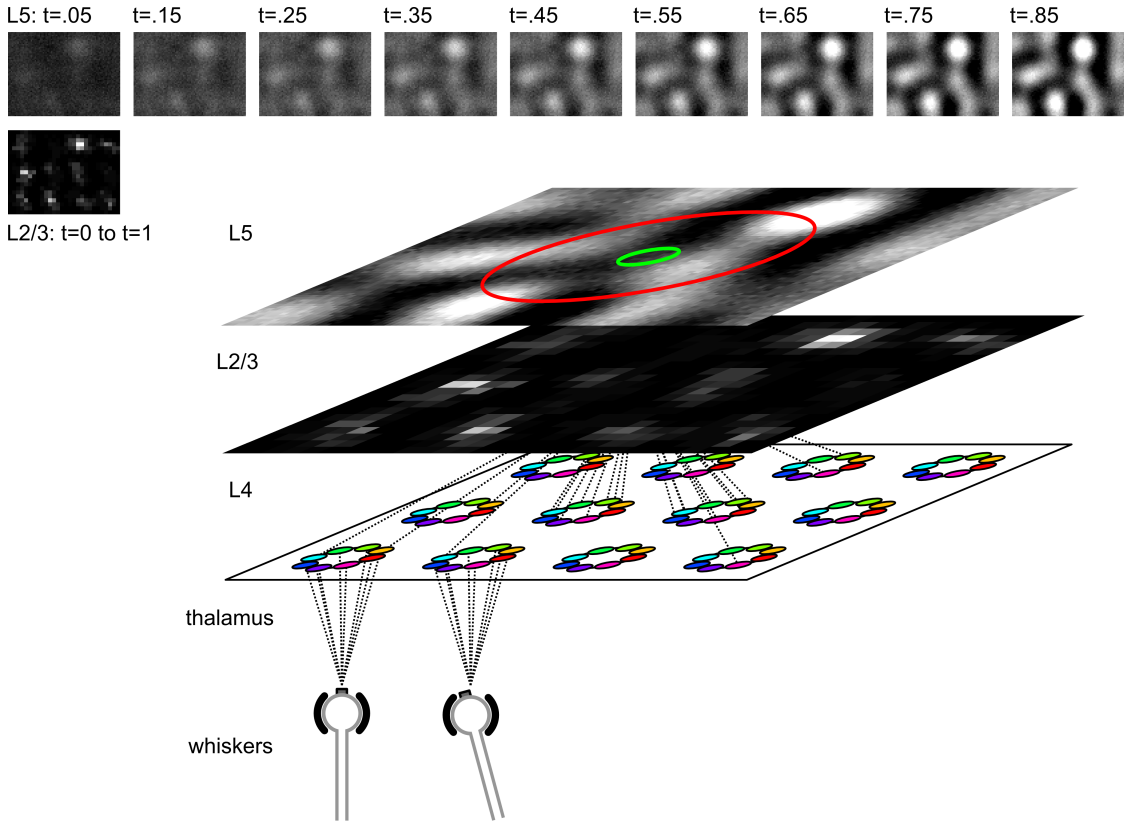

Figure 5.1. Model architecture and initial activity. When whiskers in a 3 by 4 array are moved by a tactile stimulus, changes in whisker position cause changes in voltage, measured on sensors aligned to the X and Y axes (one resting and one deflected whisker is illustrated). Thalamic neurons respond to high-velocity deflections of a principal whisker in a particular direction, and relay spikes to layer 4 (L4) barrel cortex neurons, which are positioned by whisker and direction preference (colour indicates the direction preference). Layer 2/3 (L2/3) barrel cortex neurons are arranged in a sheet above L4, and register spikes at each L4 position as one excitatory and one inhibitory conductance change (EPSC and IPSC) after delays proportional to the straight-line distance from the pre-synaptic neuron. These distance-dependent delays differ for EPSCs and IPSCs, and render L2/3 neurons at particular locations selective to particular time-differences in the onset of L4 spikes, thus converting L4 inter-spike intervals to patterns of firing rate across L2/3. Initial responses in a dense sheet of layer 5 (L5) neurons are the weighted sum over firing rates of all L2/3 afferents. L5 neurons then interact laterally, cooperating and competing via short-range excitatory and longer-range inhibitory weighted connections respectively (the ranges of connection onto the center neuron are shown as a green and red disk). The settling of recurrent interactions forms blobs of activity in L5, as shown in successive panels above. The settled activity in L5 is used to update both afferent and lateral connection weights by Hebbian learning, before activity is zeroed and a new randomly chosen multi-whisker movement pattern is presented.

positioning robot, was moved through the center of the whisker array in one of eight directions (Θ), at one of ten speeds (S). Each combination of R, Θ, and S, was repeated five times; hence 2,000 multi-whisker deflection patterns were collected in total. The deflection of each whisker was defined by a deflection magnitude and a deflection direction time-series.

High-velocity displacements of the whiskers were used to elicit spikes, in simulation, in eight directionally tuned L4 units per whisker (96 L4 units in total). The layout of the L4 units in a cortical sheet reflects their whisker and deflection direction preferences. For example, a unit tuned to rightwards deflections of the whisker in the top-left corner of the whisker array is located to the right of a barrel center at the top-left corner of the L4 sheet.

Based on neurophysiological observations (Shimegi et al., 1999, 2000; Feldmeyer et al., 2002; Helmstaedter et al., 2009), an organisation of inter-soma distance-dependent axonal delay lines was used to model the L4 to L2/3 projection. This organisation renders L2/3 neurons closer to a particular barrel center selective for stimuli in which an adjacent whisker is deflected before the whisker associated with the nearest barrel (Wilson et al., 2011). Upon registering its preferred whisker stimulus, each L4 unit elicits an immediate excitatory spike and a latent inhibitory spike, which propagate to L2/3 neurons tiling a sheet located directly above L4. The inhibitory potential travels faster, such that L2/3 neurons nearest to the L4 unit register the excitatory input first but neurons further away register the inhibitory input first.

Activity in L2/3 is computed as the maximum response, over one second post-stimulus, to the individually delayed excitatory and inhibitory potentials from each of the 96 L4 units, after leaky integration and subsequent squashing using a sigmoid. The distribution of spiking probabilities across L2/3 encodes the pattern of whisker deflections by their spatial and temporal

profile. Specifically, the projection to L4 explicitly encodes the whisker identity and deflection direction and the L4 to L2/3 projection encodes the inter-deflection interval.

According to analyses presented in chapter 4, maximal performance in classifying the tactile stimulus features (R, Θ, and S) could be achieved using the responses of around 550 L2/3 neurons at randomly chosen positions on the sheet. To use similar numbers of neurons, whilst keeping the indexing of those neurons simple, a dense L2/3 sheet comprising 90 by 120 neurons was discretised into 21 by 28 squares and all but a single randomly chosen neuron from each square were discarded. This procedure leaves 588 pseudo-randomly selected neurons in a contiguous arrangement across L2/3.

5.2.3 A self-organising model of layer 5 barrel cortex development

L5 was simulated as a sheet of 63 by 84 self-organising neurons, using the LISSOM algorithm (laterally interconnected synergistically self-organising map: Sirosh and Miikkulainen, 1997; Miikkulainen et al., 2005; Wilson et al., 2010). On each iteration, each L5 neuron computes its response as the weighted sum of the activity in separate afferent, recurrent excitatory, and recurrent inhibitory connection fields. Model afferent connections are received from all L2/3 neurons and are excitatory; short-range excitatory connections are received from all L5 neurons within a 0.2 barrel-width radius of the target neuron; longer-range inhibitory connections are from all L5 neurons within a 1.0-barrel radius. All connection weights had initially random values in the range 0.0 to 1.0, which were multiplied by a two-dimensional Gaussian kernel centred on the position of the L5 neuron in the sheet. Gaussian kernels applied to the initial afferent, excitatory, and inhibitory connections were computed using $\sigma = 0.5$, $\sigma = 0.5$, and

$\sigma = 1$ respectively (in units of between-neuron spacings on the pre-synaptic sheet), and the weights in each connection field were normalised to sum to 5, 0.6, and 1.0.

In response to each pattern of whisker deflections, the L2/3 activity pattern is fixed for 17 steps, during which the L5 activity patterns are allowed to settle via the lateral interactions; the weighted sum over the three connection fields is recomputed on every settling step. The recurrent settling process collects the activity into localised blobs across the L5 sheet (Figure 5.1), and the settled activity pattern is used to update all of the connection weights. Weights are updated using a Hebbian learning rule, using a divisive re-normalisation of the weights in each connection field to keep them plastic and bounded (see Wilson et al., 2010 for discussion). Activity is then reset to zero in preparation for processing of the next pattern of whisker deflections. In total, 60,000 whisker deflection patterns were presented to the network during training; each was chosen randomly from the 2,000 distinct multi-whisker deflection patterns.

5.2.4 Measuring tactile stimulus feature maps in L5

Maps for tactile stimulus feature preferences and for the receptive-field structure were constructed from the responses of L5 neurons after every 1,000 pattern presentations. To compute the preferred tactile stimulus parameter for the $k\mathrm{th}$ L5 neuron, all 2,000 whisker deflection patterns were presented to the network, and the response to each pattern, r_k, was computed (with learning turned off). The preferred stimulus parameter, with respect to features R, Θ, and S, was computed by summing the responses to all patterns involving a given parameter, and then

taking the maximum:

$$
\begin{aligned}
R'_k &= \arg\max_c \sum_{c=1}^{5} r_k(R_c, \Theta, S) \\
\Theta'_k &= \arg\max_c \sum_{c=1}^{8} r_k(R, \Theta_c, S) \\
S'_k &= \arg\max_c \sum_{c=1}^{10} r_k(R, \Theta, S_c)
\end{aligned}
\tag{5.1}
$$

Hence, each L5 neuron could be labelled by its preferred stimulus shape (R'_k), by its preferred stimulus movement direction (Θ'_k), and by its preferred stimulus movement speed (S'_k). Responses were recorded either before or after propagation of activity through the lateral connections, and these responses are referred to as the afferent or settled response respectively.

5.2.5 Measuring the receptive field structure of L5 neurons

Several measures of the L5 neuron receptive field structure were employed to investigate how preferences for particular tactile stimuli evolved during self-organisation, i.e., by examining the distribution of responses to isolated whisker deflections. The measures are summarised in Table 5.1.

For each measure, the response of the kth L5 neuron, $r_k(w, \theta)$, was recorded after simulating an isolated deflection of each whisker w, in each of eight directions θ. Deflections were simu-

Table 5.1. Summary of measures of the preferred stimulus for the $k\mathrm{th}$ neuron.

Measure	Description
PW_k	Principal whisker (PW)
$\hat{\mathrm{PW}}_k$	Selectivity to the PW
$\mathrm{PW}\theta_k$	Angle of the PW from the array center
$\mathrm{PW}\rho_k$	Distance of the PW from the array center
$\mathrm{MW}\theta_k$	Angle of center of mass
$\mathrm{MW}\rho_k$	Magnitude of center of mass
$\mathrm{PD}\theta_k$	preferred direction of the PW
$\mathrm{PD}\rho_k$	Selectivity for preferred direction of the PW
$\mathrm{MD}\theta_k$	Preferred direction over all whiskers
$\mathrm{MD}\rho_k$	Selectivity for preferred direction over all whiskers

lated by evoking a spike in each of the 96 L4 units in turn. The resulting L2/3 activities were multiplied by a factor of three, as determined in pilot work to evoke a strong response in L5, which would otherwise respond weakly to patterns involving less than two whisker deflections.

From the response $r_k(w, \theta)$, the preference and selectivity of the neuron for the identity of deflected whisker, and for the deflection direction could be evaluated. The principal whisker was defined as that which elicited the maximum summed response over eight directions of deflection:

$$\mathrm{PW}_k = \arg\max_w \sum_\theta r_k(w, \theta) \tag{5.2}$$

The selectivity of the neuron for deflection of the principal whisker was defined by comparing the principal whisker response with the summed response over all other whiskers:

$$\hat{\mathrm{PW}}_k = \frac{\max_w \sum_\theta r_k(w, \theta)}{\sum_w \sum_\theta r_k(w, \theta)} \tag{5.3}$$

It is useful to describe the identity of the principal whisker in polar coordinates, using the coordinates of the whisker in the whisker array ($X_w \in \{-1.5, -0.5, 0.5, 1.5\}, Y_w \in \{-1, 0, 1\}$):

$$\begin{aligned} \mathrm{PWx}_k &= X_{\mathrm{PW}_k}, \\ \mathrm{PWy}_k &= Y_{\mathrm{PW}_k}, \\ \mathrm{PW}\theta_k &= \mathrm{atan2}(\mathrm{PWy}_k, \mathrm{PWx}_k), \\ \mathrm{PW}\rho_k &= \sqrt{{\mathrm{PWy}_k}^2 + {\mathrm{PWx}_k}^2}. \end{aligned} \tag{5.4}$$

We will make similar use of the polar transform for the receptive field measures that follow, so henceforth we will define the Cartesian components of the measure explicitly, and use the suffix θ or ρ to denote its polar representation.

The center of gravity of multi-whisker responses, in co-ordinates of the whisker array, is defined by:

$$\begin{aligned} \mathrm{MWx}_k &= \sum_w \left(X_w \sum_\theta r_k(w,\theta) \right), \\ \mathrm{MWy}_k &= \sum_w \left(Y_w \sum_\theta r_k(w,\theta) \right), \end{aligned} \tag{5.5}$$

The measures MWx_k and MWy_k were used to construct the angle of the center of gravity from the center of the whisker array $\mathrm{MW}\theta_k$, and the magnitude of the center of gravity $\mathrm{MW}\rho_k$.

The preferred direction for principal whisker deflections (or the principal direction; PD) was defined as:

$$\begin{aligned} \mathrm{PDx}_k &= \sum_\theta \left[r_k(\mathrm{PW}_k,\theta)\cos(\theta) \right], \\ \mathrm{PDy}_k &= \sum_\theta \left[r_k(\mathrm{PW}_k,\theta)\sin(\theta) \right], \end{aligned} \tag{5.6}$$

and PDx_k and PDy_k were used to construct the preferred deflection direction $\mathrm{PD}\theta_k$, and the selectivity to that deflection direction $\mathrm{PD}\rho_k$.

Similarly, the distribution of preferred deflection directions, across all whiskers, was sum-

marised by the mean deflection direction, using:

$$\begin{aligned} \mathrm{MDx}_k &= \sum_w \sum_\theta \left[r_k(w,\theta) \cos(\theta) \right], \\ \mathrm{MDy}_k &= \sum_w \sum_\theta \left[r_k(w,\theta) \sin(\theta) \right], \end{aligned} \tag{5.7}$$

from which the preferred multi-whisker deflection direction $\mathrm{MD}\theta_k$, and the multi-whisker direction selectivity $\mathrm{MD}\theta_k$, were computed.

5.2.6 Simulating whisker deflections

To control for the effects of unforeseen artefacts in the data, i.e., a dependency between the stimulus direction and the stimulus speed, we ran a second network using simulated whisker deflection patterns that consisted of no such dependency. Whisker deflection onset times T_w and deflection directions Φ_w, on a four-by-four whisker array, were generated using the following model of the geometry of whisker-stimulus interactions:

$$\begin{aligned} \Theta' &= -\Theta - \pi/2, \\ X'_w &= X_w \cos\Theta' - Y_w \sin\Theta', \\ Y'_w &= X_w \sin\Theta' + Y_w \cos\Theta', \\ T_w(R,\Theta,S) &= \frac{\mathrm{sgn}(R)\sqrt{R^2 - {X'_w}^2} - Y'_w}{S}, \\ \Phi_w(R,\Theta) &= \mathrm{atan2}\left(-\sqrt{R^2 - {X'_w}^2}, -\mathrm{sgn}(R) X'_w \right) - \Theta', \end{aligned} \tag{5.8}$$

and hence deflection directions were computed as the outwardly pointing normal to the tangent of the semi-circle edge, at the time of each whisker contact. Accordingly, convex shapes ($R < 0$) deflect the whiskers away from one another, whereas concave stimuli ($R > 0$) deflect the whiskers towards one another.

Based on inspection of the robot stimulation data, the mean latency between deflection onset and subsequent offset events varied systematically with the stimulus movement speed, with latencies given approximately by $\tau = \frac{13.1\,\mathrm{ms}}{S}$. Thus for the simulated deflections, each onset was followed by an offset in the opposite direction $\Phi_w + \pi$, at $T_w + \tau$. The minimum value of $T_w + \tau$ was subtracted from all deflection times so that the first whisker deflection began at the start of each iteration of self-organisation.

Self-organisation progressed as for the robot data, but using simulated deflections allowed for stimuli to be drawn from simpler (i.e., continuous) parameter distributions. As well as a straight edge, one concave and one convex stimulus were simulated at the minimum radius required to always deflect all whiskers; movement directions were uniform around the circle, and speeds were uniformly random in the range of faster speeds $360\,\mathrm{mm/s}$ to $720\,\mathrm{mm/s}$. On each training iteration, a pattern of activity in L2/3 was generated in the usual way, using tactile stimuli with combinations of parameters drawn on each iteration randomly from these simpler distributions of radius, direction and speed.

We note that this approach required recomputing input patterns 'on the fly', and thus it took longer to simulate than for the physical model in which L2/3 activity patterns could be pre-computed. Using 28^2 L2/3 neurons and 84^2 L5 neurons, simulations took around 17 hours, with full map measurement after every 1,000 training patterns, running optimised C++ code

(interfaced using BRAHMS: Mitchinson et al., 2010) on a dual-core 2.66 GHz processor (although pre-computation of L2/3 patterns for map measurement would have allowed significant speed-up). Note also that to obtain similar responses in L5 to those evoked by physical-whisker stimulation, the afferent projection strength was doubled.

5.3 Results

5.3.1 A map for stimulus shape in simulated L5 barrel cortex

The L5 neurons were labelled first by their preferences for the tactile stimulus shape, as shown in Figure 5.2A. Prior to training, the organisation of responses to different shapes was random, except for a component at low spatial frequency in which responses to either convex shape dominated. This component is due to the initial spatial arrangement of afferent connection fields, which biases nearby neurons to have similar initial responses; that convex shapes dominate the initial responses is not important, because the selectivity of those responses was weak. After training on 60,000 input patterns, however, the shape map revealed an organisation of responses into patches of neurons, and the arrangement of patches had a regular, repeating structure. For example patches of neurons preferring movements of the straight edge tended to be below and to the right of patches for concave stimulus edges, and to the left of patches for the large convex stimulus. The repeating structure indicates that the self-organising process had promoted some form of continuity in representing shape. As expected, the size and spacing between patches was on the order of the radius of the lateral inhibitory connection fields.

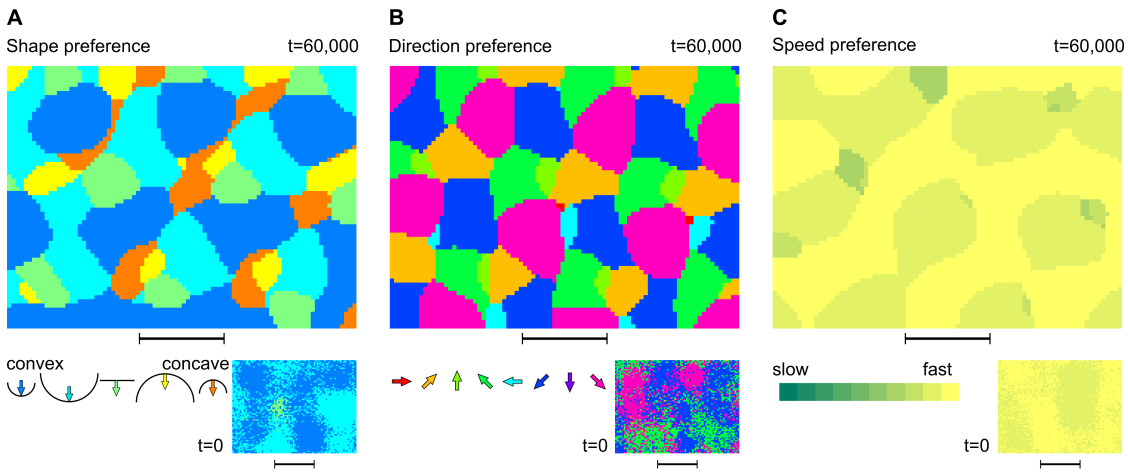

Figure 5.2. Maps for tactile stimulus features measured in simulated L5. L5 neurons (one pixel represents one neuron) were tested for their preferences for features of the tactile stimulus after training on 60,0000 example multi-whisker deflection patterns. Neurons are coloured by their maximum summed activity, over all 2,000 stimulus patterns that were parameterized by the feature indicated by the colour key. Preferences were measured in this way for **A** the shape of the stimulus edge, **B** the direction in which the edge was moved through the 3 by 4 whisker field or **C** the speed applied to the robot motors to generate the movements. Inset maps show the organisation prior to any learning or settling, which is random but for a low spatial-frequency component owing to the Gaussian kernel on the initial afferent weights. Black scale bars in each panel (and in all subsequent figures) indicate one spacing between barrel centers.

It is conceivable that instead of learning to represent tactile stimulus shape per se, as we have chosen to parameterise it (or indeed direction or speed), the self-organising process discovered structure in the whisker deflection patterns beyond our knowledge of how those patterns were generated. For example, the deflection patterns owing to different stimulus shapes could have instead been labelled by the stimulus size, i.e., by using the radii of the semi-circular edges and ignoring the distinctions between convex and concave orientations. Relabelled in this way, the straight edge stimulus has the largest size, and thus the largest size was under-represented in the dataset, with 400 patterns generated using the straight edge but 800 patterns generated using either of the other two stimulus sizes. This alternative encoding did not seem to be developed by the network, because learnt preferences for each of the five shapes dominated similar proportions of the shape map. However, it is worth noting the potential for bias when using the maximum response over chosen stimulus features to label neuronal feature preferences.

5.3.2 An anisotropic map for stimulus direction reflects a bias for faster stimuli

The same neurons were coloured next by their preferences for particular stimulus movement directions, as shown in Figure 5.2B. As in the shape map, patches of neurons displaying similar direction preferences replaced an essentially random initial organisation of responses. As in the shape map, the arrangement of direction-selective patches had a regular structure. There was a consistent relationship between patches of neurons preferring directions labelled pink and the nearest patches of neurons preferring yellow, for example, and similar relationships for any other pair of represented stimulus directions. There was a strong tendency for the four

cardinal movement directions to be underrepresented in the direction map, compared with the four diagonal movement directions. For example, there were almost no neurons that ended up preferring rightward movements, and hence very little red in the direction map, and few cyan neurons representing leftward movements. This bias may be due to a relationship between the stimulus speed and direction in the whisker deflection dataset, as diagonal movements were associated with faster movement speeds (see chapter 4).

In the speed map (Figure 5.2C), the faster movements completely dominated the organisation of L5 responses, but for a few disparate patches of neurons responding maximally to slower stimuli. Stimulus movement speed was therefore poorly represented in the organised map, whereas different stimulus shapes and directions were comparably well-covered and well-separated. A possible explanation is that the distribution of inter-whisker deflection intervals (and deflection directions) in the physical-whisker dataset is less informative about the stimulus speed than it is about shape or direction. However this is unlikely to be the case, because L2/3 activity patterns associated with different stimulus speeds were more easily separable by a linear classifier than were those associated with different shapes or directions (chapter 4). If the effect is not due to the input to L5 then it must have originated from within L5.

Faster stimulus movements give rise to shorter inter-spike intervals in L4, which tend to activate all L2/3 neurons more strongly. The recurrent interactions in L5 separate responses to different input patterns based primarily on differences in the identity of active input neurons in L2/3. This is because the dynamics of settling, via short-range excitatory and longer-range inhibitory connections, sharpen regions of contrast in the distribution of afferent responses across the L5 sheet (Figure 5.1). Although stronger inputs yield stronger responses, it is the input contrasts rather than their intensities that determine the patterns of settled activity across the sheet. Thus

the separation of input pattern representations, after consolidation of the settled responses by Hebbian learning, is driven primarily by differences in activation between rather than within input neurons. Faster speeds correspond to increased L2/3 activities, and hence faster speeds dominate even the initial L5 map organisation; differences in activity due to the stimulus speed do not sufficiently break symmetry in L5 to allow slower speeds to compete for cortical territory as self-organisation continues.

5.3.3 Orthogonal coding of tactile stimulus features in L5

To investigate a potential interaction between map organisations for the various stimulus feature spaces, we overlaid the shape, direction, and speed maps. In Figure 5.3, the direction map in Figure 5.2B was reproduced and the contours of the shape and speed map were overlaid as white and black lines respectively. It is important to clarify that each feature map was measured from the responses across the same sheet of L5 neurons, from the same simulation, and thus the three feature maps are coextensive across L5.

The overlay of feature maps revealed a tendency of the contours in each to intersect at right angles. That is, the boundary drawn between adjacent patches in one feature map is likely to be perpendicular to the boundary drawn between adjacent patches in another, at the point where those two boundaries cross. As a consequence of this organisation, patches of neurons preferring a particular shape were bisected by contours of low selectivity to the stimulus movement direction and/or speed. Therefore, at a given location in L5, stimulus shape and direction feature spaces (but not speed) were well covered. The organisation indicates that L5 responses had become self-organised, reducing the high-dimensional input space of possible combinations of

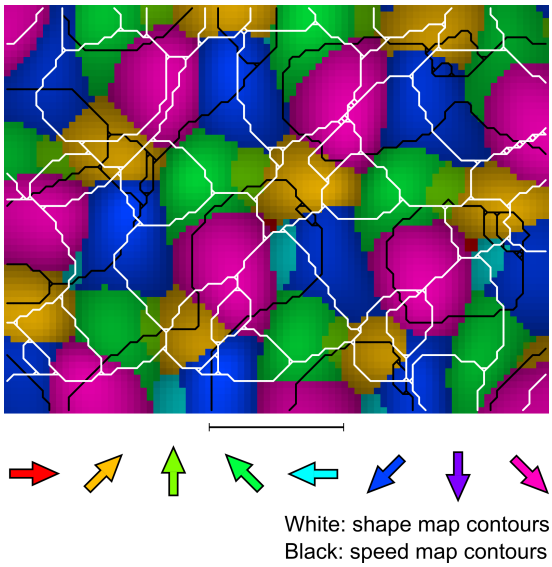

Figure 5.3. Feature separation indicated by non-overlapping map contours. The self-organised map for stimulus motion direction preferences is shown with pixel brightness indicating the selectivity of the neuron. Contours of maps for the stimulus shape (white lines) and speed (black lines). If the learnt feature representations corresponded to selectivity for particular examples of whisker deflection, then the contours of all three maps would overlap. Instead they tend to intersect at right angles, indicating a genuine separation (i.e., orthogonal encoding) of response preferences within and between feature spaces.

whisker deflection directions and relative timings, down to the three components by which the multi-deflection patterns were constrained (or at least down to two dimensions, discounting the poor-resolution speed map). Hence the interaction between feature map organisations suggests a separation of cortical representations according to the three stimulus feature spaces.

With respect to each feature map, L5 neurons with different preferences to the vertically or horizontally adjacent neuron were selected as markers for within-map contours. Neurons selected as such with respect to both in a pair of different feature maps (e.g., shape and direction), were selected as markers for between-map contour intersections. Each neuron was taken to mark an exact orthogonal map intersection if it was spatially isolated from all other neurons selected in this way, whereas intersection neurons adjacent to one other marked one of two ends of a non-orthogonal map intersection (i.e., diagonal or collinear boundaries). The proportion of exactly orthogonal versus non-orthogonal intersections for shape versus direction was $38/(38+29) = 0.57$, for shape versus speed was $32/(32+26) = 0.55$, and for direction versus speed was $31/(31+21) = 0.60$.

5.3.4 Feature map periodicity is reflected in patchy lateral connection fields

To explore how preferences for stimulus features were constructed during map formation, we first plotted the learnt connection weights onto individual L5 neurons in Figure 5.4. Weights were plotted in coordinates of the pre-synaptic sheet (i.e., L2/3 for the afferent connections and L5 for recurrent connections), for five post-synaptic neurons at equal spacings along a strip through the middle of the L5 sheet. Although the initial random weights were distributed under

a two-dimensional Gaussian kernel, after training a clear and very different spatial organisation was apparent in the weight plots.

Afferent connection weights picked out activity hotspots in L2/3 which correspond with the barrel column centers, whereas the strongest lateral inhibitory connection weights traced distinct patches in the surrounding L5. Patches in the distribution of lateral weights were on the same spatial scale as that separating patches of similar parameter preferences in the stimulus feature maps. The structure was revealed by an analysis of the periodicity between likewise-tuned neurons in the feature maps: Laid out over simulation time, histograms of the average distance separating like-tuned neurons displayed stable ridges along the time axis, which repeated at around 20-25 between-neuron spacings (i.e., one barrel-width; see Figure 5.5). The map organisation was stable throughout training, but for several step-changes in direction map periodicity, corresponding to the bleeding of smaller patches into larger neighbouring patches.

The feature map periodicity was around one barrel width (i.e., the radius we allowed for long-range lateral connection fields), which corresponds physiologically to $\approx 0.4\,\mathrm{mm}$, and is consistent with a typical feature-map periodicity of 0.5–$1.0\,\mathrm{mm}$ in cat V1 (Issa et al., 2008). Therefore feature maps that might be measured in the barrel cortex should be expected to have similar periodicity to those generated here in simulation. The patchy organisation of lateral connections is a key prediction of LISSOM, which is supported by observations in V1, and which distinguishes LISSOM from other dimension-reduction models that do not explicitly simulate lateral interactions (see Miikkulainen et al., 2005; Wilson et al., 2010).

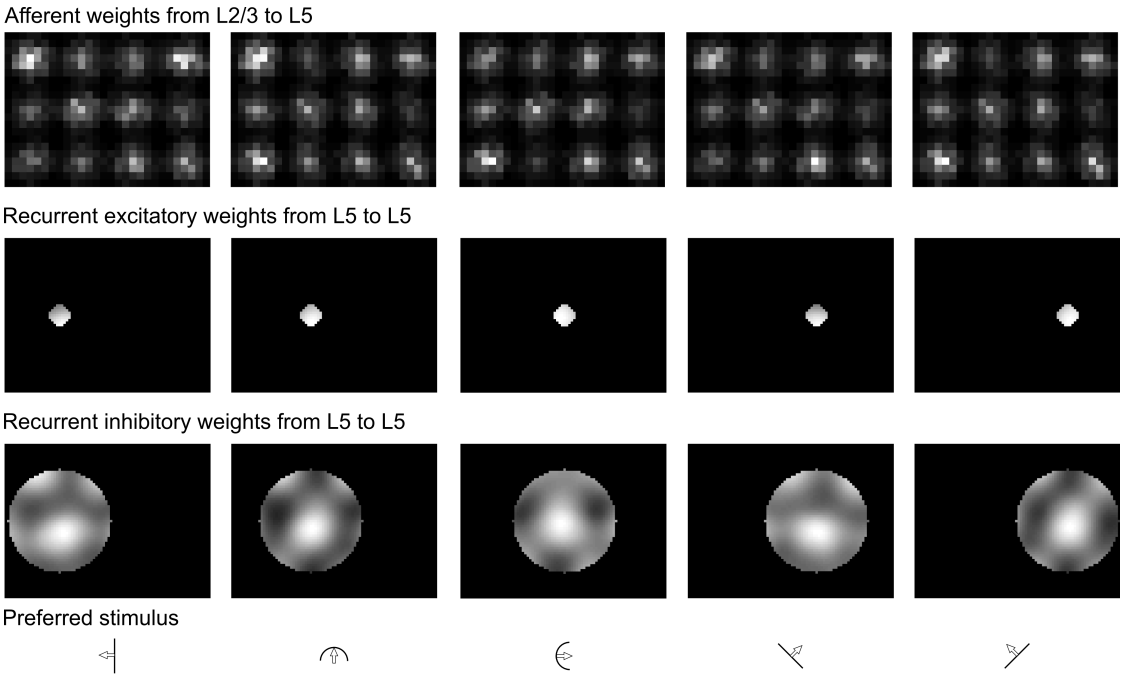

Figure 5.4. Learnt connection weights onto five L5 neurons. Connection weights onto five L5 neurons (five columns), located at varying horizontal locations along the central vertical location, are plotted in co-ordinates of the sheet to which the pre-synaptic neuron belongs. The pixel intensity indicates the connection strength after training on 60,000 stimulus presentations; pixel intensities were normalised separately in each plot to aid visualization. The top row of panels shows connection weights from the afferent neurons in L2/3. The 4 by 3 discretisation apparent in each panel reflects a tendency for L5 neurons to develop stronger connections to L2/3 neurons clustered around the barrel centers. The middle row of panels shows the learnt excitatory connection weights within L5, which in each case reveal the development of strong weights from all surrounding neurons within the short-ranging connection field. Note that these plots give a good visual impression of the location of the post-synaptic neuron in the sheet. The bottom row shows the strength of learnt lateral inhibitory connection weights, revealing a patchy structure often present in mammalian primary visual cortex. The patches are on the order of the separation between patches of likewise tuned neurons in the various multi-whisker feature maps. Symbols below the plot for each neuron indicate its preferred stimulus; each preferred the fastest speed, except the center neuron which preferred the second fastest.

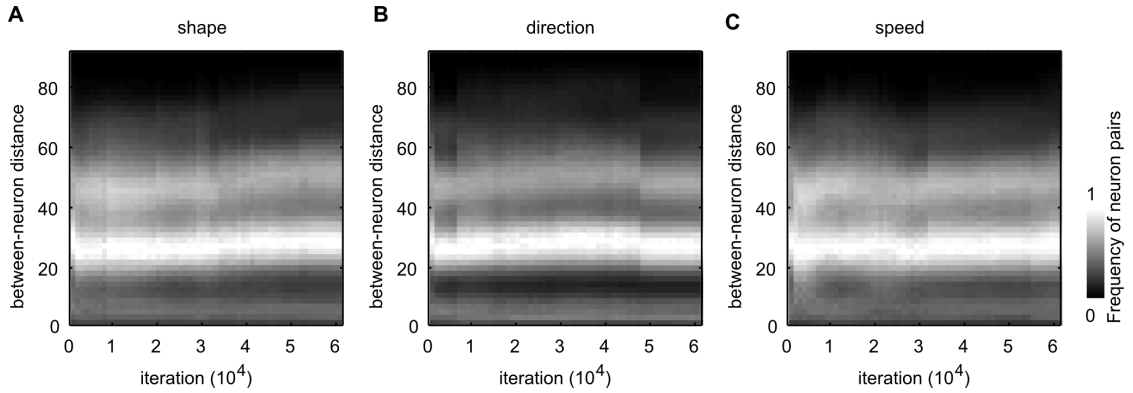

Figure 5.5. Analysis of feature-map periodicity over simulation time. Over simulation time, the distance separating pairs of neurons with the same feature preferences was measured, and histograms were constructed from the number of observed pairs at a given between-neuron distance. Plots for **A** shape preference, **B** direction preference, and **C** speed preference are shown. A horizontal band of bright pixels at under 15 between-neuron distance indicates the grouping of neurons into clusters of similar feature preference. A brighter band at distances of around 30 indicates the separation between nearby clusters. Bands at lower map spatial-frequencies (i.e., at greater between-neurons distances) indicate the separation between more distal clusters. The separation between clusters in maps for stimulus shape (**A**) increases smoothly as L5 self-organises, whereas discontinuities at iterations 6,000 and at 49,000 in maps for the stimulus movement direction (**B**), and in the map for stimulus speed at iteration 32,000 represent subsumption of smaller clusters into larger neighbouring clusters. Maps measured since these times tended to be stable. The histogram represented by each vertical column of pixels was independently normalised to aid the visualisation.

5.3.5 Self-organisation represents a transition from single-whisker to multi-whisker receptive fields

To further explore the organisation of L5, receptive-field maps were constructed using the variety of measures described in Table 5.1, based on responses to isolated whisker deflections (see Figure 5.6).

Prior to training, maps measured for stimulus features defined on single-whiskers, namely for the preferred whisker and for the preferred direction in which that whisker was deflected, dominated the organisation of L5. This is because the initial L5 responses were essentially the spatial average of the L2/3 responses, which were determined by an explicit representation of the whisker identity and deflection direction in the arrangement of units in L4 (see Figure 5.1). However after training, the organisation of L5 responses based on single-whisker preferences, in particular based on the principal whisker deflection direction (as defined by Equation 5.6), was disordered (Figure 5.6C). Instead maps measured for multi-whisker stimulus features, namely for the center of gravity of the receptive field and for the mean preferred direction, became smoother during training (Figure 5.6B & Figure 5.6B). In particular, Figure 5.6B reveals a repeating mosaic of complete somatotopic maps for the layout of the whiskers in the array, tiling L5. Thus, a single global-scale representation of the array layout was overturned during map self-organisation, suggesting a transition from a receptive-field structure based on single-whisker preferences to one based on the combination of multi-whisker preferences.

To explore this idea further, we looked at how the correlation (the circular-circular correlation coefficient; Fisher, 1993) between the single-whisker and multi-whisker receptive-field com-

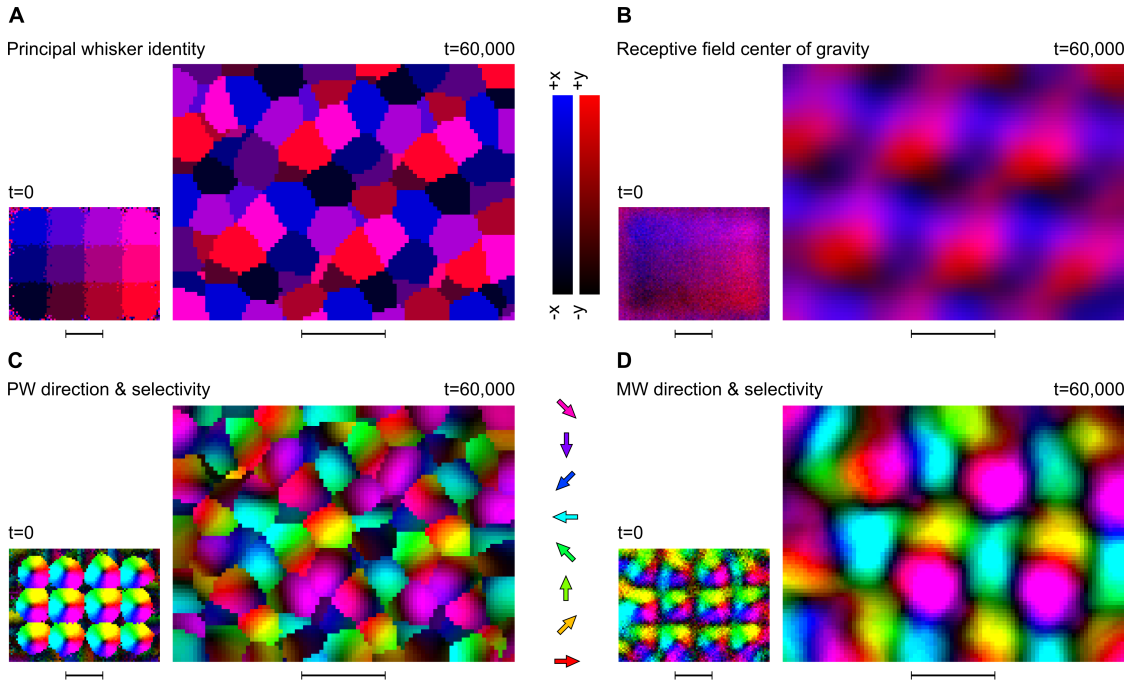

Figure 5.6. Organisation and development of whisker preference maps. A L5 neurons are coloured by the whisker which when deflected in isolation evokes the greatest response; responses to each whisker were the sum activity over deflections in eight directions. The afferent responses at time zero reveal a rigid topographic map for the principal whisker, which is inherited from the initial weights to the topographically organised L2/3 response. **B** Preferences for the identity of multiple whiskers were constructed from the center of gravity of responses to all twelve whiskers, when deflected in isolation (shown by the X and Y components on blue and red colour channels respectively), with a global organisation again present at $t = 0$. After training, plots in **A** and **B** reveal a re-organisation of whisker preferences into multiple, regularly repeating topological maps for the layout of whiskers in the whisker array. **C** L5 neurons are coloured by their direction preference for the principal whisker, with pixel intensity weighted by the selectivity of the neuron to principal whisker deflections in the preferred direction. At $t = 0$ a regular tiling of outwardly-radiating pinwheels are inherited from L2/3, but after training the mapping is irregular and discontinuous, indicating that L5 neuron representations are no longer governed by correlations within a whisker. **D** Multi-whisker direction preferences, defined as the vector average over the preferred direction for each whisker become organised into regular, repeating topological maps on the scale of those for the multi-whisker identity. These results indicate a re-organisation during training, from maps dominated by single-whisker preferences and inherited from L2/3, to maps reflecting multi-whisker preferences.

ponents varied during the self-organising process (Figure 5.7). L5 neuron preferences for the principal whisker identity and the multi-whisker identity (MW), as well as for the preferred principal whisker deflection direction (PD) and the mean preferred deflection direction over all whiskers (MD) were each expressed in radians, and a circular-circular correlation coefficient was computed over all L5 neurons. This allows inspection of the neuronal receptive-field structures in terms of the relationship between MW and MD, and between PW and PD. As L5 self-organised, single-whisker correlations (between PW & PD) stayed small or slightly negative for both the afferent and settled responses, supporting the idea that learnt stimulus preferences do not reflect single-whisker components. Conversely, the correlation between multi-whisker features (between MW and MD) increased steadily over time in the afferent response. Over time the settled responses steadily de-correlated the two multi-whisker components. This suggests that as self-organisation progressed, the lateral inhibitory weights served to separate responses based on the combination of whiskers from those based on deflection directions.

These dynamics confirm our intuition about how self-organisation unfolds. At the beginning of training, recurrent interactions dictate where activity settles on the cortical sheet, during which time a general consistency between the identity and direction of whisker deflections is learnt. This consistency can be thought of as description of the stimulus motion direction. As learning continues, the afferent connection weights consolidate this description (hence the steady rise in afferent correlations in Figure 5.7), allowing the recurrent interactions to pick out the structure in whisker-deflection patterns that is superimposed on that describing stimulus direction; i.e., that describing shape. 'Picking out' is manifest as a de-correlation of the multi-whisker identity and direction measures of the receptive field (hence the steady fall in settled correlations in Figure 5.7).

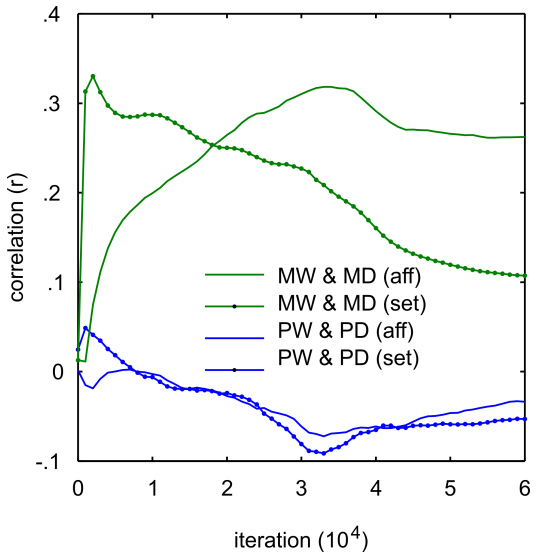

Figure 5.7. Development of relationships between represented multi-whisker features. Based on either the afferent response or the settled response in L5 ('aff' and 'set' in the legend), the correlation between the principal whisker identity (PW) and the preferred principal whisker deflection direction (PD) remained low (blue), with a slight anti-correlation between the two. However, the correlation between the angle of the receptive field center of mass (MW) and the mean preferred deflection direction over all whiskers (MD) became large in the settled responses after presentation of just 1,000 whisker-deflection patterns (green). This suggests that from the beginning of the self-organising process the lateral interactions were driven by a consistency between the identity and direction of whisker deflections. As self-organisation progressed, this consistency between deflections was consolidated in the afferent responses, and as training continued these features became increasingly de-correlated in the settled response.

According to this explanation, maps for stimulus shape (but not direction) should be better defined in the settled responses than in the afferent responses. This is what we observed; specifically, patches corresponding to the curved edge preferences were expanded in the settled versus the afferent maps. Hence the model predicts that in young animals selectivity for the stimulus movement direction will be present in the initial responses of L5 barrel cortex neurons. However selectivity for stimulus shape, as it is defined in the plane perpendicular to the motion direction, will be present only in older animals. Moreover it will be pronounced in latent responses recorded after the settling of recurrent intra-cortical dynamics.

5.3.6 Predicting selectivity for one stimulus feature from knowledge of another

A second self-organising model was run, this time using simulated whisker-deflection patterns (Figure 5.8). The stimulus features maps that emerged validate the previous results. In addition, the simpler training paradigm, in which stimulus direction and speed were drawn from continuous distributions, revealed the structure of each feature map in finer detail (Figure 5.8A).

The speed map was again dominated by faster speeds, suggesting that the effect is attributable to the process of self-organisation, rather than to the statistics of the physical-whisker dataset. The effects may by compensated by controlling the dynamics of L5 neurons differently, for example by modifying the neuronal input-output transfer function. We used a sigmoidal transfer function to prevent runaway recurrent excitation that can cause unstable network oscillations; however by balancing the recurrent excitatory and inhibitory interaction strengths more carefully, use of a non-saturating output function could provide a larger dynamic range of input-output relation-

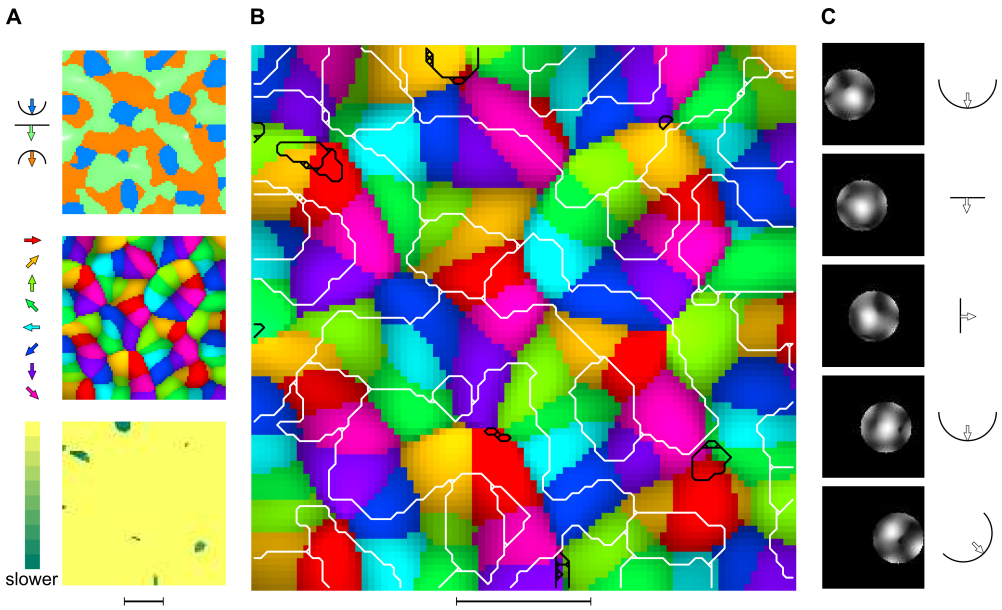

Figure 5.8. Maps generated using simulated whisker deflections. Self-organisation in L5 was driven by simulated whisker deflections, using a four-by-four whisker array. Maps generated in this way had similar form to those generated using physical whisker deflections, but were locally smoother and the discontinuities were less apparent. **A** The individual shape, direction, and speed maps are shown. Note, first that only three stimulus shapes were used for map training and testing, and hence that three colours indicate shape preferences; second, that the direction map is locally smooth, comprised of several large pinwheel-type structures, and; third, that faster speed preferences again dominate the map organisation, even though speeds were selected from a smaller range than in the physical whisker model. **B** When the tactile feature maps were overlaid, there was again evidence of orthogonal coding, with map contours tending to intersect at right angles, at least for stimulus shape and direction. The proportion of exactly orthogonal versus non-orthogonal intersections for shape versus direction was $59/(59 + 44.5) = 0.57$, for shape versus speed was $1/(1 + 0) = 1$, and for direction versus speed was $2/(2 + 7.5) = 0.21$. The figure facilitates stronger predictions about map L5 organisation. First, preferences for convex stimulus shapes, which deflect the whiskers away from one-another, are overlaid on discontinuities in the direction map that resemble pinwheel centers. Second, preferences for straight edge stimuli are overlaid on regions of local continuity in the direction map. Third, preferences for concave stimuli are overlaid at the linear fractures in the direction map. **C** Patches in the lateral inhibitory connections were delineated more strongly in the map organised using simulated multi-whisker deflection patterns (compare with Figure 5.4). Preferred stimuli for each of the five example neurons are indicated by symbols, with each preferring the fastest speed.

ships. Over larger ranges, smaller contrasts in the afferent activations of L5 neurons could break the symmetry of responses to different movement speeds, and thus aid their separation during self-organisation.

Compared with the stimulus-direction map organised using physical-whisker deflections, in which direction and speed were confounded, the map for simulated stimulus-direction preferences was locally smooth with each direction occupying equal cortical territory. As a consequence, the direction map was composed of large-scale circular structures, reminiscent of orientation pinwheels measured in visual cortex. Hence the self-organised mapping for stimulus direction promoted both coverage and continuity. Orthogonal coding was also evident when the direction map was overlaid with the self-organised map for stimulus shape preferences (Figure 5.8B).

L5 preferences were measured for the three stimulus shapes; a straight edge, a concave edge, and a convex edge. The organisation of preferences for each shape was clearly related to the structure of the direction map. For example, neurons preferring the straight edge encapsulated regions in which direction preferences varied continuously. Presumably this is because, unlike for the curved stimuli, there was no information in the identity or direction of whisker deflections in the plane perpendicular to that describing the movement direction. Preferences for the convex edge were confined to neurons representing discontinuities in the direction map, at the centers of pinwheel-like structures. At these regions of the direction map, directional preferences radiate outwardly, reflecting a major feature of the convex stimuli that they deflect the whiskers in a similar outwardly-radiating profile (Equation 5.8). Likewise, clusters of neurons preferring concave stimuli, which deflect the whiskers towards one-another, gathered at the fractures of low directional selectivity delineating the boundaries between the pinwheel-like

structures. Situated in these regions, nearby neurons can have maximally similar directional preferences based on their afferent connections, whilst maintaining lateral access to the range of deflection directions required to discriminate shape. This explanation was again supported by the observation that neuronal clusters preferring curved stimuli were expanded in maps measured using the settled responses, compared with those using the afferent responses.

These observations indicate that representations of more complex stimulus shapes will be found in the discontinuous regions of the stimulus-direction map. Thus, given knowledge of how a L5 neuron participates in the stimulus direction map, and particularly given a measure of its relative directional selectivity, we might infer its tactile stimulus shape preference. The interactions between shape and direction maps revealed here may also explain a tendency for convex shapes to dominate maps organised using physical whisker deflections (Figure 5.2A). The under-representation of cardinal directions led to a distortion of the directional pinwheels, such that regions representing whiskers deflected towards one-another were expanded in the direction map. These regions of the direction map correspond with the representation of convex stimuli in the shape map (as convex stimuli deflect the whiskers towards each other) and hence an apparent over-representation of convex stimuli in the shape map of Figure 5.2A.

5.4 Discussion

L5 barrel cortex was modelled as a self-organising network, and trained on patterns of simulated L2/3 activity that were derived from physical interactions between an array of artificial whiskers and a variety of tactile stimuli. After training on many examples of multi-whisker deflection

patterns, responses across a sheet of L5 neurons were used to construct maps from neuronal preferences for particular features of the tactile stimuli. As these feature maps developed, preferences for particular whiskers, for their deflection directions, and for particular combinations of stimulus shape, direction, and speed, became separated across L5.

Several lines of evidence suggest that the self-organisation of L5 connectivity patterns corresponded with a genuine separation of responses according to the tactile stimulus feature spaces, rather than one based on specific examples of whisker-deflection pattern. Firstly, the contours in maps measured for stimulus shape, direction, and speed preference, tended to intersect at right angles. If neurons had instead become organised into patches, each corresponding to one shape, one direction, and one speed, then the respective map contours would have been superposed, and thus L5 would have learnt preferences for individual examples of multi-whisker input rather than for the stimulus parameters represented by those examples. Secondly, inspection of maps generated using different realisations of each stimulus parameter combination revealed similar structures, as did maps generated by combining over realisations. Thus learnt representations were robust against sources of noise in the whisker movements that were uncorrelated with particular stimulus features. We can also be reasonably confident that representations were not based on noise correlated to particular stimulus parameters, because a previous analysis suggested that at least the timings of whisker deflections were dictated by the geometry of whisker-stimulus interactions (chapter 4). Therefore the network seems to have learnt representations of the tactile stimuli that were abstract with respect to specific examples of individual whisker movement.

The separation of L5 responses was due to a re-organisation of whisker representations, from those pertaining to individual whisker movements, to those pertaining to relationships between

multiple whisker movements (as suggested by Figure 5.7). Prior to training, a mapping for the identity of the whisker in the whisker array was inherited from an initial topographic organisation of L2/3 to L5 connections. However, this organisation was quickly overturned during learning, in favour of a repeating mosaic of smaller-scale maps for the array layout, in which responses reflected movements between rather than within the whiskers. The implication is that in areas downstream of L2/3, an organisation of responses based on the principal whisker identity may be secondary to one based on representations of more abstract multi-whisker features.

To what extent can the predictions of this high-level model of cortical development be expected to translate to the biology? Our previous model of barrel cortex map self-organisation used LISSOM to explore the development of maps for the principal whisker deflection direction (Wilson et al., 2010). In a more recent study (Kremer et al., 2011), the results of our model were validated using a network in which many of the biological assumptions implicit in LISSOM were made explicit. The model of Kremer et al. (2011) included realistic synaptic dynamics (as used here to simulate the L4 to L2/3 but not the L2/3 to L5 interaction), and the synaptic weights were modified in continuous-time using a spike-timing dependent plasticity learning rule in place of our rate-based approximation. Despite these modifications, at the level of map-organisation, the results of Wilson et al. (2010) and Kremer et al. (2011) were identical; for example, both models predict that map singularities are located further from the map center in more eccentric barrels. It is also interesting that Kremer et al. (2011) were able to generate the short-range excitatory and long-range inhibitory lateral interactions required for map self-organisation, using shorter-range inhibitory connections that are more biologically plausible; note that this paradox has also been resolved using LISSOM-like models of map development (Law, 2009). Overall, the consistency between map organisations predicted by the two types of model, suggest that predictions generated using our top-down approach can inform models that

are subjected to additional biological constraints.

Although based on only two network simulations, which grossly simplify the physical system in numerous ways, we can ask of the present results whether the structure of L5 receptive fields generated in simulation are consistent with those observed in the barrel cortex. Firstly, whereas an earlier study found consistency in the preferences of a given neuron for the direction in which adjacent whiskers are deflected (Kida et al., 2005), a more recent study found a null relationship between preferred deflection directions amongst whiskers (Hemelt et al., 2010). In line with the latter study, we observed only a weak correlation between the preferred deflection direction for the principal whisker and the mean direction computed across all other whiskers; i.e., a circular-circular correlation coefficient around 0.1 was measured throughout development, based on either the afferent or settled responses. Therefore, as seems to be the case in the biology, the model does not predict that L5 receptive-fields reflect simple co-linear deflection patterns. Secondly, Le Cam et al. (2011) recently found that for the majority of barrel cortex neurons, the center of gravity of responses across the whisker field depends on the direction in which the whiskers are deflected: In L5, they found that the center of gravity was shifted by between 0.6 and 0.7 whisker spacings, depending on whether whiskers were deflected to the left or to the right. An equivalent analysis in the model, averaging over four pairs of opposite deflection directions, yielded a mean shift of 0.59 ± 0.22 whiskers. Thus the simulations also predict that the whisker receptive field can be significantly modulated by the direction in which the whiskers are deflected. A final comparison can be drawn with the data of Jacob et al. (2008), which revealed selectivity in L5 neurons to the stimulus direction implied by the whisker deflection sequence, but no consistency between these preferences and the preferred principal-whisker deflection direction. To the extent that these two receptive field measures are approximated by those used to construct Figure 5.2B and Figure 5.2C, this null relationship was also true

in simulated L5. However, the dominance of preferences for faster speeds in simulation may be inconsistent with the data of Jacob et al. (2008), in which neurons displayed a degree of tuning for moderate movement speeds; the simulation result was explained earlier by a lack of symmetry breaking in the L5 recurrent connections.

The structure of maps generated using simulated deflections (Figure 5.8) may serve as more accurate predictions about the structure of maps in real barrel cortex based on real whisker experiences, during which there would be no reason for stimuli to be drawn from the discrete parameter sets used in the physical-whisker setup. The drawback to using simulated deflection patterns is that the distributions from which whisker movements are drawn, and indeed the choice of geometric model and the parameters to be varied, require us to introduce additional assumptions. By using deflections of physical whiskers, we at least introduced sources of external noise into the network that are analogous to those which may be experienced naturally, and against which we demonstrated robustness in the encoding and learning of feature representations. These types of noise are likely to better characterise biological noise than, for example, independent normally-distributed noise added to the deflection times and directions, that we might have introduced in simulation. Thus the implication is that robustness to noise at the sensory periphery is also a feature of biological cortical maps.

Short of training the network using statistics obtained from analyses of real whisker experiences, a better approach for a more comprehensive version of this study in the future, is to collect data from artificial whiskers mounted on autonomous, biomimetic robot platforms. Important questions, about how the interplay between the agent and its environment may shape cortical representations, can then be addressed by manipulating the environment, and then comparing learnt structure in simulated cortex with that in the cortices of animals reared under similar

conditions. This is the goal of our forthcoming research program. In this context, the present results, obtained using inputs gathered under controlled conditions will serve as a benchmark, against which to test hypotheses about how the nature of somatosensory inputs shapes their representation in the brain.

Chapter 6

General discussion

Chapter summary

The central thesis, as posed in chapter 1, is that sensory motion may be represented in the sensory cortex by spatial coding. This is the problem referred to as *Figuring Time by Space*. Specifically, the thesis has provided evidence that first order motion, as represented by the movement of one of the facial whiskers, and second order motion, as represented by the inter-whisker deflection interval, are encoded in the somatosensory barrel cortex in topological and/or topographical maps. The thesis set out to formulate the idea of *Figuring Time by Space* as a scientific theory, by constructing top down models of sensory motion processing in the whisker-barrel system. In this general discussion, the main findings of the thesis are reiterated, the modelling approach is evaluated, specific suggestions for further experimental work are presented, and some general implications of the research are offered.

6.1 Summary of main findings

Chapter 2 presented the hypothesis that input driven self-organisation can explain how a somatotopically aligned pinwheel mapping for the whisker movement direction (first order motion) can emerge across the supra-barrels. The explanation is that typical multi-whisker deflection patterns, coupled with cortical interactions that result in the settling of activity in regions of high contrast in afferent inputs, become associated with particular layer 2/3 neurons during post-natal development. The pinwheel mapping emerges if typical whisker deflection patterns are spatially coherent, i.e., if first- and second-order motions are colinear. Essentially, in a generic model of sensory cortex, previously investigated by analogy with the visual cortex, visual inputs were substituted for tactile inputs and tactile maps emerged. Therefore, in answer to the first research question, a general model of cortical development can explain the existence of a whisker direction map in the barrel cortex.

Chapter 3 presented the distance-dependent delay hypothesis. The hypothesis explained existing data, relating the relative timing of multi-whisker deflections (second order motion) to the location of active barrel cortex neurons, as a reflection of an underlying continuum of differences in axonal signalling delays. Inspired by an existing theory of how inter-ear timing differences are resolved in the auditory midbrain (place theory; Jeffress, 1948), a simple model that incorporated plausible connection distances, geometry, and speeds, reproduced a range of complex response properties measured in the barrel cortex. Therefore, in answer to the second research question, a general model for resolving the relative timing of sensory inputs can explain neuronal responses to differing whisker timings in the barrel cortex.

In chapter 4 the research question was whether the spatial coding mechanisms identified in the

previous chapters could be used to reconstruct tactile stimulus features from real (i.e., physical) multi-whisker deflection patterns. The answer is that features could be reconstructed after cortical re-mapping, at least as well as they could be reconstructed after remapping via a sensible control operation. Processing inputs from a physical model of whisker-stimulus interactions, chapter 4 showed how cortical responses predicted by the distance-dependent delay hypothesis translate from a one-dimensional string of neurons to a two-dimensional sheet of neurons. The process revealed robustness of the neural encoding to sources of external noise and it forced more of the assumptions involved in constructing the encoding to become explicit.

In chapter 5 cortical responses to the artificial whisker deflection signals, collected as part of chapter 4, were processed by the model developed in chapter 3, and used to drive the self-organising algorithm presented in chapter 2. Hence after a full exploration of the behaviour at each level of processing, the full model presented in chapter 5 was used to generate predictions about the functional organisation of layer 5 barrel cortex, about which there is relatively little data. As the biological constraints were more relaxed, chapter 5 represents an exploratory modelling study, with a focus on generating qualitative predictions about the cortical organisation. This approach generated specific predictions that can guide future experimental work on an important and difficult area of research. For example, the major prediction is that components of the multi-whisker deflection pattern that describe orthogonal features of a tactile stimulus, such as its shape and motion direction, will be represented in coextensive topological maps across layer 5, with contours that intersect at right angles. Hence, whilst some of the details may be shown in future experiments to be wrong, the model makes falsifiable predictions about the functional organisation of responses in layer 5, and therefore it is useful (Box and Draper, 1987).

6.2 All models are wrong, but some are useful

Chapters 2 and 3 each explained a range of complex neuronal stimulus-response interactions in terms of simple organisational principles. Although it is important to clarify that these explanations do not in themselves rule out alternatives, no explicit, verifiable, falsifiable explanation had been formulated beforehand. Hence the contribution of chapters 2 and 3 has been to formulate the first explicit theories of the functional organisation in the barrel cortex. Each model represents, at best, a theory of cortical computation, and at worst, a straw-man to be knocked down in a step towards a deeper understanding. Formulated as they are as computational models, it is clear how each theory can be knocked down. For example, if anti-correlation of a particular whisker's deflection direction failed, in a future experiment, to anti-correlate the corresponding whisker direction map (Figure 2.7), then we would know that the self-organising model of pinwheel map development must be wrong. Similarly, if the preferred inter-whisker deflection interval can be shown not to be correlated with the specified differences in axonal path lengths, then we would know that the distance-dependent delay hypothesis must be wrong.

Like any other theoretical formulation, if the model is revealed to be wrong then it can be revised or discarded. For example, when the work in chapter 2 was first submitted for publication, reviewers challenged an original assumption that whisker deflection magnitudes are graded across the whisker field in the direction of stimulus movement. The model was therefore revised to include a simpler binary deflection gradient, where some whiskers are deflected and other whiskers are not. Thus the hypothesised role of recurrent dynamics in amplifying afferent activity gradients was revealed to be more general and thus more powerful than first anticipated, extending to the simpler case of binary deflections. Similarly, when the distance-dependent

delay hypothesis was originally submitted for publication, reviewers challenged an original assumption that the major inhibitory influence on the L2/3 responses originates in L2/3 rather than in L4. As suggested by the reviewers, this is inconsistent with the known anatomy because any plausible inter-connection geometry based on this assumption would require differences in axonal path lengths that are too large to be generated within rather than between cortical laminae. The description of the model was therefore revised, and the process revealed the specific model prediction that L4 to L2/3 inhibitory axonal conduction speeds must be faster than their excitatory counterparts.

In order to process inputs from physical whisker sensors in chapter 4, the model required an explicit representation of thalamic neuronal processing, which based on the available data was assumed to act as a filter for the velocity of single-whisker movements. The process of making this type of assumption explicit revealed some of the technical and practical challenges that may face attempts to mimic the capabilities of biological whisker systems in robots. For example, it became clear that a system based on isolating high-velocity whisker movements will be significantly affected by whisker deflection offsets, unless offsets are actively controlled at the sensory periphery. The impact of the offsets on the cortical responses, such as through an increase in afferent activity and through a correlation between afferent neurons of opposite directional tuning, appears obvious only in retrospect.

6.3 Future directions: suggestions for experiments

Inputs to the model presented in chapter 2 were derived via the exact same analogy as that used to derive the inputs to the model of Kremer et al. (2011), that of a straight edge moving through the whisker field. In the model of Kremer et al. (2011) the relative whisker deflection times were communicated to a network of spiking unit as its dynamics unfolded in continuous time. However in the model of chapter 2 relative whisker deflections were communicated to the network implicitly by collapsing the full spatial-temporal evolution of the stimulus down to a snapshot of whisker activity at a single point in time. The history of the stimulus motion was captured by the binary activation of whiskers that would, at that point in time, have recently been deflected by the stimulus. Although the same stimulus movement was presented to the two models using slightly different methods, at the level of the map organisation both models produce identical results. Maps generated in both models result from unsupervised learning which reveals the statistical structure in the input patterns. Therefore any important additional structure that may have been communicated to the network of Kremer et al. (2011), by representing time explicitly, should have resulted in differences in map structure. The Kremer et al. (2011) model provides an important validation of the results in chapter 2, using a more realistic network. However it may be more interesting in a future study to ask further questions of this model relating to stimulus features that require an explicit representation of time, e.g., by trying to measure a stimulus speed map.

A particular strength of the computational model is in its power to predict, and several predictions have been derived during the presentation of this thesis. A central prediction of the distance-dependent delay hypothesis is that the position of the layer 2/3 neuron, relative to two

underlying barrels, is correlated with its preferred inter-whisker deflection interval. Specifically, deflection of whisker A before whisker B will evoke selective responses in neurons located closer to barrel B, and vice versa; thus position x should be anti-correlated with the maximally effective inter-whisker interval (IWI). As presented in Figure 6.1, the original data of Shimegi et al. (2000) were very kindly supplied for reanalysis by S. Shimegi and H. Sato of Osaka University Japan. The analysis is presented in this section on future directions because it is not complete, and as such the details are presented only briefly in the figure caption. However the initial results of the analysis are promising; smoothing over conditions to estimate the preferred IWIs of thirty-one layer 2/3 neuronal response profiles a regression of preferred-IWI onto x revealed a fit $\mathrm{IWI} = -3.61x + .26$; Pearson's correlation coefficient $r_{(29)} = .44$, $p = .0124$. Four neurons were excluded from the analysis based on inspection of the spike-histograms, either because their spikes were relatively poorly time-locked to the stimulus or because the smoothing generated artificially large preferred IWIs (see Figure 6.1D); we note that for each excluded neuron secondary peaks were evident at IWIs consistent with the overall trend, although it is difficult to draw out this relationship using transparent statistics. Excluding these neurons, the general relationship between x and the preferred IWI is as predicted by the distance-dependent delay hypothesis. Thus we might expect that a future experiment in which data like those of Shimegi et al. (2000) are collected to explicitly test the distance-dependent hypothesis will be fruitful. This is an important experiment to conduct.

It is constructive to detail a particular experiment suggested by the model presented in chapter 5. A key prediction of the model is that orthogonal components of second-order whisker motion, describing the shape and direction of a tactile stimulus moving through many whiskers, are represented by spatial coding across the sheet of layer 5 barrel cortex, in topological maps whose contours intersect at right angles. To test the hypothesis one would record somatosensory-

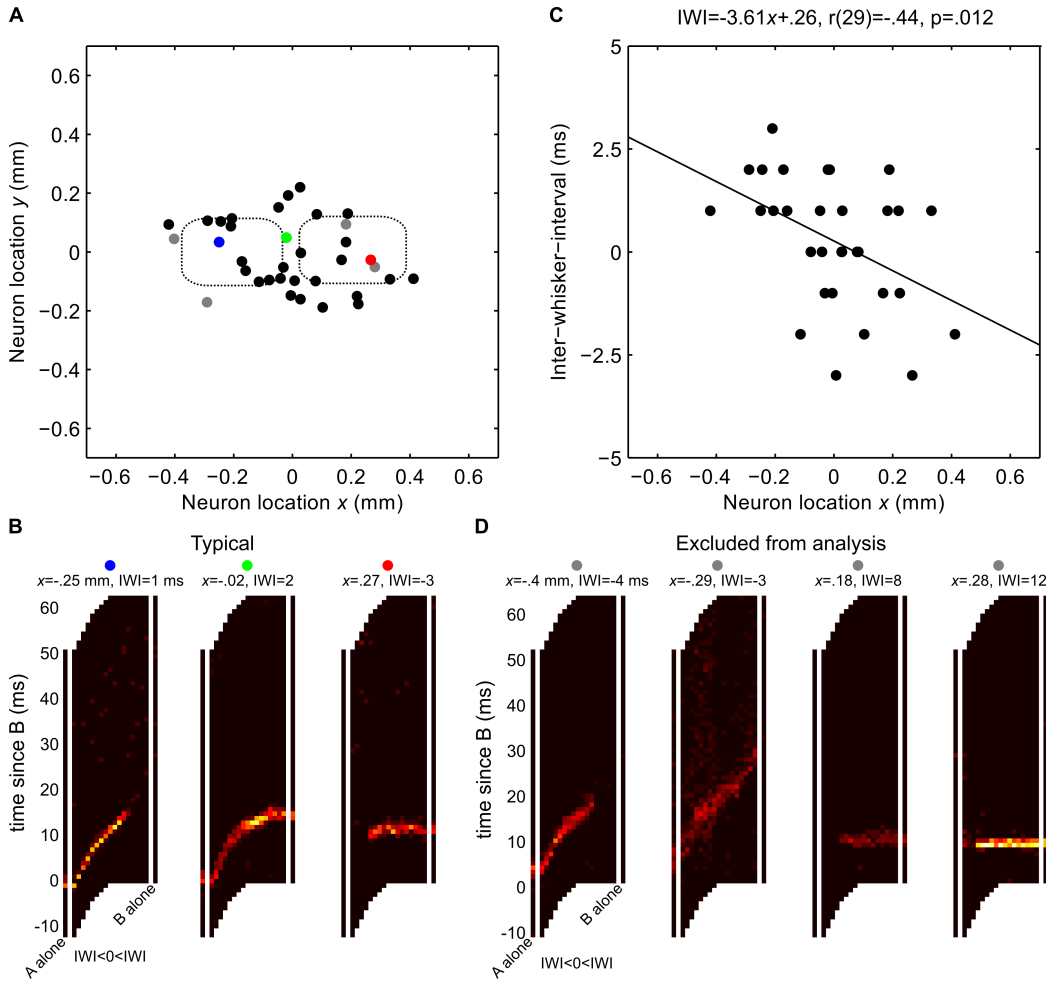

Figure 6.1. Pilot analysis of Shimegi et al., (2000) data confirms the model. S. Shimegi and H. Sato most kindly recovered and supplied 35 L2/3 neuronal response profiles to adjacent-whisker inter-deflection-intervals $\mathrm{IWI} \in \pm\{0, 1, 2, 3, 4, 6, 8, 10, 12\}$. Response profiles for 26 neurons (9 tested using two whisker-pairs) consisted of histograms of mean spikes over 25 or 50 trials in $1\,\mathrm{ms}$ bins beginning at the onset of the first whisker deflection. **A** Neuron location (x, y) in the tangential plane, was estimated histologically, and $0.4\,\mathrm{mm}$ spacing between barrel (dotted) centers was assumed *post hoc*. Neurons located above a particular barrel (e.g., blue/red) typically spiked a fixed time after deflection of the corresponding whisker, whereas neurons towards the midline (e.g., green) tended to spike a fixed latency following the earliest deflection; see **B** for individual responses. **C** Response profiles $r_{t,i}$ were smoothed across ascending $\mathrm{IWI_i}$: $r'(i) = \sum_t(\tau_2 r_{t,i-1} + (\tau_1 + \tau_2)r_{t,i} + \tau_1 r_{t,i+1})/2(\tau_1 + \tau_2)$, $\tau_1 = \mathrm{IWI}(i) - \mathrm{IWI}(i-1)$, where $\tau_2(i) = \mathrm{IWI}(i+1) - \mathrm{IWI}(i)$, and we specify $\tau_1 = \tau_2$ for $\mathrm{IWI} = \pm 12\,\mathrm{ms}$. The preferred IWI, estimated as $\arg\max_{\mathrm{IWI_i}} r'(i)$, is plotted against x and fit by linear regression. A significant anti-correlation was consistent with the predictions of the distance-dependent delay hypothesis. **D** Due mainly to smoothing artefacts responses of the grey neurons in **A** were excluded from **C**. Statistics without exclusion: $\mathrm{IWI} = 2.29x + .61$, $r_{(33)} = .16$, $p = .35$.

evoked responses across a hemisphere of barrel cortex, targeting layer 5 *in vivo* in adult rats at day P81+ (Kremer et al., 2011), using two-photon calcium imaging to capture map-level organisation at high spatial and temporal resolution (see Kerr et al., 2007; Kremer et al., 2011, but note that at the time of writing two-photon recordings in L5 have only been achieved in mouse cortex; Mittmann et al., 2011). All contralateral whiskers would be stimulated, using a matrix of omni-directional actuators (Jacob et al., 2008, 2010; Le Cam et al., 2011) to imply the variety of semi-circular edge movements defined by Equation 5.8. Stimuli would be delivered in pseudo-random order to control for the possibility of map smoothing by adaptation to consecutively presented stimuli, and responses to identical stimuli would be compared by presentation order to rule out map entraining (see Li et al., 2008). Finally alignment of the images to the barrel layout would be confirmed *post mortem* by histology.

Validating the prediction of orthogonal coding in an experiment like this is very important. Falsification, for example if two-photon imaging revealed a random map in adult layer 5, would be interesting because it would suggest that cortical areas processing information from different modalities and in different species employ specialised organisational principles. This is the implication of recent results showing a random map for orientation preferences in the primary visual cortex of certain rodent species (van Hooser et al., 2005), as well as a lack of patchy lateral connectivity between similar orientation domains (van Hooser et al., 2006); although LISSOM-like simulations have recently demonstrated how orientation selectivity in the absence of orientation maps can arise from input driven self-organisation, as a result of biologically plausible levels of retinotopic scattering in the thalamo-cortical projection (Law, 2009). Conversely, confirmation of orthogonal coding would be strong evidence that input-driven self-organisation in mammalian primary sensory cortex serves as a general purpose mechanism for representing the world, by reducing it to the most relevant feature dimensions, at least in vision

and touch. In essence, confirmation of orthogonal coding would be evidence that the sensory cortex does what this thesis set out to acheive. That is, to reduce the dimensions of the problem; to describe what is important by abstracting over the details. Perhaps then, the brain itself should be considered as a modeller?

6.4 When is a topological map necessary?

This thesis has presented evidence suggesting that topological feature maps characteristic of those in primate primary visual cortex are also present in rodent barrel cortex. However not all stimulus features appear to be mapped topologically in rodent primary cortical areas. For example, whilst the retinotopic map in rodent V1 has been well characterised (e.g., Gias et al., 2005) maps for visual edge orientation in rodent V1 appear to be random (van Hooser et al., 2005). If we assume that topological maps for alternative features do not preside over the rodent V1 orientation map, then the apparent discrepancy between rodent and primate maps raises the question of exactly when a topological map is necessary. Why should projections from a high-dimensional stimulus feature space onto two cortical sheet dimensions preserve feature space topology (Durbin and Mitchison, 1990)?

Answers to this question have often appealed to the idea of minimal wiring lengths (Koulakov and Chklovskii, 2001). The idea is that random maps minimise metabolic and structural costs associated with the lengths of connections between neurons that represent similar features, whilst maximising feature space coverage across local regions of the map (e.g., a neuron tuned for ‘up’ is equidistant from neighbours representing all angles). Conversely, topological maps

minimise wiring lengths whilst maximising feature space continuity across local regions of the map (e.g., a neuron tuned for 'up' is closer to other 'up' neurons and further from 'down' neurons). This minimal wiring length argument is by itself unsatisfying because it does not explain the functional significance of representing feature space continuously.

Preserving continuity in feature space preserves also notional distances between features present in a stimulus. Therefore, unlike a random map, a topological map allows a comparison between features to be computed in units of inter-neuronal connection distance. This means that any computation based on the degree of similarity between stimulus features can be implemented on a topological map using monotonic functions of the inter-neuronal distance. For example, relative to a topological orientation map, lateral inhibition that increases in strength with inter-neuronal distance will enhance responses to edges of novel orientation against a background of similar (and thus mutually suppressive) orientations. However, it is not difficult to conceive of appropriate non-monotonic connectivity in random maps that can achieve identical functionality. Therefore any comparison between stimulus features that requires a topological map should utilise some network property that is constrained to vary monotonically with inter-connection distance.

A candidate network property is the signalling latency, which must increase monotonically with inter-connection distance if axonal and dendritic propagation speeds are finite and essentially homogeneous. As we saw in Chapter 3, measuring distances in feature space in terms of relative signalling latencies fulfils the basic requirements for second order motion detection outlined by Borst and Egelhaaf (1989). Therefore topological maps are required for the use of distance dependent signalling delays to measure the velocity of stimulus motion through feature space. For example, the rotation of a visual edge defines a velocity vector in the orientation domain, and

hence distance dependent signalling delays can be used to compute the speed and direction of rotation in a topological orientation map. Similar mechanisms could in principle resolve vectors defined in arbitrary feature spaces using distance dependent delays and topological maps. Thus *Figuring Time by Space* may well be the primary function of topological maps.

The argument can be summarised as follows. i) By definition, topological maps preserve continuity and thus notional distances in feature space; ii) Distances in feature space correspond to differences between features present in a stimulus; iii) Computations based on these differences alone can be resolved in random maps using non-monotonic functions of inter-neuronal distance; iv) However computations based on differences between features and relying on monotonic functions of inter-neuronal distance necessitate topological maps; v) These include any computation relying on finite, homogeneous inter-neuronal connection speeds to resolve motion velocities through arbitrary feature spaces; vi) Thus the topological map may be necessary for any computation that requires figuring time by space.

6.5 The best model for a rat is another, or preferably the same rat

Rosenblueth and Wiener (1945) were of course being flippant when they declared that '...the best material model for a cat is another, or preferably the same cat' (page 320). What they meant is that the system is necessarily the most accurate *description* of itself. My cat is called Dinah. A perfect description of Dinah's brain, down to the quantum state(s) of every molecule flowing at every synapse, in itself offers no better explanation for how Dinah perceives her world than

does Dinah herself, nor can it predict how she will behave next. One could argue that new insights would be gained by constructing such a detailed model, or that once constructed, the model would be more amenable to scientific investigation. These are both valid points only if at some stage we start to abstract over the details, i.e., by making a model of the model. Else, as Rosenblueth and Wiener (1945) conclude, for anybody to comprehend the original model, to the point that they may elaborate upon it, would require a level of comprehension that would render such a modelling effort unnecessary. If this is true, then how can progress be made?

By adopting a top down approach to modelling, the work of this thesis has provided insights into the functional organisation of the barrel cortex that may have been difficult to establish using only a bottom up approach. For example, imagine for the sake of argument that evolution has selected the structure of the barrel column for the property that it discretises the location of neurons in cortical space and thus supports a Jeffress-like place coding for the inter-whisker interval. It is difficult to imagine how this could have been revealed by bottom up models, simply because current models have necessarily been simulating the neuronal and synaptic processes in single columns that are isolated from sensory input. Of course, bottom up models have an important role to play in understanding brain function. For example the model of Wilson et al. (2011) presented in chapter 3 leaned heavily on the equations and parameters used by Sarid et al. (2007) in order to represent processes of synaptic integration in the barrel cortex with confidence. This serves to illustrate how the bottom up approach to modelling can inform models constructed from the top down. Imagine now that the primary function of the barrel column were instead to learn the topology of the space of typical whisker deflection directions. According to the self-organisation hypothesis, the minimum requirements for this organisation to emerge are inputs from multiple whiskers, spatial coherence between experienced whisker deflections, and Hebbian learning. Again, even if the next generation of bottom up models

simulated more than one column, it would be a long time before the function of the system as a whole could be elucidated. The interplay between the studies of Wilson et al. (2010) and Kremer et al. (2011), in which the details of the relatively abstract model of chapter 2 were verified in simulations that filled in some of the biological details, serves to illustrate how the top down approach to modelling can inform models constructed from the bottom up. Thus it seems that bottom up models like those of Sarid et al. (2007) and Lefort et al. (2009) provide essential tools for informing higher-level models, and *vice versa*, in equal measures. The truth, so to speak, will almost certainly lie at the point where top down, bottom up, and experimental approaches converge; i.e., in a collaborative cycle of top down prediction, experimental validation, and bottom up verification. Perhaps it is only through such a cyclical process that we can progress towards understanding how high level phenomena like perception and consciousness are subserved by neural circuitry (but see Markram, 2006).

6.6 Conclusion: 'seeing' with whiskers

By way of a conclusion, the thesis will end by taking the liberty to discuss the potential role of spatial coding in perception; or 'seeing' (see Frisby and Stone, 2010 on seeing in the context of visual perception).

The evidence for *Figuring Time by Space*, from which the models presented in this thesis were derived, was measured almost exclusively from neurons of the lemniscal pathway (barrelette, barreloid, barrel, supra/infra-barrels and beyond), whereas much of the evidence for figuring space by time is provided instead in paralemniscal pathways that deviate from the lemniscal

pathway at the brainstem (Ahissar and Arieli, 2001). Therefore it may be useful to consider these two pathways as separate streams for processing temporal and spatial information. Seeing is about figuring both time and space, and thus it surely involves both streams. Note that the dichotomy between processing streams is presented with the caveat that there is likely to be considerable interplay between the two, as representations become increasingly abstract along the neuraxis with respect to simple motion primitives like the whisker deflection direction (see Bale and Petersen, 2009).

From the perspective of Gibson (1962), seeing might be recast as a more general problem of active sensing, where the observer seeks to elicit the behaviours that are afforded by stimulus objects, i.e., a mug affords grasping, a wedge of cheese affords eating, and, to an Etruscan shrew at least (Anjum et al., 2006), a cricket leg affords attack. Like all mammalian sensory systems, the whisker system is dynamic and active; rats, for example, palpate the whiskers at around ten 'whisks' per second (Welker, 1964; Kleinfeld et al., 2006; Grant et al., 2009, 2011). In light of evidence from the whisker system, the role of spatial coding during perception might be explained as follows. Topographical cortical maps for first-order sensory motion (i.e., chapter 2; Wilson et al., 2010) and second-order sensory motion (i.e., chapter 3; Wilson et al., 2011), are each in spatial register with an overall map of the body (Stafford and Wilson, 2007), anchored as they are to the layout of cortical columns. Spatial relationships in the sensory environment are therefore preserved, and thus stimuli are played out onto a kind of Cartesian screen (Dennett, 1991). Projections onto the cortical screen are gated by the thalamus, which itself contains a mapping of the sensory cortex (Hartings et al., 2000), and which illuminates salient regions of cortical feature maps (Crick, 1984). In turn representations of salient stimuli are attended to, without invoking a homunculus, but as manifest in the dynamic shaping of thalamic maps by cortical activity (Li and Ebner, 2007). Topological maps for higher-order

stimulus features are maintained in projections through deep brain structures (Welker et al., 1988; Mercier et al., 1990; Hoover et al., 2003; Hoffer et al., 2005), such as the basal ganglia which resolve competing requests for access to motor resources (Redgrave et al., 1999; Gurney et al., 2001a,b). Preservation of the topology of sensory input spaces through the brain may ensure efficiency in fulfilling the affordances of salient sensory stimuli, as mammalian sensory-motor systems interact dynamically with the sensory environment.

To conclude, during the course of this thesis the idea that sensory motion is represented in the sensory cortex via a series of coextensive spatial codes was developed into the theory of *Figuring Time by Space*. The theory was formulated scientifically using a series of top down systems-level computational neuroscience models of the whisker barrel system. Based on simple and local principles of functional organisation between cortical neurons, *Figuring Time by Space* represents a general theory of neural computation in the mammalian sensory cortex.

References

Adesnik, H. and Scanziani, M. (2010). Lateral competition for cortical space by layer-specific horizontal circuits. *Nature*, 464(7292):1155–1160.

Ahissar, E. (1998). Temporal-code to rate-code conversion by neuronal phase-locked loops. *Neural Comput*, 10(3):597–650.

Ahissar, E. and Arieli, A. (2001). Figuring space by time. *Neuron*, 32(2):185–201.

Ahissar, E. and Staiger, J. (2010). S1 laminar specialization. *Scholarpedia*, 5(8):7457.

Ahl, A. S. (1986). The role of vibrissae in behavior: a status review. *Vet Res Commun*, 10(4):245–268.

Ajima, A. and Tanaka, S. (2006). Spatial patterns of excitation and inhibition evoked by lateral connectivity in layer 2/3 of rat barrel cortex. *Cereb Cortex*, 16(8):1202–1211.

Alloway, K. D. (2008). Information processing streams in rodent barrel cortex: the differential functions of barrel and septal circuits. *Cereb Cortex*, 18(5):979–989.

Andermann, M. L. and Moore, C. I. (2006). A somatotopic map of vibrissa motion direction within a barrel column. *Nat Neurosci*, 9(4):543–551.

Andermann, M. L. and Moore, C. I. (2008). Mechanical resonance enhances the sensitivity of the vibrissa sensory system to near-threshold stimuli. *Brain Res*, 1235:74–81.

Andermann, M. L., Ritt, J., Neimark, M. A., and Moore, C. I. (2004). Neural correlates of vibrissa resonance; band-pass and somatotopic representation of high-frequency stimuli. *Neuron*, 42(3):451–463.

Anjum, F., Turni, H., Mulder, P. G. H., van der Burg, J., and Brecht, M. (2006). Tactile guidance of prey capture in Etruscan shrews. *Proc Natl Acad Sci U S A*, 103(44):16544–16549.

Arabzadeh, E., Panzeri, S., and Diamond, M. E. (2004). Whisker vibration information carried by rat barrel cortex neurons. *J Neurosci*, 24(26):6011–6020.

Arabzadeh, E., van Heimendal, M., and Diamond, M. (2009). Vibrissal texture decoding. *Scholarpedia*, 4(4):6640.

Arabzadeh, E., Zorzin, E., and Diamond, M. E. (2005). Neuronal encoding of texture in the whisker sensory pathway. *PLoS Biol*, 3(1):e17.

Armstrong-James, M., Fox, K., and Das-Gupta, A. (1992). Flow of excitation within rat barrel cortex on striking a single vibrissa. *J Neurophysiol*, 68(4):1345–1358.

Auer, P., Burgsteiner, H., and Maass, W. (2008). A learning rule for very simple universal approximators consisting of a single layer of perceptrons. *Neural Netw*, 21(5):786–795.

Bale, M. R. and Petersen, R. S. (2009). Transformation in the neural code for whisker deflection direction along the lemniscal pathway. *J Neurophysiol*, 102(5):2771–2780.

Barth, D. S. (2003). Submillisecond synchronization of fast electrical oscillations in neocortex. *J Neurosci*, 23(6):2502–2510.

Basole, A., Kreft-Kerekes, V., White, L. E., and Fitzpatrick, D. (2006). Cortical cartography revisited: A frequency perspective on the functional architecture of visual cortex. *Prog Brain Res*, 154:121–134.

Beaulieu, C. (1993). Numerical data on neocortical neurons in adult rat, with special reference to the gaba population. *Brain Res*, 609(1-2):284–292.

Bednar, J. A. (2012). Building a mechanistic model of the development and function of the primary visual cortex. *Journal of Physiology (Paris)*, In Press.

Bednar, J. A., Choe, Y., De Paula, J., Miikkulainen, R., Provost, J., and Tversky, T. (2004). Modeling cortical maps with Topographica. *Neurocomputing*, 58-60:1129–1135.

Bednar, J. A. and Miikkulainen, R. (2003). Self-organization of spatiotemporal receptive fields and laterally connected direction and orientation maps. *Neurocomputing*, 52-54:473–480.

Beierlein, M., Gibson, J. R., and Connors, B. W. (2003). Two dynamically distinct inhibitory networks in layer 4 of the neocortex. *J Neurophysiol*, 90(5):2987–3000.

Benison, A. M., Ard, T. D., Crosby, A. M., and Barth, D. S. (2006). Temporal patterns of field potentials in vibrissa/barrel cortex reveal stimulus orientation and shape. *J Neurophysiol*, 95(4):2242–2251.

Benucci, A., Frazor, R. A., and Carandini, M. (2007). Standing waves and traveling waves distinguish two circuits in visual cortex. *Neuron*, 55(1):103–117.

Benusková, L., Ebner, F. F., Diamond, M. E., and Armstrong-James, M. (1999). Computational study of experience-dependent plasticity in adult rat cortical barrel-column. *Network*, 10(4):303–323.

Birdwell, J. A., Solomon, J. H., Thajchayapong, M., Taylor, M. A., Cheely, M., Towal, R. B., Conradt, J., and Hartmann, M. J. Z. (2007). Biomechanical models for radial distance determination by the rat vibrissal system. *J Neurophysiol*, 98(4):2439–2455.

Blakemore, C. and Cooper, G. F. (1970). Development of the brain depends on the visual environment. *Nature*, 228(5270):477–478.

Blakemore, C., Movshon, J. A., and van Sluyters, R. C. (1978). Modification of the kitten's visual cortex by exposure to spatially periodic patterns. *Exp Brain Res*, 31(4):561–572.

Blasdel, G. G., Mitchell, D. E., Muir, D. W., and Pettigrew, J. D. (1977). A physiological and behavioural study in cats of the effect of early visual experience with contours of a single orientation. *J Physiol*, 265(3):615–636.

Borghuis, B. G., Perge, J. A., Vajda, I., van Wezel, R. J. A., van de Grind, W. A., and Lankheet, M. J. M. (2003). The motion reverse correlation (MRC) method: a linear systems approach in the motion domain. *J Neurosci Methods*, 123(2):153–166.

Borst, A. and Egelhaaf, M. (1989). Principles of visual motion detection. *Trends Neurosci*, 12(8):297–306.

Bosking, W. H., Zhang, Y., Schofield, B., and Fitzpatrick, D. (1997). Orientation selectivity and the arrangement of horizontal connections in tree shrew striate cortex. *J Neurosci*, 17(6):2112–2127.

Box, G. and Draper, N. (1987). *Empirical model-building and response surfaces*. Wiley series in probability and mathematical statistics: Applied probability and statistics. Wiley.

Braitenberg, V. (1984). *Vehicles, experiments in synthetic psychology*. MIT Press, Cambridge, Mass.

Branco, T., Clark, B. A., and Hausser, M. (2010). Dendritic discrimination of temporal input sequences in cortical neurons. *Science*, 329(5999):1671–1675.

Brecht, M. (2006). Good vibrations. focus on "texture signals in whisker vibrations". *J Neurophysiol*, 95(3):1307–1308.

Brecht, M., Preilowski, B., and Merzenich, M. M. (1997). Functional architecture of the mystacial vibrissae. *Behav Brain Res*, 84(1-2):81–97.

Brecht, M. and Sakmann, B. (2002). Whisker maps of neuronal subclasses of the rat ventral posterior medial thalamus, identified by whole-cell voltage recording and morphological reconstruction. *J Physiol*, 538(Pt 2):495–515.

Brumberg, J. C., Pinto, D. J., and Simons, D. J. (1996). Spatial gradients and inhibitory summation in the rat whisker barrel system. *J Neurophysiol*, 76(1):130–140.

Brumberg, J. C., Pinto, D. J., and Simons, D. J. (1999). Cortical columnar processing in the rat whisker-to-barrel system. *J Neurophysiol*, 82(4):1808–1817.

Bruno, R. M., Hahn, T. T. G., Wallace, D. J., de Kock, C. P. J., and Sakmann, B. (2009). Sensory experience alters specific branches of individual corticocortical axons during development. *J Neurosci*, 29(10):3172–3181.

Bruno, R. M., Khatri, V., Land, P. W., and Simons, D. J. (2003). Thalamocortical angular tuning domains within individual barrels of rat somatosensory cortex. *J Neurosci*, 23(29):9565–9574.

Bruno, R. M. and Simons, D. J. (2002). Feedforward mechanisms of excitatory and inhibitory cortical receptive fields. *J Neurosci*, 22(24):10966–10975.

Burger, T. and Lang, E. W. (2001). Self-organization of local cortical circuits and cortical orientation maps: a nonlinear Hebbian model of the visual cortex with adaptive lateral couplings. *Z Naturforsch [C]*, 56(5-6):464–478.

Carvell, G. E. and Simons, D. J. (1990). Biometric analyses of vibrissal tactile discrimination in the rat. *J Neurosci*, 10(8):2638–2648.

Carvell, G. E. and Simons, D. J. (1995). Task- and subject-related differences in sensorimotor behavior during active touch. *Somatosens Mot Res*, 12(1):1–9.

Cavanagh, P. and Mather, G. (1989). Motion: The long and short of it. *Spat Vis*, 4(2-3):103–129.

Celikel, T. and Sakmann, B. (2007). Sensory integration across space and in time for decision making in the somatosensory system of rodents. *Proc Natl Acad Sci U S A*, 104(4):1395–1400.

Chakrabarti, S. and Alloway, K. D. (2009). Differential response patterns in the SI barrel and septal compartments during mechanical whisker stimulation. *J Neurophysiol*, 102(3):1632–1646.

Chernova, O. F. and Kulikov, V. F. (2011). Structural differences between the shafts of mammalian vibrissae and hairs and their causes. *Dokl Biol Sci*, 438:182–185.

Civillico, E. F. and Contreras, D. (2006). Integration of evoked responses in supragranular cortex studied with optical recordings in vivo. *J Neurophysiol*, 96(1):336–351.

Cohen, J. (1968). Weighted kappa: Nominal scale agreement with provision for scaled disagreement or partial credit. *Psychol Bull*, 70(4):213–220.

Crick, F. (1984). Function of the thalamic reticular complex: The searchlight hypothesis. *Proc Natl Acad Sci U S A*, 81(14):4586–4590.

Dayan, P. and Abbott, L. (2001). *Theoretical neuroscience: Computational and mathematical modeling of neural systems*. MIT Press.

Dehnhardt, G., Mauck, B., Hanke, W., and Bleckmann, H. (2001). Hydrodynamic trail-following in harbor seals (phoca vitulina). *Science*, 293(5527):102–104.

Dennett, D. (1991). *Consciousness explained*. The Penguin Press.

Derdikman, D., Hildesheim, R., Ahissar, E., Arieli, A., and Grinvald, A. (2003). Imaging spatiotemporal dynamics of surround inhibition in the barrels somatosensory cortex. *J Neurosci*, 23(8):3100–3105.

Diamond, M. E., von Heimendahl, M., Knutsen, P. M., Kleinfeld, D., and Ahissar, E. (2008). 'where' and 'what' in the whisker sensorimotor system. *Nat Rev Neurosci*, 9(8):601–612.

Drew, P. J. and Feldman, D. E. (2007). Representation of moving wavefronts of whisker deflection in rat somatosensory cortex. *J Neurophysiol*, 98(3):1566–1580.

Durbin, R. and Mitchison, G. (1990). A dimension reduction framework for understanding cortical maps. *Nature*, 343(6259):644–647.

Ebara, S., Kumamoto, K., Matsuura, T., Mazurkiewicz, J. E., and Rice, F. L. (2002). Similarities and differences in the innervation of mystacial vibrissal follicle-sinus complexes in the rat and cat: a confocal microscopic study. *J Comp Neurol*, 449(2):103–119.

Ego-Stengel, V., Mello e Souza, T., Jacob, V., and Shulz, D. E. (2005). Spatiotemporal characteristics of neuronal sensory integration in the barrel cortex of the rat. *J Neurophysiol*, 93(3):1450–1467.

Epstein, J. M. (2008). Why model? *Journal of Artificial Societies and Social Simulation*, 11(4):12.

Ermentrout, B., Simons, D. J., and Land, P. W. (2009). Subbarrel patterns in somatosensory cortical barrels can emerge from local dynamic instabilities. *PLoS Comput Biol*, 5(10):e1000537.

Evans, M. H., Fox, C. W., Pearson, M. J., and Prescott, T. J. (2010). Tactile discrimination using template classifiers: Towards a model of feature extraction in mammalian vibrissal systems. In *From Animals to Animats (Proc. 11th Int. Conf. Simulation of Adaptive Behavior)*. Berlin, Springer.

Farah, M. J. (1998). Why does the somatosensory homunculus have hands next to face and feet next to genitals? A hypothesis. *Neural Comput*, 10(8):1983–1985.

Farley, B. J., Yu, H., Jin, D. Z., and Sur, M. (2007). Alteration of visual input results in a coordinated reorganization of multiple visual cortex maps. *J Neurosci*, 27(38):10299–10310.

Feldman, D. E. and Brecht, M. (2005). Map plasticity in somatosensory cortex. *Science*, 310(5749):810–815.

Feldmeyer, D., Lübke, J., and Sakmann, B. (2006). Efficacy and connectivity of intracolumnar pairs of layer 2/3 pyramidal cells in the barrel cortex of juvenile rats. *J Physiol*, 575(Pt 2):583–602.

Feldmeyer, D., Lübke, J., Silver, R. A., and Sakmann, B. (2002). Synaptic connections between layer 4 spiny neurone-layer 2/3 pyramidal cell pairs in juvenile rat barrel cortex: physiology and anatomy of interlaminar signalling within a cortical column. *J Physiol*, 538(Pt 3):803–822.

Fisher, N. I. (1993). *Statistical analysis of circular data.* Cambridge University Press.

Fitzpatrick, D. C., Kuwada, S., and Batra, R. (2000). Neural sensitivity to interaural time differences: beyond the Jeffress model. *J Neurosci*, 20(4):1605–1615.

Fox, C. W., Mitchinson, B., Pearson, M. J., Pipe, A. G., and Prescott, T. J. (2009). Contact type dependency of texture classification in a whiskered mobile robot. *Auton Robot*, (18 March) doi:10.1007/s10514-009-9109-z.

Fox, K. (2008). *Barrel Cortex*. Cambridge University Press: Cambridge, UK.

Fox, K. and Wong, R. O. L. (2005). A comparison of experience-dependent plasticity in the visual and somatosensory systems. *Neuron*, 48(3):465–477.

Frisby, J. P. and Stone, J. V. (2010). *Seeing, second edition: The computational approach to biological vision*. MIT Press.

Furuta, T., Nakamura, K., and Deschênes, M. (2006). Angular tuning bias of vibrissa-responsive cells in the paralemniscal pathway. *J Neurosci*, 26(41):10548–10557.

Garabedian, C. E., Jones, S. R., Merzenich, M. M., Dale, A., and Moore, C. I. (2003). Band-pass response properties of rat si neurons. *J Neurophysiol*, 90(3):1379–1391.

Ghazanfar, A. A. and Nicolelis, M. A. (1997). Nonlinear processing of tactile information in the thalamocortical loop. *J Neurophysiol*, 78(1):506–510.

Ghazanfar, A. A. and Nicolelis, M. A. (1999). Spatiotemporal properties of layer V neurons of the rat primary somatosensory cortex. *Cereb Cortex*, 9(4):348–361.

Gias, C., Hewson-Stoate, N., Jones, M., Johnston, D., Mayhew, J. E., and Coffey, P. J. (2005). Retinotopy within rat primary visual cortex using optical imaging. *Neuroimage*, 24(1):200–206.

Gibson, J. J. (1962). Observations on active touch. *Psychol Rev*, 69:477–491.

Golomb, D., Ahissar, E., and Kleinfeld, D. (2006). Coding of stimulus frequency by latency in thalamic networks through the interplay of GABA-B-mediated feedback and stimulus shape. *J Neurophysiol*, 95(3):1735–1750.

Goodhill, G. J. and Sejnowski, T. J. (1997). A unifying objective function for topographic mappings. *Neural Computation*, 9(6):1291–1303.

Gopal, V. and Hartmann, M. J. Z. (2007). Using hardware models to quantify sensory data acquisition across the rat vibrissal array. *Bioinspir Biomim*, 2(4):S135–S145.

Grant, R. A., Mitchinson, B., Fox, C. W., and Prescott, T. J. (2009). Active touch sensing in the rat: Anticipatory and regulatory control of whisker movements during surface exploration. *J Neurophysiol*, 101(2):862–874.

Grant, R. A., Mitchinson, B., and Prescott, T. J. (2011). The development of whisker control in rats in relation to locomotion. *Developmental Psychobiology*, page DOI: 10.1002/dev.20591.

Grothe, B. (2003). New roles for synaptic inhibition in sound localization. *Nat Rev Neurosci*, 4(7):540–550.

Gurney, K., Prescott, T. J., and Redgrave, P. (2001a). A computational model of action selection in the basal ganglia. i. a new functional anatomy. *Biol Cybern*, 84(6):401–410.

Gurney, K., Prescott, T. J., and Redgrave, P. (2001b). A computational model of action selection in the basal ganglia. ii. analysis and simulation of behaviour. *Biol Cybern*, 84(6):411–423.

Hanke, W., Witte, M., Miersch, L., Brede, M., Oeffner, J., Michael, M., Hanke, F., Leder, A., and Dehnhardt, G. (2010). Harbor seal vibrissa morphology suppresses vortex-induced vibrations. *J Exp Biol*, 213(Pt 15):2665–2672.

Hartings, J. A., Temereanca, S., and Simons, D. J. (2000). High responsiveness and direction sensitivity of neurons in the rat thalamic reticular nucleus to vibrissa deflections. *J Neurophysiol*, 83(5):2791–2801.

Hartmann, M. J. Z. (2011). A night in the life of a rat: vibrissal mechanics and tactile exploration. *Ann N Y Acad Sci*, 1225:110–118.

Helmstaedter, M., de Kock, C. P. J., Feldmeyer, D., Bruno, R. M., and Sakmann, B. (2007). Reconstruction of an average cortical column in silico. *Brain Res Rev*, 55(2):193–203.

Helmstaedter, M., Sakmann, B., and Feldmeyer, D. (2009). L2/3 interneuron groups defined by multiparameter analysis of axonal projection, dendritic geometry, and electrical excitability. *Cereb Cortex*, 19(4):951–962.

Helmstaedter, M., Staiger, J. F., Sakmann, B., and Feldmeyer, D. (2008). Efficient recruitment of layer 2/3 interneurons by layer 4 input in single columns of rat somatosensory cortex. *J Neurosci*, 28(33):8273–8284.

Hemelt, M. E., Kwegyir-Afful, E. E., Bruno, R. M., Simons, D. J., and Keller, A. (2010). Consistency of angular tuning in the rat vibrissa system. *J Neurophysiol*, 104(6):3105–3112.

Higley, M. J. and Contreras, D. (2003). Nonlinear integration of sensory responses in the rat barrel cortex: an intracellular study in vivo. *J Neurosci*, 23(32):10190–10200.

Higley, M. J. and Contreras, D. (2005). Integration of synaptic responses to neighboring whiskers in rat barrel cortex in vivo. *J Neurophysiol*, 93(4):1920–1934.

Higley, M. J. and Contreras, D. (2007). Cellular mechanisms of suppressive interactions between somatosensory responses in vivo. *J Neurophysiol*, 97(1):647–658.

Hoffer, Z. S., Arantes, H. B., Roth, R. L., and Alloway, K. D. (2005). Functional circuits mediating sensorimotor integration: quantitative comparisons of projections from rodent barrel cortex to primary motor cortex, neostriatum, superior colliculus, and the pons. *J Comp Neurol*, 488(1):82–100.

Hoover, J. E., Hoffer, Z. S., and Alloway, K. D. (2003). Projections from primary somatosensory cortex to the neostriatum: the role of somatotopic continuity in corticostriatal convergence. *J Neurophysiol*, 89(3):1576–1587.

Hubel, D. H. and Wiesel, T. N. (1959). Receptive fields of single neurones in the cat's striate cortex. *J Physiol*, 148:574–591.

Hubel, D. H. and Wiesel, T. N. (1965). Receptive fields and functional architecture in two nonstriate visual areas (18 and 19) of the cat. *J Neurophysiol*, 28:229–289.

Hubel, D. H. and Wiesel, T. N. (1974). Sequence regularity and geometry of orientation columns in the monkey striate cortex. *J Comp Neurol*, 158(3):267–293.

Hübener, M., Shoham, D., Grinvald, A., and Bonhoeffer, T. (1997). Spatial relationships among three columnar systems in cat area 17. *J Neurosci*, 17(23):9270–9284.

Issa, N. P., Rosenberg, A., and Husson, T. R. (2008). Models and measurements of functional maps in v1. *J Neurophysiol*, 99(6):2745–2754.

Ito, M. (1992). Simultaneous visualization of cortical barrels and horseradish peroxidase-injected layer 5b vibrissa neurones in the rat. *J Physiol*, 454:247–265.

Izhikevich, E. M. and Hoppensteadt, F. C. (2009). Polychronous wavefront computations. *International Journal of Bifurcation and Chaos*, 19:1733–1739.

Jacob, V., Cam, J. L., Ego-Stengel, V., and Shulz, D. E. (2008). Emergent properties of tactile scenes selectively activate barrel cortex neurons. *Neuron*, 60(6):1112–1125.

Jacob, V., Estebanez, L., Cam, J. L., Tiercelin, J.-Y., Parra, P., Parsys, G., and Shulz, D. E. (2010). The matrix: a new tool for probing the whisker-to-barrel system with natural stimuli. *J Neurosci Methods*, 189(1):65–74.

Jacob, V., Petreanu, L., Wright, N., Svoboda, K., and Fox, K. (2012). Regular spiking and intrinsic bursting pyramidal cells show orthogonal forms of experience-dependent plasticity in layer V of barrel cortex. *Neuron*, 73(2):391–404.

Jeffress, L. A. (1948). A place theory of sound localization. *J Comp Physiol Psychol*, 41(1):35–39.

Kapfer, C., Glickfeld, L. L., Atallah, B. V., and Scanziani, M. (2007). Supralinear increase of recurrent inhibition during sparse activity in the somatosensory cortex. *Nat Neurosci*, 10(6):743–753.

Kerr, J. N. D., de Kock, C. P. J., Greenberg, D. S., Bruno, R. M., Sakmann, B., and Helmchen, F. (2007). Spatial organization of neuronal population responses in layer 2/3 of rat barrel cortex. *J Neurosci*, 27(48):13316–13328.

Khatri, V. and Simons, D. J. (2007). Angularly nonspecific response suppression in rat barrel cortex. *Cereb Cortex*, 17(3):599–609.

Kida, H., Shimegi, S., and Sato, H. (2005). Similarity of direction tuning among responses to stimulation of different whiskers in neurons of rat barrel cortex. *J Neurophysiol*, 94(3):2004–2018.

Killackey, H. (1980). Pattern formation in the trigeminal system of the rat. *Trends in Neurosciences*, 3(12):303 – 306.

Kim, D. and Möller, R. (2007). Biomimetic whiskers for shape recognition. *Robot. Autonom. Syst.*, 55(3):229–243.

Kimura, F., Itami, C., Ikezoe, K., Tamura, H., Fujita, I., Yanagawa, Y., Obata, K., and Ohshima, M. (2010). Fast activation of feedforward inhibitory neurons from thalamic input and its relevance to the regulation of spike sequences in the barrel cortex. *J Physiol*, 588(Pt 15):2769–2787.

Kleinfeld, D., Ahissar, E., and Diamond, M. E. (2006). Active sensation: insights from the rodent vibrissa sensorimotor system. *Curr Opin Neurobiol*, 16(4):435–444.

Kohonen, T. (1982). Self-organized formation of topologically correct feature maps. *Biological Cybernetics*, 43:58–69.

Koulakov, A. A. and Chklovskii, D. B. (2001). Orientation preference patterns in mammalian visual cortex: a wire length minimization approach. *Neuron*, 29(2):519–527.

Kremer, Y., Léger, J.-F., Goodman, D., Brette, R., and Bourdieu, L. (2011). Late emergence of the vibrissa direction selectivity map in the rat barrel cortex. *J Neurosci*, 31(29):10689–10700.

Krupa, D. J., Brisben, A. J., and Nicolelis, M. A. (2001a). A multi-channel whisker stimulator for producing spatiotemporally complex tactile stimuli. *J Neurosci Methods*, 104(2):199–208.

Krupa, D. J., Matell, M. S., Brisben, A. J., Oliveira, L. M., and Nicolelis, M. A. (2001b). Behavioral properties of the trigeminal somatosensory system in rats performing whisker-dependent tactile discriminations. *J Neurosci*, 21(15):5752–5763.

Kwegyir-Afful, E. E., Bruno, R. M., Simons, D. J., and Keller, A. (2005). The role of thalamic inputs in surround receptive fields of barrel neurons. *J Neurosci*, 25(25):5926–5934.

Kyriazi, H. T., Carvell, G. E., Brumberg, J. C., and Simons, D. J. (1996). Quantitative effects of GABA and bicuculline methiodide on receptive field properties of neurons in real and simulated whisker barrels. *J Neurophysiol*, 75(2):547–560.

Kyriazi, H. T. and Simons, D. J. (1993). Thalamocortical response transformations in simulated whisker barrels. *J Neurosci*, 13(4):1601–1615.

Land, P. W. and Erickson, S. L. (2005). Subbarrel domains in rat somatosensory (S1) cortex. *J Comp Neurol*, 490(4):414–426.

Lavallée, P. and Deschênes, M. (2004). Dendroarchitecture and lateral inhibition in thalamic barreloids. *J Neurosci*, 24(27):6098–6105.

Law, J. S. (2009). *Modeling the Development of Organization for Orientation Preference in Primary Visual Cortex.* PhD thesis, School of Informatics, The University of Edinburgh, Edinburgh, UK.

Le Cam, J., Estebanez, L., Jacob, V., and Shulz, D. E. (2011). The spatial structure of multi-whisker receptive fields in the barrel cortex is stimulus-dependent. *J Neurophysiol*, 1:1.

Lee, S. and Simons, D. J. (2004). Angular tuning and velocity sensitivity in different neuron classes within layer 4 of rat barrel cortex. *J Neurophysiol*, 91(1):223–229.

Lefort, S., Tomm, C., Sarria, J.-C. F., and Petersen, C. C. H. (2009). The excitatory neuronal network of the C2 barrel column in mouse primary somatosensory cortex. *Neuron*, 61(2):301–316.

Li, L. and Ebner, F. F. (2007). Cortical modulation of spatial and angular tuning maps in the rat thalamus. *J Neurosci*, 27(1):167–179.

Li, Y., Fitzpatrick, D., and White, L. E. (2006). The development of direction selectivity in ferret visual cortex requires early visual experience. *Nat Neurosci*, 9(5):676–681.

Li, Y., Hooser, S. D. V., Mazurek, M., White, L. E., and Fitzpatrick, D. (2008). Experience with moving visual stimuli drives the early development of cortical direction selectivity. *Nature*, 456(7224):952–956.

Lichtenstein, S. H., Carvell, G. E., and Simons, D. J. (1990). Responses of rat trigeminal ganglion neurons to movements of vibrissae in different directions. *Somatosens Mot Res*, 7(1):47–65.

Lottem, E. and Azouz, R. (2009). Mechanisms of tactile information transmission through whisker vibrations. *J Neurosci*, 29(37):11686–11697.

Lottem, E. and Azouz, R. (2011). A unifying framework underlying mechanotransduction in the somatosensory system. *J Neurosci*, 31(23):8520–8532.

Louderback, K. M., Glass, C. S., Shamalla-Hannah, L., Erickson, S. L., and Land, P. W. (2006). Subbarrel patterns of thalamocortical innervation in rat somatosensory cortical barrels: Organization and postnatal development. *J Comp Neurol*, 497(1):32–41.

Lübke, J., Egger, V., Sakmann, B., and Feldmeyer, D. (2000). Columnar organization of dendrites and axons of single and synaptically coupled excitatory spiny neurons in layer 4 of the rat barrel cortex. *J Neurosci*, 20(14):5300–5311.

Lungarella, M., Hafner, V. V., Pfeifer, R., and Yokoi, H. (2002). Whisking: An unexplored sensory modality. In *From Animals to Animats (Proc. 7th Int. Conf. Simulation of Adaptive Behavior)*. Cambridge, MA:MIT Press.

Ma, P. M. and Woolsey, T. A. (1984). Cytoarchitectonic correlates of the vibrissae in the medullary trigeminal complex of the mouse. *Brain Res*, 306(1-2):374–379.

Maier, D. L., Mani, S., Donovan, S. L., Soppet, D., Tessarollo, L., McCasland, J. S., and Meiri, K. F. (1999). Disrupted cortical map and absence of cortical barrels in growth-associated protein (gap)-43 knockout mice. *Proc Natl Acad Sci U S A*, 96(16):9397–9402.

Manns, I. D., Sakmann, B., and Brecht, M. (2004). Sub- and suprathreshold receptive field properties of pyramidal neurones in layers 5a and 5b of rat somatosensory barrel cortex. *J Physiol*, 556(Pt 2):601–622.

Markram, H. (2006). The blue brain project. *Nat Rev Neurosci*, 7(2):153–160.

Martin, K. A. C. (2002). Microcircuits in visual cortex. *Curr Opin Neurobiol*, 12(4):418–425.

McAlpine, D. and Grothe, B. (2003). Sound localization and delay lines – do mammals fit the model? *Trends Neurosci*, 26(7):347–350.

Mercier, B. E., Legg, C. R., and Glickstein, M. (1990). Basal ganglia and cerebellum receive different somatosensory information in rats. *Proc Natl Acad Sci U S A*, 87(11):4388–4392.

Miikkulainen, R., Bednar, J. A., Choe, Y., and Sirosh, J. (2005). *Computational maps in the visual cortex*. Springer, Berlin.

Miller, K. D. and Mackay, D. J. C. (1994). The role of constraints in Hebbian learning. *Neural Computation*, 6:100–126.

Mirabella, G., Battiston, S., and Diamond, M. E. (2001). Integration of multiple-whisker inputs in rat somatosensory cortex. *Cereb Cortex*, 11(2):164–170.

Mitchinson, B., Arabzadeh, E., Diamond, M. E., and Prescott, T. J. (2008). Spike-timing in primary sensory neurons: A model of somatosensory transduction in the rat. *Biol Cybern*, 98(3):185–194.

Mitchinson, B., Arkley, K., Grant, R., Rankov, V., and Prescott, T. J. (2011). Active vibrissal sensing in rodents and marsupials. *Proceedings of the Royal Society.*, 1:1.

Mitchinson, B., Gurney, K. N., Redgrave, P., Melhuish, C., Pipe, A. G., Pearson, M., Gilhespy, I., and Prescott, T. J. (2004). Empirically inspired simulated electro-mechanical model of the rat mystacial follicle-sinus complex. *Proc Biol Sci*, 271(1556):2509–2516.

Mitchinson, B., Martin, C. J., Grant, R. A., and Prescott, T. J. (2007). Feedback control in active sensing: rat exploratory whisking is modulated by environmental contact. *Proc Biol Sci*, 274(1613):1035–1041.

Mitchinson, B., Pearson, M. J., Melhuish, C., and Prescott, T. J. (2006). A model of sensorimotor coordination in the rat whisker system. In *SAB'06*, pages 77–88.

Mitchinson, B., Pearson, M. J., Pipe, A. G., and Prescott, T. J. (2010). *Neuromorphic and Brain-Based Robots: Trends and Perspectives*, chapter Biomimetic robots as scientific models: A view from the whisker tip. Cambridge University Press.

Mittmann, W., Wallace, D. J., Czubayko, U., Herb, J. T., Schaefer, A. T., Looger, L. L., Denk, W., and Kerr, J. N. D. (2011). Two-photon calcium imaging of evoked activity from l5 somatosensory neurons in vivo. *Nat Neurosci*, 14(8):1089–1093.

Moore, C. and Andermann, M. (2005). *Somatosensory Plasticity*, chapter 2. The vibrissa resonance hypothesis, pages 21–60. CRC Press.

Moore, C. I., Nelson, S. B., and Sur, M. (1999). Dynamics of neuronal processing in rat somatosensory cortex. *Trends Neurosci*, 22(11):513–520.

Neimark, M. A., Andermann, M. L., Hopfield, J. J., and Moore, C. I. (2003). Vibrissa resonance as a transduction mechanism for tactile encoding. *J Neurosci*, 23(16):6499–6509.

Oberlaender, M., Boudewijns, Z. S. R. M., Kleele, T., Mansvelder, H. D., Sakmann, B., and de Kock, C. P. J. (2011). Three-dimensional axon morphologies of individual layer 5 neurons indicate cell type-specific intracortical pathways for whisker motion and touch. *Proc Natl Acad Sci U S A*, 108(10):4188–4193.

O'Connor, D. H., Peron, S. P., Huber, D., and Svoboda, K. (2010). Neural activity in barrel cortex underlying vibrissa-based object localization in mice. *Neuron*, 67(6):1048–1061.

Ohki, K., Chung, S., Ch'ng, Y. H., Kara, P., and Reid, R. C. (2005). Functional imaging with cellular resolution reveals precise micro-architecture in visual cortex. *Nature*, 433(7026):597–603.

Ohki, K., Chung, S., Kara, P., Hübener, M., Bonhoeffer, T., and Reid, R. C. (2006). Highly ordered arrangement of single neurons in orientation pinwheels. *Nature*, 442(7105):925–928.

Park, C., Choi, H., and Choe, Y. (2009). Self-organization of tactile receptive fields: Exploring their textural origin and their representational properties. In *Proceedings of the 7th International Workshop on Advances in Self-Organizing Maps*, WSOM '09, pages 228–236, Berlin, Heidelberg. Springer-Verlag.

Pearson, M. J., Pipe, A. G., Melhuish, C., Mitchinson, B., and Prescott, T. J. (2007). Whiskerbot: A robotic active touch system modeled on the rat whisker sensory system. *Adaptive Behaviour*, 15(3):223–240.

Petersen, C. C. and Sakmann, B. (2000). The excitatory neuronal network of rat layer 4 barrel cortex. *J Neurosci*, 20(20):7579–7586.

Petersen, C. C. H., Grinvald, A., and Sakmann, B. (2003). Spatiotemporal dynamics of sensory responses in layer 2/3 of rat barrel cortex measured in vivo by voltage-sensitive dye imaging combined with whole-cell voltage recordings and neuron reconstructions. *J Neurosci*, 23(4):1298–1309.

Petersen, R. S., Brambilla, M., Bale, M. R., Alenda, A., Panzeri, S., Montemurro, M. A., and Maravall, M. (2008). Diverse and temporally precise kinetic feature selectivity in the VPm thalamic nucleus. *Neuron*, 60(5):890–903.

Petersen, R. S., Panzeri, S., and Maravall, M. (2009). Neural coding and contextual influences in the whisker system. *Biol Cybern*, 100(6):427–446.

Pinto, D. J., Brumberg, J. C., Simons, D. J., and Ermentrout, G. B. (1996). A quantitative population model of whisker barrels: Re-examining the Wilson-Cowan equations. *J Comput Neurosci*, 3(3):247–264.

Pisano, R. G. and Storer, T. I. (1948). Burrows and feeding of the Norway rat. *J. Mammalogy*, 29(4):374–383.

Polley, D. B., Rickert, J. L., and Frostig, R. D. (2005). Whisker-based discrimination of object orientation determined with a rapid training paradigm. *Neurobiol Learn Mem*, 83(2):134–142.

Porter, J. T., Johnson, C. K., and Agmon, A. (2001). Diverse types of interneurons generate thalamus-evoked feedforward inhibition in the mouse barrel cortex. *J Neurosci*, 21(8):2699–2710.

Prescott, T. J., Pearson, M., Mitchinson, B., Sullivan, J. C. W., and Pipe, A. G. (2009). Whisking with robots: From rat vibrissae to biomimetic technology for active touch. *IEEE Robotics and Automation Magazine*, 6(3):42–50.

Puccini, G. D., Compte, A., and Maravall, M. (2006). Stimulus dependence of barrel cortex directional selectivity. *PLoS ONE*, 1:e137.

Quiroga, R. Q., Reddy, L., Kreiman, G., Koch, C., and Fried, I. (2005). Invariant visual representation by single neurons in the human brain. *Nature*, 435(7045):1102–1107.

Rall, W. (1964). *Theoretical significance of dendritic trees for neuronal input-output relations*. In Neural Theory and Modeling, Ed. R F Reiss. Stanford Univ. Press.

Redgrave, P., Prescott, T. J., and Gurney, K. (1999). The basal ganglia: A vertebrate solution to the selection problem? *Neuroscience*, 89(4):1009–1023.

Reichardt, W. (1961). *Autocorrelation, a principle for the evaluation of sensory information by the central nervous system*. In Sensory Communication, Ed W A Rosenblith; New York: New York.

Ren, M., Yoshimura, Y., Takada, N., Horibe, S., and Komatsu, Y. (2007). Specialized inhibitory synaptic actions between nearby neocortical pyramidal neurons. *Science*, 316(5825):758–761.

Ritt, J. T., Andermann, M. L., and Moore, C. I. (2008). Embodied information processing: Vibrissa mechanics and texture features shape micromotions in actively sensing rats. *Neuron*, 57(4):599–613.

Roberts, S. and Pashler, H. (2000). How persuasive is a good fit? A comment on theory testing. *Psychol Rev*, 107(2):358–367.

Roberts, W. M., Howard, J., and Hudspeth, A. J. (1988). Hair cells: Transduction, tuning, and transmission in the inner ear. *Annu Rev Cell Biol*, 4:63–92.

Rosenblueth, A. and Wiener, N. (1945). The role of models in science. *Philosophy of Science*, 12(4):316–321.

Roth-Alpermann, C., Anjum, F., Naumann, R., and Brecht, M. (2010). Cortical organization in the Etruscan shrew (Suncus etruscus). *J Neurophysiol*, 104(5):2389–2406.

Roy, N. C., Bessaih, T., and Contreras, D. (2011). Comprehensive mapping of whisker-evoked responses reveals broad, sharply tuned thalamocortical input to layer 4 of barrel cortex. *Journal of Neurophysiol*, 105(5):2421–2437.

Russell, R. A. and Wijaya, J. A. (2005). Recognising and manipulating objects using data from a whisker sensor arrays. *Robotica*, 5:653–664.

Sachdev, R. N., Sellien, H., and Ebner, F. (2001). Temporal organization of multi-whisker contact in rats. *Somatosens Mot Res*, 18(2):91–100.

Sachdev, R. N. S., Sato, T., and Ebner, F. F. (2002). Divergent movement of adjacent whiskers. *J Neurophysiol*, 87(3):1440–1448.

Sarid, L., Bruno, R., Sakmann, B., Segev, I., and Feldmeyer, D. (2007). Modeling a layer 4-to-layer 2/3 module of a single column in rat neocortex: Interweaving in vitro and in vivo experimental observations. *Proc Natl Acad Sci U S A*, 104(41):16353–16358.

Sato, H., Shimanuki, Y., Saito, M., Toyoda, H., Nokubi, T., Maeda, Y., Yamamoto, T., and Kang, Y. (2008). Differential columnar processing in local circuits of barrel and insular cortices. *J Neurosci*, 28(12):3076–3089.

Sato, T. R., Gray, N. W., Mainen, Z. F., and Svoboda, K. (2007). The functional microarchitecture of the mouse barrel cortex. *PLoS Biol*, 5(7):e189.

Schubert, D., Kotter, R., Luhmann, H. J., and Staiger, J. F. (2006). Morphology, electrophysiology and functional input connectivity of pyramidal neurons characterizes a genuine layer Va in the primary somatosensory cortex. *Cereb Cortex*, 16(2):223–236.

Schubert, D., Staiger, J. F., Cho, N., Kotter, R., Zilles, K., and Luhmann, H. J. (2001). Layer-specific intracolumnar and transcolumnar functional connectivity of layer V pyramidal cells in rat barrel cortex. *J Neurosci*, 21(10):3580–3592.

Schuett, S., Bonhoeffer, T., and Hübener, M. (2002). Mapping retinotopic structure in mouse visual cortex with optical imaging. *J Neurosci*, 22(15):6549–6559.

Senft, S. L. and Woolsey, T. A. (1991). Mouse barrel cortex viewed as Dirichlet domains. *Cereb Cortex*, 1(4):348–363.

Seriès, P., Georges, S., Lorenceau, J., and Frégnac, Y. (2002). Orientation dependent modulation of apparent speed: A model based on the dynamics of feed-forward and horizontal connectivity in V1 cortex. *Vision Res*, 42(25):2781–2797.

Seth, A. K., andG M Edelman, J. L. M., and Krichma, J. L. (2004). Active sensing of visual and tactile stimuli by brain-based devices. *Int. J. Robot. Automat.*, 19(4):222–238.

Sharma, J., Angelucci, A., and Sur, M. (2000). Induction of visual orientation modules in auditory cortex. *Nature*, 404(6780):841–847.

Shimegi, S., Akasaki, T., Ichikawa, T., and Sato, H. (2000). Physiological and anatomical organization of multiwhisker response interactions in the barrel cortex of rats. *J Neurosci*, 20(16):6241–6248.

Shimegi, S., Ichikawa, T., Akasaki, T., and Sato, H. (1999). Temporal characteristics of response integration evoked by multiple whisker stimulations in the barrel cortex of rats. *J Neurosci*, 19(22):10164–10175.

Shoykhet, M. and Simons, D. J. (2008). Development of thalamocortical response transformations in the rat whisker-barrel system. *J Neurophysiol*, 99(1):356–366.

Silberberg, G. and Markram, H. (2007). Disynaptic inhibition between neocortical pyramidal cells mediated by Martinotti cells. *Neuron*, 53(5):735–746.

Simons, D. J. (1978). Response properties of vibrissa units in rat si somatosensory neocortex. *J Neurophysiol*, 41(3):798–820.

Simons, D. J. (1983). Multi-whisker stimulation and its effects on vibrissa units in rat SmI barrel cortex. *Brain Res*, 276(1):178–182.

Simons, D. J. (1985). Temporal and spatial integration in the rat SI vibrissa cortex. *J Neurophysiol*, 54(3):615–635.

Simons, D. J. and Carvell, G. E. (1989). Thalamocortical response transformation in the rat vibrissa/barrel system. *J Neurophysiol*, 61(2):311–330.

Simons, D. J., Carvell, G. E., Kyriazi, H. T., and Bruno, R. M. (2007). Thalamocortical conduction times and stimulus-evoked responses in the rat whisker-to-barrel system. *J Neurophysiol*, 98(5):2842–2847.

Sirosh, J. and Miikkulainen, R. (1997). Topographic receptive fields and patterned lateral interaction in a self-organizing model of the primary visual cortex. *Neural Comput*, 9(3):577–594.

Solomon, J. and Hartmann, M. (2008). Artificial whiskers suitable for array implementation: Accounting for lateral slip and surface friction. *Robotics, IEEE Transactions on*, 24(5):1157 –1167.

Solomon, J. H. and Hartmann, M. J. (2006). Biomechanics: Robotic whiskers used to sense features. *Nature*, 443(7111):525.

Somers, D. C., Todorov, E. V., Siapas, A. G., Toth, L. J., Kim, D. S., and Sur, M. (1998). A local circuit approach to understanding integration of long-range inputs in primary visual cortex. *Cereb Cortex*, 8(3):204–217.

Stafford, T. and Wilson, S. P. (2007). Self-organisation can generate the discontinuities in the somatosensory map. *Neurocomputing*, 70:1932–1937.

Sullivan, J., Mitchinson, B., Pearson, M., Evans, M., Lepora, N., Fox, C., Melhuish, C., and Prescott, T. (2011). Tactile discrimination using active whisker sensors. *Sensors Journal, IEEE*, PP(99):1.

Sun, Q.-Q., Huguenard, J. R., and Prince, D. A. (2006). Barrel cortex microcircuits: Thalamocortical feedforward inhibition in spiny stellate cells is mediated by a small number of fast-spiking interneurons. *J Neurosci*, 26(4):1219–1230.

Swadlow, H. A. (2002). Thalamocortical control of feed-forward inhibition in awake somatosensory 'barrel' cortex. *Philos Trans R Soc Lond B Biol Sci*, 357(1428):1717–1727.

Swadlow, H. A. and Gusev, A. G. (2002). Receptive-field construction in cortical inhibitory interneurons. *Nat Neurosci*, 5(5):403–404.

Swindale, N. V. (1996). The development of topography in the visual cortex: A review of models. *Network: Comput Neural Syst*, 7(2):161–247.

Swindale, N. V., Shoham, D., Grinvald, A., Bonhoeffer, T., and Hübener, M. (2000). Visual cortex maps are optimized for uniform coverage. *Nat Neurosci*, 3(8):822–826.

Szwed, M. and Ahissar, E. (2006). Mapping the gates. Focus on "Relationship between physiological response type (RA and SA) and vibrissal receptive field of neurons within the rat trigeminal ganglion". *J Neurophysiol*, 95(5):2729–2730.

Temereanca, S. and Simons, D. J. (2004). Functional topography of corticothalamic feedback enhances thalamic spatial response tuning in the somatosensory whisker/barrel system. *Neuron*, 41(4):639–651.

Tieman, S. B. and Hirsch, H. V. (1982). Exposure to lines of only one orientation modifies dendritic morphology of cells in the visual cortex of the cat. *J Comp Neurol*, 211(4):353–362.

Timofeeva, E., Lavallée, P., Arsenault, D., and Deschênes, M. (2004). Synthesis of multiwhisker-receptive fields in subcortical stations of the vibrissa system. *J Neurophysiol*, 91(4):1510–1515.

Timofeeva, E., Mérette, C., Emond, C., Lavallée, P., and Deschênes, M. (2003). A map of angular tuning preference in thalamic barreloids. *J Neurosci*, 23(33):10717–10723.

Towal, R. B., Quist, B. W., Gopal, V., Solomon, J. H., and Hartmann, M. J. Z. (2011). The morphology of the rat vibrissal array: A model for quantifying spatiotemporal patterns of whisker-object contact. *PLoS Comput Biol*, 7(4):e1001120.

Tsytsarev, V., Pope, D., Pumbo, E., Yablonskii, A., and Hofmann, M. (2010). Study of the cortical representation of whisker directional deflection using voltage-sensitive dye optical imaging. *Neuroimage*, 53(1):233–238.

van der Loos, H. (1976). Barreloids in mouse somatosensory thalamus. *Neurosci Lett*, 2(1):1–6.

van Hooser, S. D., Heimel, J. A., Chung, S., and Nelson, S. B. (2006). Lack of patchy horizontal connectivity in primary visual cortex of a mammal without orientation maps. *J Neurosci*, 26(29):7680–7692.

van Hooser, S. D., Heimel, J. A. F., Chung, S., Nelson, S. B., and Toth, L. J. (2005). Orientation selectivity without orientation maps in visual cortex of a highly visual mammal. *J Neurosci*, 25(1):19–28.

Veinante, P., Lavallée, P., and Deschênes, M. (2000). Corticothalamic projections from layer 5 of the vibrissal barrel cortex in the rat. *J Comp Neurol*, 424(2):197–204.

Vincent, S. B. (1912). The function of the vibrissae in the behavior of the white rat. *Behav Monographs*, 1:1–82.

von der Malsburg, C. (1973). Self-organization of orientation sensitive cells in the striate cortex. *Kybernetik*, 14(2):85–100.

Wallace, H. and Fox, K. (1999). The effect of vibrissa deprivation pattern on the form of plasticity induced in rat barrel cortex. *Somatosens Mot Res*, 16(2):122–138.

Weliky, M., Bosking, W. H., and Fitzpatrick, D. (1996). A systematic map of direction preference in primary visual cortex. *Nature*, 379(6567):725–8.

Weliky, M., Kandler, K., Fitzpatrick, D., and Katz, L. C. (1995). Patterns of excitation and inhibition evoked by horizontal connections in visual cortex share a common relationship to orientation columns. *Neuron*, 15(3):541–552.

Welker, C. and Woolsey, T. A. (1974). Structure of layer IV in the somatosensory neocortex of the rat: Description and comparison with the mouse. *J Comp Neurol*, 158(4):437–453.

Welker, E., Hoogland, P. V., and van der Loos, H. (1988). Organization of feedback and feed-forward projections of the barrel cortex: A PHA-L study in the mouse. *Exp Brain Res*, 73(2):411–435.

Welker, W. I. (1964). Analysis of sniffing of the albino rat. *Behaviour*, 22:223–244.

White, L. E. and Fitzpatrick, D. (2007). Vision and cortical map development. *Neuron*, 56(2):327–338.

Wieskotten, S., Mauck, B., Miersch, L., Dehnhardt, G., and Hanke, W. (2011). Hydrodynamic discrimination of wakes caused by objects of different size or shape in a harbour seal (Phoca vitulina). *J Exp Biol*, 214(Pt 11):1922–1930.

Wilent, W. B. and Contreras, D. (2005). Dynamics of excitation and inhibition underlying stimulus selectivity in rat somatosensory cortex. *Nat Neurosci*, 8(10):1364–1370.

Williams, C. M. and Kramer, E. M. (2010). The advantages of a tapered whisker. *PLoS One*, 5(1):e8806.

Willmore, B. and Smyth, D. (2003). Methods for first-order kernel estimation: Simple-cell receptive fields from responses to natural scenes. *Network*, 14(3):553–577.

Wilson, S. P. (2007). Self-organisation can explain the mapping of angular whisker deflections in the barrel cortex. Master's thesis, School of Informatics, The University of Edinburgh, Edinburgh, UK.

Wilson, S. P., Bednar, J. A., Prescott, T. J., and Mitchinson, B. (2011). Neural computation via neural geometry: A place code for inter-whisker timing in the barrel cortex? *PLoS Computational Biology*, 1(1):1.

Wilson, S. P., Law, J. S., Mitchinson, B., Prescott, T. J., and Bednar, J. A. (2010). Modeling the emergence of whisker direction maps in rat barrel cortex. *PLoS One*, 5(1):e8778.

Wirth, C. and Lüscher, H.-R. (2004). Spatiotemporal evolution of excitation and inhibition in the rat barrel cortex investigated with multielectrode arrays. *J Neurophysiol*, 91(4):1635–1647.

Wolfe, J., Hill, D. N., Pahlavan, S., Drew, P. J., Kleinfeld, D., and Feldman, D. E. (2008). Texture coding in the rat whisker system: Slip-stick versus differential resonance. *PLoS Biol*, 6(8):e215.

Woolsey, C. N. and LeMessurier, D. H. (1948). The pattern of cutaneous representation in the rat's cerebral cortex. *Fed Proc*, 7(1 Pt 1):137.

Woolsey, T. A. and van der Loos, H. (1970). The structural organization of layer IV in the somatosensory region (SI) of mouse cerebral cortex. The description of a cortical field composed of discrete cytoarchitectonic units. *Brain Res*, 17(2):205–242.

Wright, N. and Fox, K. (2010). Origins of cortical layer V surround receptive fields in the rat barrel cortex. *J Neurophysiol*, 103(2):709–724.

Yoris, P. and Yin, T. C. T. (2006). A matter of time: Internal delays in binaural processing. *Trends Neurosci*, 30:70–78.

Yu, H., Farley, B. J., Jin, D. Z., and Sur, M. (2005). The coordinated mapping of visual space and response features in visual cortex. *Neuron*, 47(2):267–280.

Zucker, E. and Welker, W. I. (1969). Coding of somatic sensory input by vibrissae neurons in the rat's trigeminal ganglion. *Brain Res*, 12(1):138–156.